Biochemical and structural studies of the FtsZ:FtsA complex and polymerising abilities of the FtsA protein

Piotr Ł. Szwedziak

College of Corpus Christi and the Blessed Virgin Mary

University of Cambridge

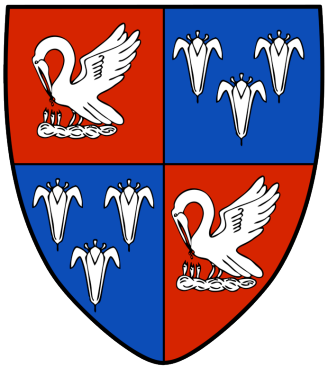

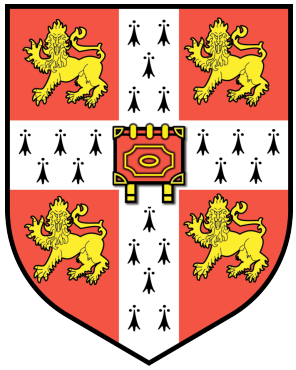

Thesis submitted to the University of Cambridge for the degree of Doctor of Philosophy

December 2011

Declaration

This thesis is the result of my own work and includes nothing that is the outcome of work done in collaboration except where specifically indicated in the text. No part of this thesis has been submitted for other qualification, in any other university. Permission is granted to copy the information contained herein for the purpose of private study, but not for publication. This thesis does not exceed the word limit prescribed by the Degree Committee of the Faculty of Biology.

Piotr Ł. Szwedziak

Acknowledgements

The work described in this dissertation was performed in the group of Jan Löwe at the Medical Research Council Laboratory of Molecular Biology. I owe a great debt of thanks to Jan for giving me the opportunity to work in such a fantastic environment and wise guidance throughout the entire period of my PhD work.

I would like to thank all members of G8C and G6 for many pieces of advice and enjoyable and stimulating discussions. I am especially grateful to Kate Michie and Fusinita van den Ent for help with starting in the lab.

I am grateful to Qing Wang for his outstanding work on visualising FtsA polymers by electron cryo-tomography and to Stefan Freund for excellent and fruitful collaboration on the NMR side of my project.

I was lucky to be supported by a PhD fellowship from Boehringer Ingelheim Fonds, which enabled me to meet and network with many brilliant fellows from all around Europe and North America.

I wish to thank all my friends in Cambridge that I have met over the past three years who made my time here such a great experience.

Finally, I would like to warmly thank my parents, Anna and Marek and my brother Krzysztof for their support, devotion and for believing in me.

Table of contents

List of abbreviations

ATP	adenosine triphosphate
ATPγS	adenosine-γ-thiotriphosphate
ATPase	adenosine triphosphatase
B. subtilis	*Bacillus subtilis*
BsFtsA	*Bacillus subtilis* FtsA
C. crescentus	*Caulobacter crescentus*
cryoET	electron cryo-tomography
csp	chemical shift perturbation
DNA	deoxyribonucleic acid
DTT	dithiotreitol
E. coli	*Escherichia coli*
EcFtsA	*Escherichia coli* FtsA
EDTA	ethylenediaminetetraacetic acid
EM	electron microscopy
GTP	guanosine triphosphate
HSQC	heteronuclear single quantum coherence
IPTG	isopropyl-β-D-thiogalactopyranoside
ITC	isothermal titration calorimetry
kDa	kilodalton
MBP	maltose binding protein
NMR	nuclear magnetic resonance spectroscopy

OD_{600}	optical density at 600 nm
PAGE	polyacrylamide gel electrophoresis
PBS	phosphate buffered saline
PCR	polymerase chain reaction
PDB	protein data bank
PMSF	phenylmethylsulfonyl fluoride
rpm	revolution per minute
SDS	sodium dodecyl sulphate
T. maritima	*Thermotoga maritima*
TmFtsA	*Thermotoga maritima* FtsA
TmFtsZ	*Thermotoga maritima* FtsZ
TROSY	transverse relaxation optimized spectroscopy
ts	temperature sensitive
wt	wild-type

Abstract

A key step in bacterial cell division is the formation of the Z-ring composed of polymers of the tubulin-like protein FtsZ. The Z-ring constricts and through interaction with other components engages in remodelling the cell wall and membranes in order to yield two daughter cells. During this process, FtsZ is known to interact with FtsA, which is an early component of the Z-ring, and then recruits other components of the divisome, the cell division apparatus. Analysis of FtsA sequences revealed a conserved C-terminal motif, which is predicted to form an amphipathic helix and has been shown to localise FtsA (and with it FtsZ) to the membrane. FtsA belongs to the actin/HSP70 family of proteins, although its fold was shown to deviate by a subdomain deletion and addition. Many members of this family are able to form filaments, and it is a long-standing question whether FtsA is able to polymerise.

In this study, I reconstituted the tethering of FtsZ to the membrane via FtsA's C-terminal amphipathic helix *in vitro* using *T. maritima* proteins. A crystal structure of the FtsA:FtsZ interaction revealed 16 amino acids of the FtsZ tail bound to subdomain 2B of FtsA. The same structure and a second crystal form of FtsA revealed that FtsA forms actin-like protofilaments with a repeat of 48 Å. An identical repeat length was observed when FtsA was polymerised using a lipid monolayer surface and FtsAs from three organisms formed polymers in cells when overexpressed, as observed by electron cryo-tomography. Mutants that disrupt polymerisation also showed a significant cell division phenotype in a temperature sensitive FtsA background, demonstrating the importance of filament formation for FtsA's function in the Z-ring.

Introduction

Bacterial cell division

One of the prerequisites for the existence of cellular forms of life is cell division after DNA's replication and distribution to two daughter cells. Both DNA segregation and cell division must be temporally and spatially resolved to ensure that the daughter cells are genetically identical. In spite of the fact that the mechanisms governing cell division are of crucial importance and must have emerged very early in evolution, there are some significant differences between prokaryotes and eukaryotes (Nanninga, 2001; Fig. 1a). Firstly, in a vast majority of prokaryotes there is no distinction between interphase and mitosis as DNA segregation proceeds simultaneously with replication (Woldringh, 1976). Secondly, an actomyosin ring, consisting of actin and a type II myosin, performs cytokinesis in eukarotyes and this is fairly well understood (Pollard, 2010). In contrast, it seems that cell division in prokaryotes is almost exclusively carried out by tubulin-like FtsZ and associated proteins (Erickson, Anderson & Osawa, 2010), except of several species that are discussed later.

The division machinery has to constrict the membrane between segregated DNA so that there is only a narrow connection between the daughter cells, which are eventually separated. In animal cells and fungi, septin filaments define the division plane and then both myosin and actin are recruited (Longtine & Bi, 2003). Actin, organised by formins (Waller & Alberts, 2003), bundles and the actomyosin sliding-filament constricts. On the other hand, cell division in bacteria is achieved by a multiprotein complex called the divisome (Adams & Errington, 2009). Its assembly starts with the polymerisation of FtsZ, a prokaryotic tubulin homologue, into the Z-ring, which subsequently recruits other protein components to the division site. The divisome is currently known to contain more than 20 components and can be divided into the inner and outer divisome (Vicente & Rico, 2006). This distinction reflects the fact that the divisome needs to remodel not only the inner cell membrane, but also the rigid cell wall and hence a direct link with enzymes for cell wall remodelling is made. The mechanism of constriction is currently unclear, but the only known sources of energy in the system (apart from binding energies) are nucleotide hydrolysis by FtsA

Figure 1. An overview of fundamental terms concerning cytokinesis.

a) Cell cycle phases in prokaryotes and eukaryotes. In *E. coli* the chromosome separates as it replicates, thus S=M. G_1 – phase prior to DNA replication, G_2 – phase between DNA replication and mitosis, M – mitosis, S – DNA synthesis phase (modified from Nanninga, 2001).
b) Cell division in rod-shaped bacteria. After DNA replication and rapid segregation the Z-ring assembles at the division site. Then the next proteins of the divisome are recruited. Finally, the ring constricts in order to obtain two daughter cells.
c) Phylogenetic distribution of known cell division mechanisms (modified from Bernander & Ettema, 2010).

Figure 1

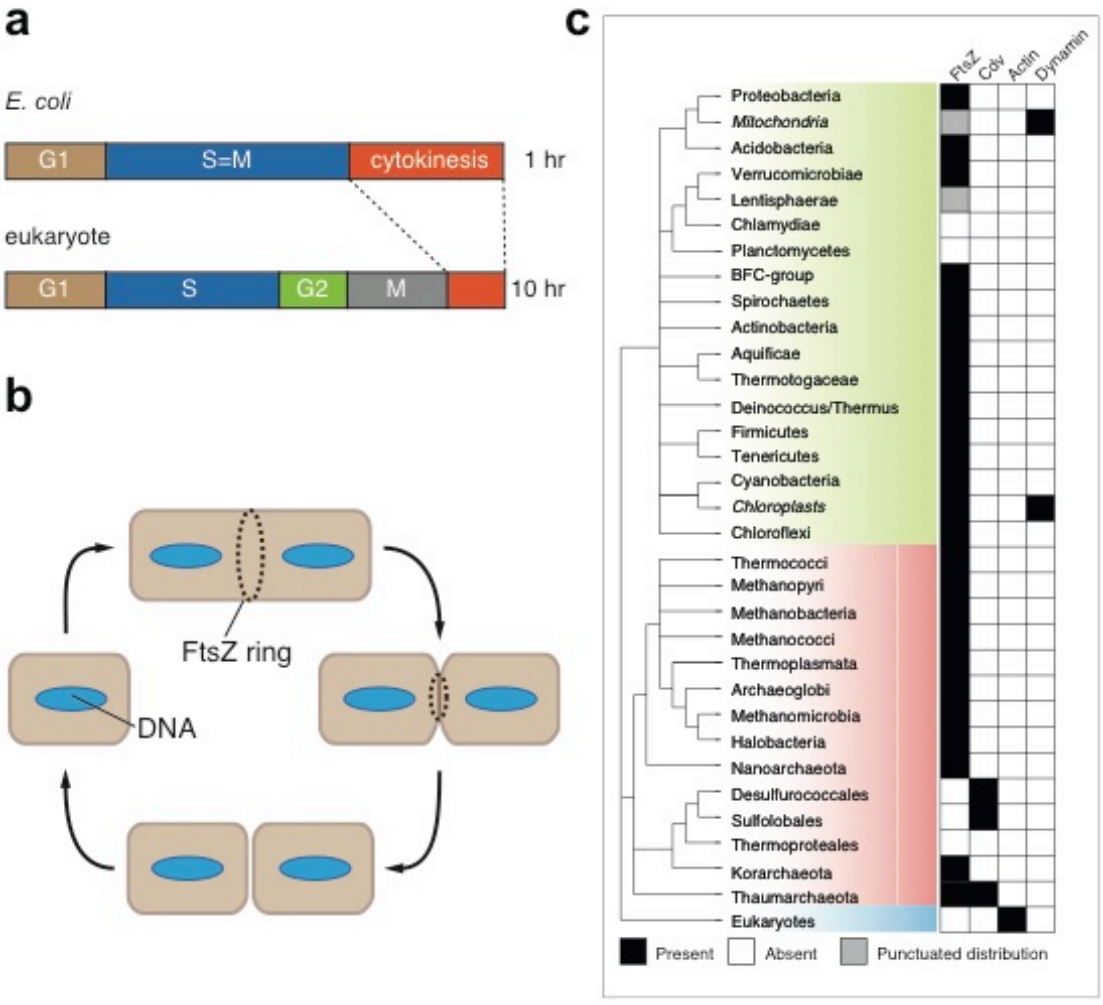
a
E. coli
G1
S=M
cytokinesis
1 hr
eukaryote
G1
S
G2
M
10 hr
b
FtsZ ring
DNA
c
FtsZ
Cdv
Actin
Dynamin
Proteobacteria
Mitochondria
Acidobacteria
Verrucomicrobiae
Lentisphaerae
Chlamydiae
Planctomycetes
BFC-group
Spirochaetes
Actinobacteria
Aquificae
Thermotogaceae
Deinococcus/Thermus
Firmicutes
Tenericutes
Cyanobacteria
Chloroplasts
Chloroflexi
Thermococci
Methanopyri
Methanobacteria
Methanococci
Thermoplasmata
Archaeoglobi
Methanomicrobia
Halobacteria
Nanoarchaeota
Desulfurococcales
Sulfolobales
Thermoproteales
Korarchaeota
Thaumarchaeota
Eukaryotes
Present
Absent
Punctuated distribution

and FtsZ (inner divisome), as well as cell wall synthesis from precursors in the periplasm (outer divisome).

Cell division has been extensively studied in three model bacteria: gram-negative *Escherichia coli* (Vicente & Rico, 2006), gram-positive *Bacillus subtilis* (Jensen, Thompson & Harry, 2005), which also has an asymmetric cell division associated with sporulation, and *Caulobacter crescentus* (Goley et al., 2011), which exhibits an unusual life cycle featuring stalked and swarmer cells. In rod-shaped cells the divisome assembles at the midpoint of the rod, between two segregated nucleoids and constriction creates two equal-sized daughter cells (Fig. 1b). Constriction in the case of *E. coli* involves three envelope layers (the outer membrane, the peptidoglycan layer and the cell membrane). In *B. subtilis* there is additionally an ingrowing septum made of the thick cell wall. Moreover, *B. subtilis* undergoes two modes of cell division (Ben-Yehuda & Losick, 2002): vegetative, where a cell divides by binary fission (as *E. coli* does) and asymmetric, where upon entry into sporulation, the division plane is switched to a position close to one pole of the developing cell. The formation of polar FtsZ polymers is mediated by Spo0A and σ^H, which govern entry into sporulation (Levin & Losick, 1996). Another example of a peculiar cell division is *C. crescentus*, which divides asymmetrically to obtain two different daughter cells, a swarmer and a stalked cell (McAdams & Shapiro, 2009). Only the latter is able to replicate its DNA and the swarmer cell eventually differentiates into the stalked cell. This lifestyle dictates a need for tight regulation of FtsZ and FtsA synthesis and stability (Kelly, Sackett, Din, Quardokus & Brun, 1998; Martin, Trimble & Brun, 2004) since merely stalked cells undergo cell division. On the other hand, no considerable changes have been reported in FtsZ's abundance in *E. coli* and *B. subtilis*. It seems that cell division in these bacteria must be regulated at the level of the divisome assembly.

Most bacteria and a branch of the archaea called the Euryarchaeota rely on FtsZ. Interestingly, some prokaryotic microorganisms have evolved other FtsZ-independent systems of cell division. Until 1998 no alternatives for the FtsZ-based apparatus in bacteria and archaea (Erickson & Osawa, 2010) had been found. Then newly sequenced genomes of *Chlamydia* and *Aeropyrum pernix*, a free-living archeon, were found to have no *ftsZ* gene (Stephens et al., 1998; Kawarabayasi, Hino, Horikawa, Yamazaki & Haikawa, 1999). Soon after it turned out that the entire kingdom of

Crenarchaea, and the phylum *Planctomycetes* and some *Mycoplasmas* among the bacteria, all live without *ftsZ* (Bernander & Ettema, 2010). Strikingly, ten years later it was discovered that the division mechanism of *Crenarchea* relies on a homologue of the eukaryotic ESCRT-III system, which is involved in vesicle trafficking and membrane scission (Lindas, Karlsson, Lindgren, Etterna & Bernander, 2008; Samson et al., 2008). ESCRT-III forms thin filaments that bind to membranes, invaginating and pinching them off and this could lead to constriction. Moreover, it has been recently reported that *Mycoplasma genitalium* with a completely deleted *ftsZ* gene has identical growth kinetics compared to the wild-type and most likely divides by using its motile apparatus to pull cells apart (Lluch-Senar, Querol & Pinol, 2010). This is so-called traction-mediated cytofission. Another example of FtsZ-less cell division is a *B. subtilis* L-form, a strain that grows without a cell wall (Leaver, Dominguez-Cuevas, Coxhead, Daniel & Errington, 2009). Propagation of L-forms does not require the normal FtsZ-dependent division machinery as shown by FtsZ depletion. In this case the authors proposed a brand-new mechanism named extrusion and resolution. The cells grow and start forming transient protrusions on the surface. Next, one of the protrusions is resolved by cleavage into small bodies, which are the progeny. The exact mechanism of this process remains unknown. Notably, the thaumarachaeon *Nitrosopumilus maritimus* has both ESCRT-III and FtsZ homologues and it has been discovered that cells divide using the former one (Pelve et al., 2011). However, the thaumarachaeal FtsZ lacks some highly conserved residues needed for GTP binding.

This redundancy in the relatively simple prokaryotic world raises questions of what the different mechanisms are needed for. One could claim that they provide a backup in case one system fails. Another option would be to use them together so that the process is more efficient. It seems that in species such as *Mycoplasma mobile*, one of the systems (traction-mediated cytofission) must have evolved to be so efficient that the other has become unnecessary and eventually been discarded (FtsZ).

Importantly, FtsZ has been found in eukaryotic organelles, both in chloroplasts derived from cyanobacteria (Martin et al., 2002) and in mitochondria derived from α-proteobacteria (Kiefel, Gilson & Beech, 2004). Here two systems (FtsZ and a dynamin-dependent system) operate in conjunction on different faces, so that FtsZ

pulls from the inside and dynamin squeezes from the outside (Erickson, 2000). Moreover, dynamin is dominant over FtsZ in higher eukaryotes.

To conclude, there are three main cell division systems: the actin-myosin, FtsZ and ESCRT-III based mechanisms (Fig. 1c). Each is assigned to well-defined taxonomic clades (Bernander & Ettema, 2010). Whereas in the eukaryotes all cytokinesis mechanisms seem to be variations on an actin-myosin ring, generalization should be avoided when one talks about archaea and bacteria since an unexpected myriad of complementary systems has been discovered. Nevertheless, the FtsZ-based mechanism is widespread and present in most major branches in the phylogenetic tree and therefore was the subject of my PhD work.

The divisome and the Z-ring

A vast majority of proteins participating in bacterial cell division have been identified through a screen to detect thermosensitive defects that cause cells to form filaments, thus they are named 'Fts', after filamentous thermal sensitive (Hirota, Ryter & Jacob, 1968). One of these proteins, FtsZ, turned out to be the homolog of eukaryotic tubulin (Löwe & Amos, 1998). First, FtsZ had been shown by means of immuno-electron microscopy to form ring-like structures that are associated with division in *E. coli* (Bi & Lutkenhaus, 1991). Furthermore it had been realised that FtsZ contains a 7 amino-acid stretch (GGGTGTG) almost identical to a highly conserved sequence within α-, β-, and γ-tubulins of eukaryotic cells, and it was subsequently demonstrated that FtsZ binds and hydrolyses GTP (de Boer, Crossley & Rothfield, 1992). Biochemical assays and electron microscopy of purified FtsZ unveiled polymerising abilities of the protein (Mukherjee & Lutkenhaus, 1994; Bramhill & Thompson, 1994; Erickson, Taylor, Taylor & Bramhill, 1996). Now FtsZ's GTP binding and hydrolysis as well as filament formation are relatively well understood and the nucleotide is efficiently hydrolysed only upon polymerisation (Oliva, Cordell & Löwe, 2004). FtsZ is a conserved ancient protein (Davis, 2002) and this is unsurprising since a mechanism for cell division would have been required at the earliest stage of evolution of a cellular life form. FtsZ consists of the core domain (residues 1-325 in *T. maritima* FtsZ), which is responsible for the GTP binding and polymerisation, and the C-terminal tail (the last 15-20 residues), which is a busy region for protein interaction

since it is known to bind FtsA, ZipA and MinC. The two FtsZ domains are connected by a flexible, unstructured linker (Erickson et al., 2010).

Importantly, FtsZ acts as a scaffold for the highly sequential recruitment of downstream components of the divisome, the cell division apparatus (Adams & Errington, 2009). First, FtsZ finds the middle of the cell through two independent mechanisms in *E. coli*, nucleoid exclusion (Bernhardt & de Boer, 2005) and the oscillating MinCDE system (Raskin & de Boer, 1999). To prevent the formation of the Z-ring over the nucleoid, Noc in *B. subtilis* and SlmA in *E. coli* interact with FtsZ, as has been shown *in vitro* (Bernhardt & de Boer, 2005). Next, the oscillating Min system inhibits the assembly of the Z-ring at the cell poles. This is achieved by a direct interaction of MinC with FtsZ, and it has been demonstrated firstly that the C-terminal domain of MinC ($MinC^C$) interacts with the highly conserved C-terminus of FtsZ, competing for a binding site with FtsA (Shen & Lutkenhaus, 2009), and secondly that the N-terminal domain of MinC ($MinC^N$) inhibits FtsZ polymerisation (Shen & Lutkenhaus, 2010). These two distinct mechanisms ensure that the process is spatially resolved and the divisome is formed only in the middle of the cell between two segregated chromosomes (Fig. 2a). The timing of ring assembly (temporal resolution) is probably dependent on the mechanism of division site placement (Errington, Daniel & Scheffers, 2003). Once formed, the Z-ring is a dynamic structure and undergoes constant remodelling with a turnover in the order of 8 seconds, as demonstrated by fluorescence recovery after photobleaching (FRAP) analyses (Stricker, Maddox, Salmon & Erickson, 2002).

Assembly of the divisome is a linear two-step process (Adams & Errington, 2009): the early-assembling proteins, directly interacting with FtsZ, are first recruited to the midcell. This includes FtsA, SepF and ZapA in *B. subtilis*. Then, after a substantial delay, late division proteins are recruited (FtsK, FtsQ, FtsL, FtsB, FtsW, FtsI etc.). Due to the complexity of the division process, these proteins are cytoplasmic, periplasmic and membrane-embedded (Goehring & Beckwith, 2005). For instance, ZapA is a cytoplasmic protein thought to stimulate FtsZ polymerisation, FtsA is a membrane-associated soluble protein that may be responsible for FtsZ binding to the lipid bilayer, and FtsK belongs to a family of proteins involved in chromosome partitioning. The carboxy-terminal cytoplasmic domain of FtsK is a hexameric DNA

Figure 2. Bacterial cell division.

a) Model for the positioning of the Z-ring by the nucleoid exclusion and Min systems. The only allowed plane of FtsZ polymerisation is in the midcell region (modified from Thanbichler, 2010).
b) Assembly of the divisome in *B. subtilis*. The cell division apparatus consists of cytoplasmic as well as membrane proteins (modified from Adams & Errington, 2009).

Figure 2

a

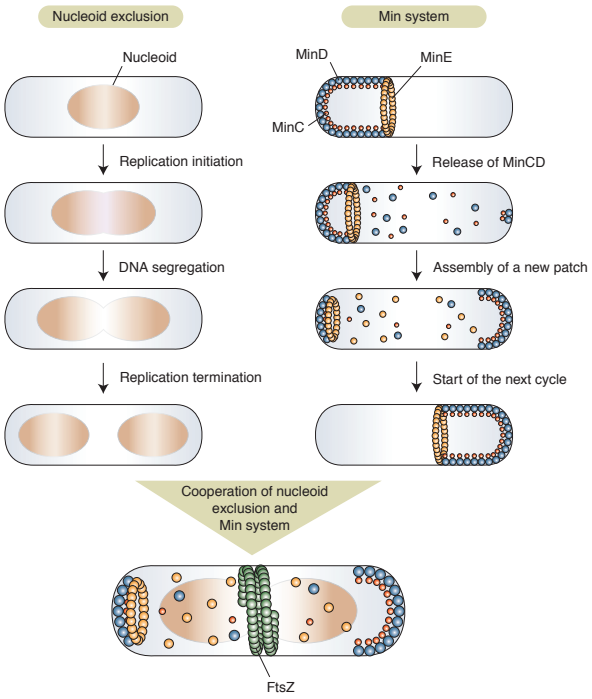
Nucleoid exclusion
Min system
Nucleoid
MinD
MinE
MinC
Replication initiation
Release of MinCD
DNA segregation
Assembly of a new patch
Replication termination
Start of the next cycle
Cooperation of nucleoid exclusion and Min system
FtsZ

b

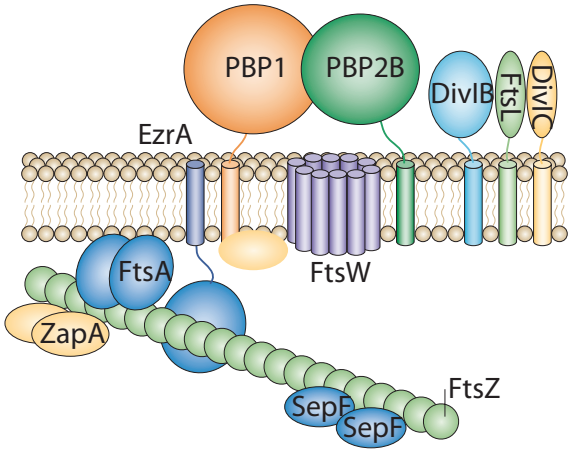
PBP1
PBP2B
DivIB
FtsL
DivIC
EzrA
FtsA
FtsW
ZapA
FtsZ
SepF
SepF

motor (Löwe et al., 2008). The N-terminal FtsK domain is a four-transmembrane segment. Finally, there are also proteins involved in cell wall synthesis. FtsI (known as penicillin-binding protein 3) is essential for cell division, but not for elongation (Bramhill, 1997) and exhibits a transpeptidase activity. FtsW is predicted to contain multiple transmembrane domains (Ikeda, Sato, Wachi, Jung & Ishino, 1989) and has recently been identified as an essential transporter of the lipid-linked peptidoglycan precursors across the cytoplasmic membrane, thus providing substrates for murein synthesis (Mohammadi et al., 2011). It is worth noting that rod-shaped bacteria switch between two kinds of cell wall synthesis. During elongation, new material is inserted along the lateral walls. When cell division takes place, cell wall incorporation is mainly confined to the septum (Goehring & Beckwith, 2005). The recruitment of FtsI and FtsW is dependent on the FtsQLB complex, whose constituents are inner membrane proteins spanning to the periplasmic space and may provide a link between the inner and the outer divisome.

To summarise, the divisome is a complex and complete multiprotein structure capable of DNA segregation (FtsK), membrane constriction (FtsZ, FtsA, other?) and cell wall remodelling (FtsI, FtsW), thus fulfilling all the requirements needed to perform cell division (Fig. 2b).

One of the key divisome subcomplexes is the FtsZ:FtsA complex. The *ftsA* gene is very often found in one operon with *ftsZ* within the *dcw* (division and cell wall; Ayala, Garrido, de Pedro & Vicente, 1994) cluster (Fig. 3a). The two proteins interact at the earliest stage of Z-ring formation and are essential for recruitment of the next proteins of the divisome. Since the Z-ring must be anchored to transmit the constriction force to the membrane, FtsA seems to be a perfect candidate to perform this job as it contains a conserved C-terminal motif, which is predicted to form an amphipathic helix (Löwe & van den Ent, 2001; Fig. 3b). Also, if FtsA is prevented from localising to FtsZ, cell division is severely impaired (Addinall & Lutkenhaus, 1996b). In the absence of FtsA, FtsZ rings are unable to contract (Addinall, Bi, & Lutkenhaus, 1996) and the proper ratio of FtsZ to FtsA is required for cell division to occur (Dai & Lutkenhaus, 1992; Dewar, Begg & Donachie, 1992). Harmful effects of the overproduction of either protein can be diminished by overproduction of the other. These reasons prompted an idea that FtsZ and FtsA may interact directly.

Subsequently, FtsZ and FtsA were shown to co-localise in living *E. coli* cells by means of green fluorescent protein (Ma, Ehrhardt & Margolin, 1996), and yeast two-hybrid analysis detected the interaction (Wang, Huang, Mukherjee, Cao & Lutkenhaus, 1997). Interestingly, FtsZ and FtsA from evolutionarily distant species such as *E. coli* and *B. subtilis* (Wang et al., 1997) or *Rhizobium meliloti* and *Agrobacterium tumefaciens* (Ma et al., 1997) were found to form a complex. Moreover, an *in vivo* genetic screen identified FtsA mutants on the surface of subdomain 2B as impaired for the FtsA-FtsZ interaction and these mutants retained the ability to bind to the membrane (Pichoff & Lutkenhaus, 2007). The interaction has also been characterised from the FtsZ perspective and the last 70 residues were demonstrated to be involved in FtsA binding (Haney et al., 2001). Later this was refined, and shown that a deletion of 12 amino acids from the highly conserved C-terminal tail of *E. coli* FtsZ failed to complement chromosomal *ftsZ* mutants and failed to interact with FtsA (Ma & Margolin, 1999). Moreover, the same FtsZ interaction site is used by another protein, ZipA (Mosyak et al., 2000), which is a bitopic protein and shows some functional overlap with FtsA despite being a very different protein in sequence. The exact functions of these proteins and their relationship with FtsZ have remained enigmatic. However, a single residue alteration in *E. coli* FtsA, the R286W mutation (FtsA*), allows efficient division in the absence of ZipA (Geissler, Elraheb & Margolin, 2003).

The C-terminal amphipathic helix of FtsA is essential for its function *in vivo* and plays a key role in targeting FtsA and with it FtsZ to the membrane (Pichoff & Lutkenhaus, 2005). Furthermore, FtsA's C-terminal motif can substitute for MinD's (another bacterial membrane-associated protein) lipid bilayer targeting sequence, and vice versa: the membrane-targeting sequence of MinD is fully functional when fused to FtsA. This also applies to the first transmembrane domain of MalF (Shiomi & Margolin, 2008). This strongly suggests that the sequence of the membrane-targeting motif is not important as such, indicating that it serves only as a generic membrane anchor. Deletions as short as 5 residues from the C-terminus destroy the biological function of FtsA, thus emphasise the role of the amphipathic helix (Yim et al., 2000). Since FtsA is widely conserved in bacterial species it probably constitutes the primary membrane anchor for the Z-ring (Fig. 3c). Furthermore, the *ftsA* gene of *E. coli* seems

Figure 3. What we have learnt about the FtsA:FtsZ:membrane complex so far.

a) Gene organisation in the *ftsZ* region of the *B. subtilis* chromosome. Arrows indicate gene orientation.
b) Helical wheel diagrams of the C-terminal motif from FtsA of *E. coli* and *B. subtilis* predicted to form an amphipathic helix (modified from Pichoff & Lutkenhaus, 2005).
c) Summarising current knowledge on the FtsZ:FtsA:membrane complex. It is not clear how the two proteins interact and what the exact boundaries of the interacting regions are.
d) A model for the Z-ring emerging from Li et al., 2007.

Figure 3

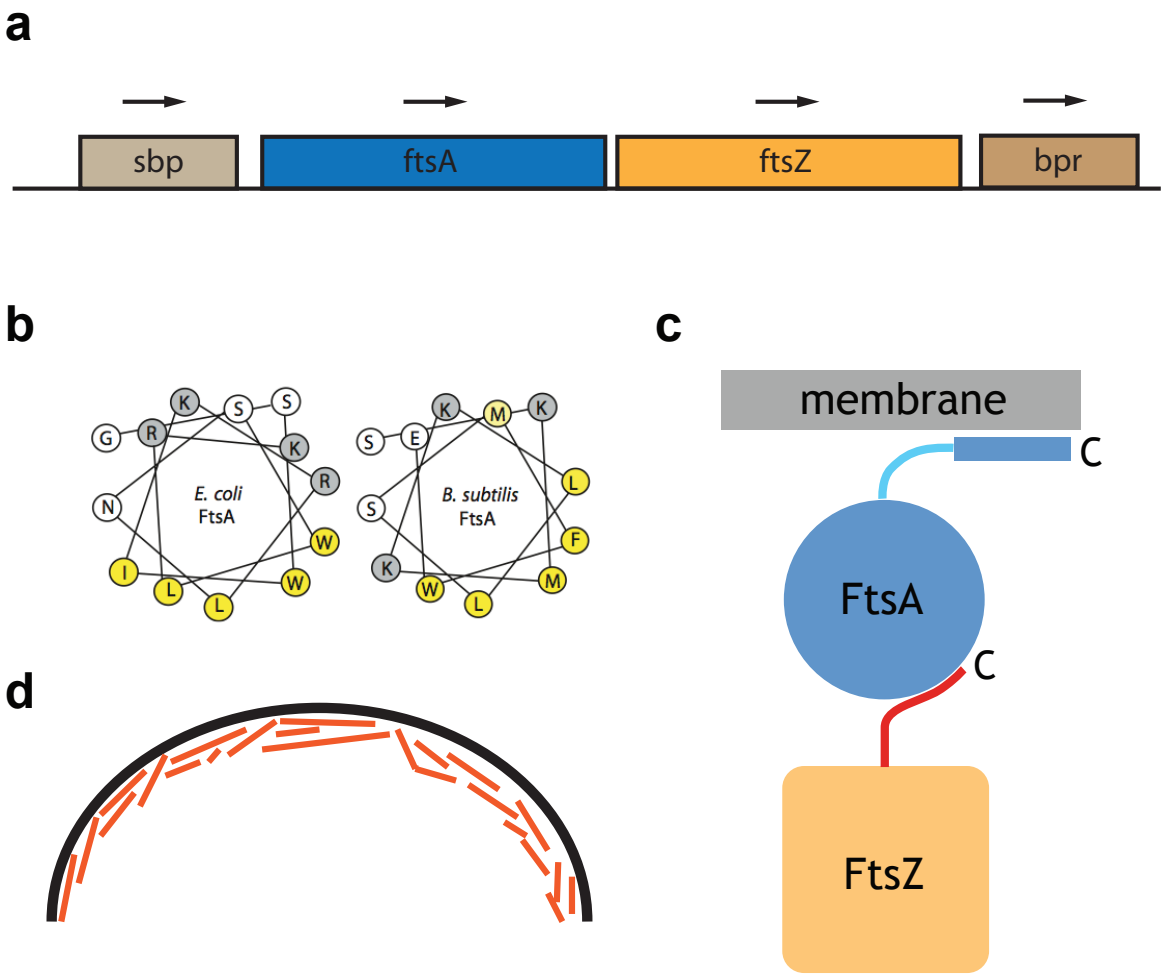
a
sbp
ftsA
ftsZ
bpr
b
E. coli
FtsA
B. subtilis
FtsA
c
membrane
C
FtsA
C
FtsZ
d

to be essential. In contrast, it can be disrupted in *B. subtilis* by insertional inactivation (Beall & Lutkenhaus, 1992; Jensen et al., 2005). In the absence of the FtsA protein cells become filamentous and growth is severely impaired. This indicates that FtsA is required for efficient Z-ring assembly.

The above pieces of evidence triggered the question of whether FtsZ and the tethering of the Z-ring to the membrane can provide the constriction force themselves without any input from the other divisome components. To test this hypothesis a series of *in vitro* experiments have been performed. In one of them the highly conserved FtsZ C-terminus was replaced with an amphipathic helix and this protein was subsequently used in a reconstitution with liposomes (Osawa, Anderson & Erickson, 2008). The authors concluded that FtsZ itself could assemble the Z-ring and be a force generator. Interestingly, when the FtsZ-amphipathic helix was added to the outside of liposomes it produced concave depressions, bending the membrane similarly to the Z-ring inside liposomes, and when another variant of the protein, N-terminal amphipathic helix-FtsZ (N and C termini are approximately 180° apart), was used, it yielded convex bulges instead (Osawa, Anderson & Erickson, 2009). This implies that FtsZ protofilaments are of a fixed direction of curvature. A more natural situation was achieved when purified FtsZ and FtsA from *E. coli* were incorporated inside giant unilamellar vesicles obtained from bacterial inner membranes (Jimenez, Martos, Vicente & Rivas, 2011) and this study may provide us with a novel *in vitro* technique to investigate interactions between the divisome components.

Recent improvements in imaging technology, especially electron cryo-tomography (cryoET) has allowed an advance in our understanding of the structure and function of the cell division apparatus (Li, Trimble, Brun & Jensen, 2007; Fig. 3d). Electron cryo-tomographic reconstruction of dividing *Caulobacter crescentus* cells visualised arc-like filaments underneath the inner membrane at the septum. These were short (~ 100 nm), erratic and overlapping filaments rather than one long and continuous polymer covering the cell circumference. A constriction model was proposed where the force is generated solely by FtsZ's cycles of GTP hydrolysis, polymerisation and depolymerisation while attached to the membrane. There have been several others models for Z-ring constriction described and crucially, all of them require the presence of an anchor to connect FtsZ to the membrane, thus making FtsA an

indispensable component of the machinery (Errington et al., 2003). One of the models utilises motor proteins to slide overlapping FtsZ protofilaments relative to one another (Bramhill, 1997). However, no motor proteins in prokaryotes have been discovered up to date and it seems that FtsZ-driven membrane constriction does not require any (Osawa et al., 2008).

At the moment it is difficult to verify any of the existing models for membrane constriction since:

- it is not clear if FtsZ may be recruited to the membrane merely by FtsA
- it remains elusive how these two proteins interact and whether there are any other components involved in the interaction
- there is no structural information available on the FtsZ:FtsA complex.

Prokaryotic actin-like proteins

Until recently, the lack of the cytoskeleton, which is needed to perform mitosis and cytokinesis in eukaryotes, defined prokaryotes as a separate domain of life (van den Ent, Amos & Löwe, 2001a). Prokaryotes were thought to maintain their shape simply through cell walls and base their metabolism mainly on diffusion. There are three types of cytoskeletal elements in eukaryotic cells: tubulin, actin and intermediate filaments (Graumann, 2007). For instance, actin polymerises into long, two-stranded, right-handed helical filaments with an axial rise of 54 Å (Oda, Iwasa, Aihara, Maeda & Narita, 2009) in order to perform its biological functions such as keeping mechanical properties and shapes of cells, and acting in endocytosis and cytokinesis together with a type II myosin (Pollard, 2009).

The first cytoskeletal elements in prokaryotes were discovered by bacterial genetics methods more than thirty years ago (Hirota, Ryter & Jacob, 1968; Lutkenhaus, Wolf-Watz & Donachie, 1980) but only the discovery that FtsZ has the tubulin signature sequence (GGGTGTG) and the use of fluorescent and electron microscopy revealed their filamentous behaviour (Addinall & Lutkenhaus, 1996a). Now it is widely accepted that prokaryotes possess homologs of tubulin (FtsZ, TubZ), actin (MreB, ParM, FtsA; Fig. 4a) and intermediate filaments (crescentin).

The discovery of bacterial relatives of actin particularly was not straightforward, since using simple sequence alignments did not reveal any homologs. It is not surprising since the closest bacterial proteins show less than 15% identity to eukaryotic actin and are extremely variable among themselves (MreB shows 40-50% sequence identity across prokaryotic species). Then a structure-based sequence alignment (Bork, Sander & Valencia, 1992) elucidated a set of common conserved residues involved in ATP binding (named PHOSPHATE 1, CONNECT 1, PHOSPHATE 2, ADENOSINE and CONNECT 2) and a sequence database search with the pattern returned members of the sugar kinases and chaperone hsp70 subfamilies as well as many prokaryotic proteins such as MreB, FtsA, ParM, all predicted to feature the actin-like fold.

The canonical actin fold is characterised by two domains (1 and 2) and a nucleotide-binding site in the interdomain cleft (Kabsch & Holmes, 1995). Each domain can be further divided into two subdomains (A and B). The two larger subdomains (1A and 2A) are of a shared fold (probably because of evolution from a common ancestral domain) and are connected (Fig. 4a). The smaller subdomains (1B and 2B) vary from one subfamily to another and seem to be inserted in different loops of the 1A and 2A domains, respectively. This fold is shared by hexokinase, hsp70 and actin as revealed by X-ray crystallography.

Bacterial actin homologs play key roles in distinct cellular processes that rely on their filamentous, actin-like nature (Fig. 4b). For example, MreB was found to possess the canonical actin-like fold (van den Ent, Amos & Löwe, 2001b) and to form filaments underneath the inner cell membrane that are required for different aspects of cell morphogenesis. They achieve this by directing the placement of elongation-specific cell wall synthesis machinery in rod-shaped bacteria (Jones, Carballido-Lopez & Errington, 2001). Two recent papers (Garner et al., 2011; Dominguez-Escobar et al., 2011) suggest that MreB assembles into discrete patches that move along tracks perpendicular to the cell axis. Another bacterial actin-like protein, ParM, is a crucial component of the low-copy-number plasmid segregation system ParMRC and seems to form a prokaryotic version of the mitotic spindle (Moller-Jensen, Jensen, Löwe & Gerdes, 2002). Interestingly, ParM has been shown to adopt two different conformations depending on the nucleotide state (van den Ent, Moller-Jensen, Amos, Gerdes & Löwe, 2002a). ParM binds to the centromere-like *parC* DNA sequences on

the plasmid through the dimeric ParR adaptor protein (Moller-Jensen, Ringgaard, Mercogliano, Gerdes & Löwe, 2007). As ParM polymerises, it forms protofilaments that push newly replicated plasmids apart to the cell poles. Compellingly, the chromosome segregation that occurs in eukaryotic mitosis is based on tubulin, and not actin.

The low sequence identity yet high structural similarity between actin, MreB, ParM and FtsA could be explained by the fact that they have evolved from the last common ancestor into structures performing a myriad of distinct tasks (Jones, Carballido-Lopez & Errington, 2007), which still depend on polymerisation. It seems that this level of conservation represents the limit of divergence that allows the performance of designed functions. However, they share one common feature, which is dynamic behaviour described as 'cytomotive' (Löwe & Amos, 2009). This means that the filaments themselves, using energy concealed in the bound nucleotide, can create linear force to push or pull objects by filament growth and shrinkage. Eukaryotic filamentous proteins (actin, tubulin) can additionally provide a track for motor proteins that move along and thus generate force.

Interestingly, an actin-like filament might be produced in many ways, especially among bacterial actin systems (Popp & Robinson, 2011). X-ray diffraction patterns from oriented gels revealed that actin is a right-handed helix with 13 subunits per helix turn (Oda et al., 2009) whereas ParM has a similar symmetry but, remarkably, the helix is left-handed (Galkin, Orlova, Rivera, Mullins & Egelman, 2009). Moreover, MreB is known to form a double, straight filament (Salje, van den Ent, de Boer & Löwe, 2011). What dictates the organisation of actin filaments then? Most likely it is triggered by interacting partners. For example, ParM left-handedness may be important for the ParR adaptor protein binding, whose geometry in turn is governed by the handedness of DNA. In this work I show that there exists yet another way to create an actin-like filament, surprisingly, by a protein of a non-canonical actin architecture.

Figure 4. Actin-like proteins of the cytoskeleton.

a) X-ray crystallography revealed a striking similarity between actin-like proteins from different domains of life.
b) Actin-like proteins act in a variety of cellular processes (modified from Gasper & Löwe, 2011).

Figure 4

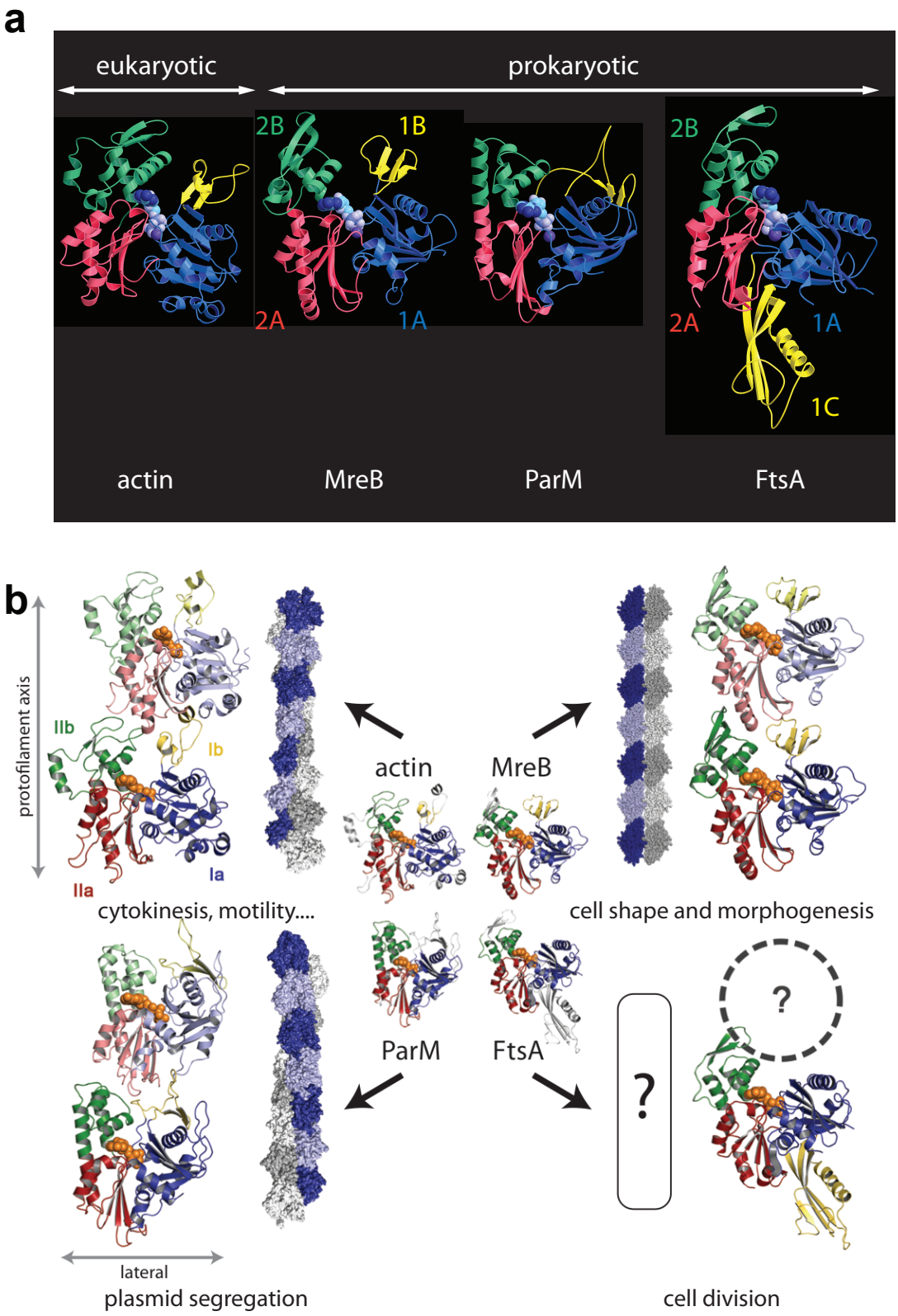
a
eukaryotic
prokaryotic
2B
1B
2A
1A
2B
2A
1A
1C
actin
MreB
ParM
FtsA
b
protofilament axis
IIb
Ib
Ia
IIa
actin
MreB
cytokinesis, motility....
cell shape and morphogenesis
ParM
FtsA
?
?
lateral
plasmid segregation
cell division

FtsA as an actin-like protein

FtsA, according to a structure-based sequence alignment, was predicted to be an actin-like protein (Bork et al., 1992). Sequence comparison revealed that the protein contains all the motifs required for ATP binding. The structure of FtsA was solved a decade ago (van den Ent & Löwe, 2000). This revealed that the protein is indeed a member of the actin/HSP70 family, although its fold was shown to considerably deviate from the canonical actin fold by a subdomain deletion (1B) and addition (1C). Three out of the four subdomains are arranged similarly in FtsA and other actin-like proteins, but the fourth (1C) is located on the opposite side of the subdomain 1A with respect to the 1B subdomain (Fig. 4a). FtsA was found to crystallise with an ATP molecule bound in the active site located in the interdomain cleft between two main domains. Two pieces of evidence currently support the idea that FtsA is a truly actin-like protein capable of forming polymers. It has been demonstrated that wild-type rod-shaped *E. coli* cells expressing the truncated *E. coli* FtsA deprived of the last 28 amino acids acquire a curved phenotype (Gayda, Henk & Leong, 1992). Visualisation of thin sections of these C-shaped cells with transmission electron microscopy revealed aggregates of cylindrical structures near centres of the cells. They extended diagonally across the cytoplasm from membrane to membrane and most likely were responsible for the curved cells (Fig. 5a). However, technical limitations at that time did not allow the accurate measurement of the longitudinal repeat along the cylinders to find out what actually constituted the cylinders. In another case, FtsA from *Streptococcus pneumoniae* has been demonstrated to form helical filaments *in vitro* (Fig. 5b) but no information is available on how that would be possible given that the canonical actin fold is incomplete in FtsA, or on what FtsA protofilaments would look like (Lara et al., 2005). This study also confirmed that purified FtsA preferentially binds nucleotide triphosphates, particularly ATP. However, no ATPase activity was detected. Work with *B. subtilis* FtsA, however, detected some trace hydrolytic activity but it is not clear if this is due to the protein itself or represents some contamination (Feucht, Lucet, Yudkin & Errington, 2001). Fractionation experiments with *E. coli* cells demonstrated that FtsA in the cytoplasm is phosphorylated and capable of binding ATP, whereas the membrane-associated form is unphosphorylated and does not bind ATP (Sanchez et al., 1994). Unfortunately, it has not been determined what the putative phosphorylation site would be or how the process would be performed.

Purified *B. subtilis* FtsA behaves as a dimer (Feucht et al., 2001). Also, *E. coli* FtsA self-interaction has been demonstrated in yeast and bacterial two-hybrid systems (Yim et al., 2000; Karimova, Dautin & Ladant, 2005), and a model for an FtsA dimer was proposed (Carettoni et al., 2003). Based on a phage-display library screen and bioinformatics analysis the authors suggested that the 1C subdomain of one monomer is inserted into the cleft between subdomains 1A, 2A and 2B of the other molecule. Also, strands S12-S13 are on the dimerization interface. This has been investigated further (Rico, Garcia-Ovalle, Mingorance & Vicente, 2004) and mutational analysis showed that deletions of subdomain 1C or the S12 and S13 β-strands result in partially functional proteins that cannot perform cell division. The Carettoni model stays in contradiction to the work presented in this dissertation.

Figure 5. Previous reports on FtsA's tendency to form aggregates.

a) Transmission electron microscopy of thin sections of curved cells. Aggregates extend from membrane to membrane (modified from Gayda et al., 1992).
b) Electron microscopy analysis of *Streptococcus pneumoniae* FtsA in the presence of ATP. Corkscrew-like structures are visible (modified from Lara et al., 2005).

Figure 5

a

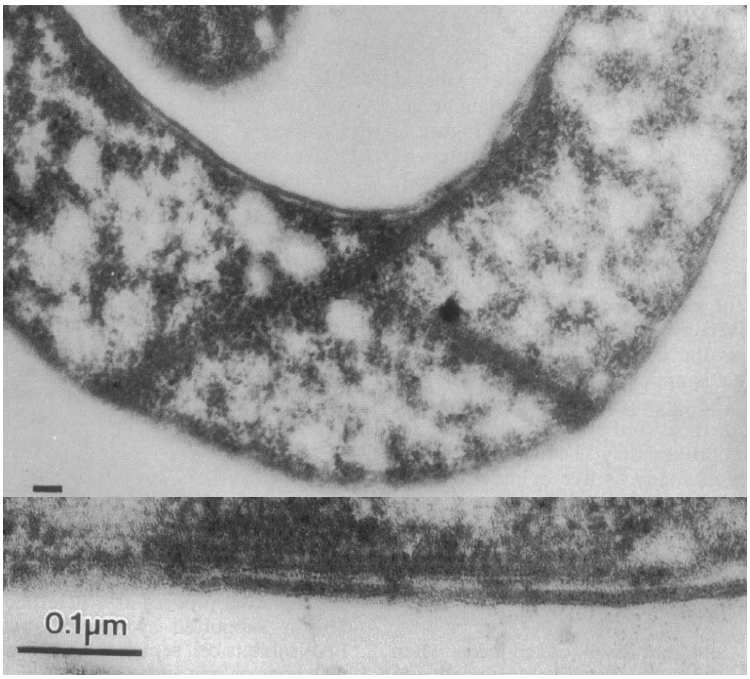

b

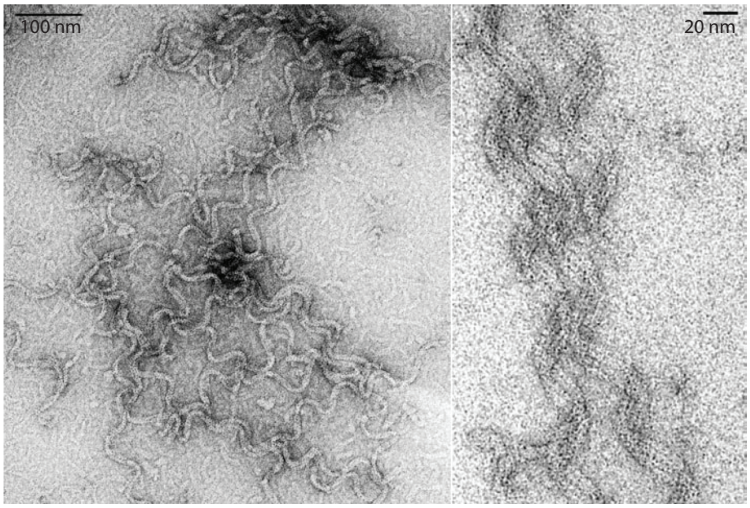

Aims and scope of the work

There are several unaddressed issues emerging from this brief literature review that concern incipient stages of bacterial cell division. Firstly, understanding how the FtsZ:FtsA complex is formed seems to be crucial in order to find out how this earliest step of bacterial cell division is regulated. Secondly, since FtsA belongs to the actin/HSP70 family of proteins, with many members being able to form filaments, is the long-standing question of whether FtsA is able to polymerise. Solving these inquiries would allow us to speculate on the cell membrane constriction mechanism and eventually arrive at a better model.

Two major lines of research have been applied in order to tackle these problems:

- biochemical and structural studies of the FtsZ:FtsA complex
- investigating the polymerising abilities of the FtsA protein

First I describe *in vitro* analysis of the FtsZ:FtsA complex using purified *Thermotoga maritima* proteins, including a high-resolution crystal structure of the interaction. This leads me to work on FtsA polymers, which in turn are characterised both *in vitro* and *in vivo* by X-ray crystallography, lipid monolayer electron microscopy, electron cryo-tomography, fluorescence microscopy and genetic complementation analysis in *Bacillus subtilis*.

Methods

Strains and plasmids

All strains and plasmids used in this work are listed in Appendix A.

Media and growth conditions

Cells were grown in 2xTY medium supplemented with antibiotics and inducers at 37°C unless otherwise stated. When necessary, cells were maintained at 4°C for short periods of time on TYE plates supplemented with the required antibiotics. Long-term storage of strains was in glycerol stocks at -80°C. Details of growth media are given in Appendix B.

Preparation of glycerol stocks

0.7 ml of fresh culture grown to OD_{600}=2-3 was mixed with 0.3 ml 50% glycerol and flash-frozen in liquid nitrogen in a freezer vial.

Preparation of electrocompetent cells

Cells were grown to OD_{600}=0.5–0.7, cooled for 20 min and transferred to pre-chilled centrifuge bottles and centrifuged at 4000 *x g* for 20 min at 4°C. The supernatant was discarded and cells were washed 3 times in ice-cold double-distilled water. Again, the supernatant was discarded and cells were re-suspended in 10% ice-cold glycerol and spun one more time. The pellet was re-suspended in an equal volume of ice-cold 10% glycerol, distributed into 50 µl aliquots in Eppendorf tubes and frozen in liquid nitrogen. Cells were stored at -80°C.

Transformation of *E. coli*

Purified plasmids were transformed into electrocompetent cells using electroporation. 5 – 10 µl (ligation) or 1 – 2 µl (purified plasmid) was mixed with 50 – 100 µl of competent cells and 200 µl of double-distilled water in a pre-chilled 2 mm electroporation cuvette, on ice. Settings for electroporation were as follows: 2.5 kV, 25 µF capacitance, 100 Ω resistance. Cells were recovered by the addition of 250 µl 2xTY and incubated at 37°C for 30 min, then spread onto TYE plates supplemented with appropriate antibiotic and grown overnight at 37°C.

Transformation of *B. subtilis*

Linearised plasmids were transformed into *B. subtillis* cells due to the ability of *B. subtilis* to develop natural competency according to Spititzen (Anagnostopoulos, 1961). 10 ml MD medium + 50 µl 20% casamino acids was inoculated with a freshly streaked strain and grown at 37°C until OD_{600} reached 1 – 1.5. Then, an equal volume (10 ml) of warm MD medium lacking casamino acids was added. After 1 hour at 37°C 800 µl of competent cells were transferred to a pre-warmed 15 ml plastic tube and DNA to final concentration of 1 µg/ml was added. Cells were agitated at 37°C for for 25 min and then 25 µl of 20% casamino acids was added. After incubation for several hours at 37°C cells were plated on selective antibiotic TYE plates and kept at 37°C overnight.

SDS-PAGE

Protein samples were separated according to their relative molecular weight by SDS-polyacrylamide gel electrophoresis according to the Laemmli method (Laemmli, 1970). Samples were mixed with protein loading buffer and loaded onto an SDS-PAGE gel (12.5% or gradient 10-20%, BioRad). Gels were run at 300 V for 30 min in 1x SDS-PAGE buffer, and proteins were visualised by staining with PAGE-blue 83 folLöwed by washing in destaining buffer.

Quantitative protein analysis

The concentration of purified proteins was determined using the BCA Protein Assay Kit according to the protocol.

Mass spectrometry

Protein masses were confirmed by electrospray mass spectrometry using an LCT electrospray mass spectrometer (Micromass). The molecular mass was calibrated using 2 µg/ml bovine myoglobin and all samples were prepared in 50 % (v/v) methanol, 1 % (v/v) formic acid and infused at 20 µl/min. Output m/z data were analysed with MassLynx's maximum likelihood function to produce a single harmonic mass series.

Cloning

The polymerase chain reaction (PCR) was employed to amplify genes of interest. A typical reaction was:

- Plasmid template 100 ng
- KOD 10x buffer 1x dilution
- dNTP mix 0.2 mM each
- forward/reverse primer 0.5 nmol easch
- KOD polymerase 5U

  Total volume 50 – 100 µl with H_2O

And the standard profile was

- Initial denaturation 94°C 2 sec
- Denaturation 94°C 15 sec
- Annealing 53-55°C 20 sec
- Elongation 68°C 1min/kb

steps denaturation, annealing and elongation repeated 25-30 times.

- Final elongation 68°C 10 min

PCR products were separated by agarose gel electrophoresis and purified using a Qiagen gel extraction kit. PCR products and vectors were digested with restriction enzymes (New England Biolabs) in buffers recommended by the supplier at 37°C for 3-4 hours. All reactions were stopped by purification of the DNA using a Qiagen gel extraction kit.

PCR products and linearised plasmids were mixed with 400 units of T4 DNA ligase (New England Biolabs) in the ligation buffer. Ligation was carried out at 20°C overnight in a total volume of 10 µl.

Site-directed mutagenesis

Site-directed mutagenesis was performed according to he QuickChange Site-Directed Mutagenesis protocol (Stratagene) using Pfu DNA polymerase.

Agarose gel electrophoresis

PCR products or vectors were separated according to molecular weight by electrophoresis in 1-2% agarose gels made in TBE buffer containing 0.4 μg/ml ethidium bromide. Gels were run at 100 V in TBE buffer for 30 min. DNA samples were mixed with DNA loading buffer and the molecular weight was judged by comparison with standard DNA ladders.

DNA sequencing

DNA sequencing was done commercially by GATC Biotech using either standard stock sequencing primers or gene-specific sequencing primers. Sequences were analysed using ApE plasmid editor.

Protein purification

Thermotoga maritima FtsA (from plasmid pSZ8) and FtsZ (pSZ7) proteins as well as the ParM-FtsZ (pSZ19) hybrid protein for *in vitro* assays were purified using the IMPACT system (NEB). The proteins were produced at 37°C in C41(DE3) cells for 4 hours. Cells were lysed in buffer A (50 mM Tris, 10 mM EDTA, 2 mM 1,10-phenantroline, 1 mM PMSF, pH 8.5) by passing through a Constant Systems cell disruptor at 25 kpsi. The soluble fraction was loaded on a chitin column (NEB), which was then thoroughly washed with buffer B (A + 50 mM NaCl) and finally with 2 column volumes of buffer C (B + 50 mM DTT) and left overnight at 4°C to cleave off the intein tag. The untagged proteins were eluted with buffer B and pooled fractions were passed over an ion-exchange Q column (HiTrap, GE Healthcare). The column was washed with buffer D (20 mM Tris, 10 mM EDTA, 2 mM 1,10-phenantroline, 1 mM PMSF, pH 7.5) and the proteins were eluted by applying a gradient of buffer E (D + 1 M NaCl). Peak fractions were pooled, concentrated and subjected to size-exclusion chromatography on Sephacryl S200 (GE Healthcare) in buffer F (50 mM Tris, 1 mM NaN_3, 1 mM EDTA, pH 7.5). Peak fractions were concentrated to 10 mg/ml and stored at -80°C. This protocol yielded full-length TmFtsA, TmFtsZ and ParM-Z. For the proteins lacking the C-terminal amino acids

the same protocol was performed but 1,10-phenantroline and PMSF were omitted, which resulted in efficient and specific cleavage of the last 8 amino acids by an unknown *E. coli* protease. The protein's identity and correct molecular masses were confirmed by N-terminal sequencing and electrospray mass spectroscopy displaying: 38307 Da for TmFtsZ, 37404 Da for TmFtsZΔ8, 47015 Da for TmFtsA, 45968 Da for TmFtsAΔ8, 42011 Da for ParM-Z and 41109 Da form ParM-ZΔ8.

Co-pelleting assay

Purified proteins were mixed at a final concentration of 15 μM each. The samples were pre-spun at 57 krpm in a Beckman TLA100 rotor for 30 minutes, supernatants transferred to new tubes and GTP (in case of FtsZ) or ATP (in case of ParM-Z hybrid) to a final concentration of 2.5 mM was added. Next, the tubes were centrifuged at 57 krpm at 20°C for 30 minutes. The supernatants were removed for analysis and the pellets washed with buffer containing the same components as the reaction buffer aside from proteins. Pellets were solubilized with SDS gel loading buffer (same volume as for the supernatants) and samples were analysed by SDS PAGE.

Co-sedimentation assay

Vesicles were prepared using *E. coli* total lipid extract (Avanti Polar Lipids) in buffer F by sonication and extrusion, using a pore size of 1 μm. Vesicles were mixed with pre-spun proteins at a final concentration of 15 μM and centrifuged at 40k rpm at 20°C for 15 minutes in a Beckman TLA100 rotor. The supernatants were removed for analysis, the pellets washed with buffer F and solubilized with SDS gel loading buffer (same volume as for the supernatants) and samples were analysed by SDS PAGE.

Crystallisation and structure determination

Full-length *Thermotoga maritima* FtsA was co-crystallised with either the C-terminal TmFtsZ peptide (336 H_2N-EGDIPAIYRYGLEGLL-COOH 351) or the peptide and ATPγS. The protein was at 10 mg/ml, the peptide at 10x molar excess and the nucleotide at 2 mM. FtsA and the peptide yielded crystals in the following conditions: 0.1 M BisTris pH 5.5, 12% (w/v) PEG 10k, 0.15 M ammonium acetate. Crystals were moved to the same conditions supplemented with 18% (v/v) PEG 200 and flash frozen in liquid nitrogen. Crystals of FtsA in complex with ATPγS grew from 0.1 M Tris pH 6.7 and 42% ethanol. Crystals were transferred into the same conditions

supplemented with 25% (v/v) PEG 200 before flash freezing. Data were collected at 100 K at ESRF in Grenoble, France (beamlines ID29 and ID23.1). Both crystal forms diffracted to 1.8 Å. The data were processed with MOSFLM and SCALA (1994). Phases were calculated by molecular replacement with TmFtsA PDB entry 1E4F as a model using PHASER (McCoy et al., 2007). The structures were refined with REFMAC (Murshudov, Vagin & Dodson, 1997) or PHENIX (Adams et al., 2010). 91.2% residues for FtsA+peptide+ATP and 91.4% residues for FtsA+ATPγS were in the most favored regions of the Ramachandran plot as determined by PROCHECK. Crystallographic data are summarised in Table 1. Structures were deposited in the Protein Data Bank (PDB) with codes 4A2A and 4A2B.

Isothermal titration calorimetry (ITC)

The experiment was performed at 35°C on an ITC_{200} instrument. The sample cell was filled with 55 μM TmFtsA in buffer F and titrated with 500 μM FtsZ peptide in buffer F while stirring at 1000 rpm. 20 aliquots of the peptide (2 μl) were injected at 120 s intervals. Data analysis was done using the Origin-ITC analysis package in 'one set of sites' mode. The experiment was repeated using 70 μM TmFtsA and 730 μM FtsZ peptide.

Solution nuclear magnetic resonance (NMR)

To assign the backbone resonances of the 47 kDa FtsA (pSZ1) protein from *Thermotoga maritima,* I over-expressed $^{15}N^{13}C^{2}H$ triple-labelled FtsA protein growing bacteria on MOPS minimal media using $^{15}NH_4Cl$ as the sole nitrogen source, $^{13}C^{2}H$ glucose as the sole carbon source and $^{2}H_2O$ as the solvent. The protein was purified using standard nickel-NTA chromatography followed by size-exclusion chromatography on Sephacryl S200 in buffer F. 3D TROSY experiments (HNCO, HN(CA)CO, HNCA, HN(CO)CA, HN(CO)CACB and HNCACB) were recorded at 50°C on a Bruker Avance II+ 700 MHz spectrometer at a sample concentration of 85 μM in buffer F. All data were processed in Topspin 2.1 (Bruker, Karlsruhe), analysed in SPARKY (Goddard & Kneller) and backbone connectivities were obtained with MARS (Jung & Zweckstetter, 2004), MAPPER (Guntert, Salzmann, Braun & Wuthrich, 2000) or in-house scripts. To confirm and extend obtained assignments, ^{15}N selectively labelled (^{15}N Leu and ^{15}N Ile) FtsA samples yielded amide resonances of Leu (Ile) residues, respectively. Weighted chemical shift perturbation (csp) maps

were based on TROSY HSQC spectra acquired in the absence or presence of the FtsZ C-terminal peptide (2.5 molar excess). Weighted csps larger than 0.04 ppm or disappearing resonances were assumed to be involved in peptide binding and mapped onto the crystal structure

Monolayer assay

2D lipid monolayers were prepared from *E. coli* total lipid extract (Avanti Polar Lipids). Teflon block wells were filled with 50 µl of buffer F, next, a drop of lipid solution in chloroform was applied on top and incubated for an hour to let the chloroform evaporate, leaving a monolayer of lipid on the surface of the buffer. EM carbon-coated grids (carbon side down) were placed on the top of each well and the protein applied into the side injection well, underneath the surface. After one hour the grids were stained with 2% uranyl acetate and visualised using a Philips EM208 electron microscope operating at 80 kV. Images were processed and Fourier transforms calculated using ImageJ (Abramoff, Magalhaes & Ram, 2004).

Electron cryo-tomography

C41(DE3) cells containing the plasmid for FtsA over-expression (pSZ6, pSZ25, pSZ41, pSZ47 or pMZ114) were grown in M9 minimal medium supplemented with 0.2% glycerol at 30˚C. FtsA over-expression was induced by adding 0.2% agarose to the cultures at an OD_{600} of 0.2. After 3 hours, the cells were collected, washed in PBS once, mixed with 10 nm protein-A coated gold beads (Sigma-Aldrich), and plunge-frozen on Quantifoil R3.5/1 holey carbon grids using an FEI Vitrobot (FEI Company, USA). Cells were imaged using an FEI Polara electron microscope operating at 300 kV, equipped with a Gatan imaging filter (GIF) set at the zero-loss peak with a slit-width of 20 eV. A Gatan Ultrascan 4000 CCD camera binned to 2k x 2k was used for imaging with SerialEM software (Mastronarde, 2005). Cells were imaged at a magnification of 41 k, corresponding to a pixel size of 5.8 Å at the specimen. The specimen was tilted from approximately -50˚ to 50˚ with a 1˚ increment during tilt series acquisition, and the defocus was set at 10 µm. The total dose for each tilt series was between 150 to 200 e/Å^2. Tomographic reconstruction was calculated using the IMOD tomography reconstruction package (Kremer, Mastronarde & McIntosh, 1996). Images were processed and Fourier transforms calculated using ImageJ (Abramoff, Magalhaes & Ram, 2004).

Confocal microscopy

E. coli C41(DE3) cells were transformed with vectors encoding N-terminal mCherry fusions to the *E. coli* (pSZ49) or *B. subtilis* FtsA (pSZ50a-e) proteins, deprived of the C-terminal amphipathic helices and expression was induced with 1 mM IPTG at OD_{600} 0.4 for 3 hours at 37°C. Cells were taken from the growth media, washed with PBS, stained with FM1-43 stain (Invitrogen) and visualised using a Zeiss LSM 510 confocal laser scanning microscope with the Argon (488 nm) and HeNe (543 nm) lasers and emission filters 505-530 and 560-750 nm.

Strain construction and *in vivo* complementation experiment

To obtain genetically modified *B. subtilis* strains I first constructed integration vectors (pSZ61a-f) consisting of a spectinomycin resistance cassette and an FtsA point mutant (K145A, M147E, I278K, Q87Stop, S46F) in between the *aprE* flanking sequences (using pAPNC213; Morimoto et al., 2002). These constructs were used to transform the *B. subtilis* S62 strain (BGSC no.: 1S62, possessing the *spoIIN279(ts) ftsA* mutation (Beall & Lutkenhaus, 1992; Karmazyn-Campelli, Fluss, Leighton & Stragier, 1992). Transformants were selected on LB plates containing spectinomycin (100 μg/ml) and the correct location and orientation of the insert was checked by PCR and sequencing. The strains were grown at 42°C (to inactivate the endogenous thermo-sensitive FtsA protein) in LB medium in the presence of 1 mM IPTG (to induce the synthesis of the FtsA mutants). At OD_{600} 0.4-0.5, cells were harvested, washed with PBS and visualized using a Zeiss LSM5 microscope. Then average cell lengths and standard deviations were calculated for each FtsA variant. Fractions of successful cell divisions were obtained as a quotient of the number of observed cells for each variant and the number of possible cells. The number of possible cells was calculated (assuming that the length per nucleoid is constant and the wild-type FtsA cells undergo correct cell divisions) by dividing the sum of all cell lengths for each variant by the average wild-type FtsA cell length.

Results

The last 8-16 residues of *T. maritima* FtsZ are necessary and sufficient to interact with *T. maritima* FtsA *in vitro*

In order to investigate the interaction between the cell division proteins FtsZ and FtsA, I reconstituted the system *in vitro* using purified *Thermotoga maritima* FtsA (TmFtsA) and FtsZ (TmFtsZ) proteins as well as liposomes made from *E. coli* total lipid extract. TmFtsA and TmFtsZ were purified as either full-length (TmFtsa 1-419, TmFtsZ 1-351) or C-terminally truncated proteins (TmFtsAΔ8 1-411, TmFtsZΔ8 1-343, Fig. 6a). The C-terminal tail of FtsZ is known to interact with FtsA (Ma & Margolin, 1999), whereas the C-terminal tail of FtsA is thought to directly interact with the membrane via an amphipathic helix (Pichoff & Lutkenhaus, 2005). No extra residues were introduced at either end and great care was taken not to lose the tails through proteolysis during purification, as I found to happen easily when monitored by high-resolution mass spectrometry. Initial purifications involved using either untagged or MBP-tagged proteins, however, in both cases for both FtsA and FtsZ proteolysis could be observed. Interestingly, FtsZ and FtsA were missing the last eight residues, which seem to be vital for the proteins' function. Thus final purifications were done utilising C-terminally intein-tagged proteins so that only full-length, uncleaved molecules are pulled down. The proteins were then tested in pelleting assays in the presence of GTP (Fig. 6b). In the presence of GTP, TmFtsZ forms polymers that sediment easily and if these polymers interact with TmFtsA, both proteins will be found in the pellet. This assay revealed that the last 8 amino acids of TmFtsZ are necessary for the interaction with TmFtsA since TmFtsZΔ8 failed to recruit TmFtsA to the pellet fraction. To discover whether or not the highly conserved C-terminal TmFtsZ fragment is sufficient for this interaction, I constructed a hybrid protein consisting of the actin-like protein ParM followed by an artificial linker and the last 16 residues of TmFtsZ. ParM is a bacterial actin-like protein involved in low copy number plasmids segregation and polymerises in an ATP-dependent manner (van den Ent, Moller-Jensen, Amos, Gerdes & Löwe, 2002b). Unmodified ParM does not interact with FtsA alone. A pelleting assay in the presence of ATP (Fig. 6c) demonstrated that the hybrid protein ParM-Z efficiently interacted with TmFtsA when

Figure 6. *In vitro* reconstitution of the FtsZ:FtsA:membrane complex using *Thermotoga maritima* proteins.

a) Schematic representation of *Thermotoga maritima* proteins used. Dotted violet squares represent enlarged views of the C-terminal regions, which are crucial for the experimental design.
b) FtsA-FtsZ co-pelleting assay. S: supernatant, P: pellet. The C-terminal 8 residues of FtsZ are necessary to interact with FtsA.
c) The C-terminal 16 residues of FtsZ are sufficient to interact with FtsA as shown in a ParM-Z-FtsA co-pelleting assay. A hybrid protein consisting of R1 ParM and the last 16 residues of FtsZ binds to FtsA.
d) Full-length FtsA binds to the membrane *via* its C-terminal amphipathic helix and tethers FtsZ to the membrane as shown by a liposome co-sedimentation assay. FtsZ does not have an affinity to lipids itself. Only pellets are shown.

Figure 6

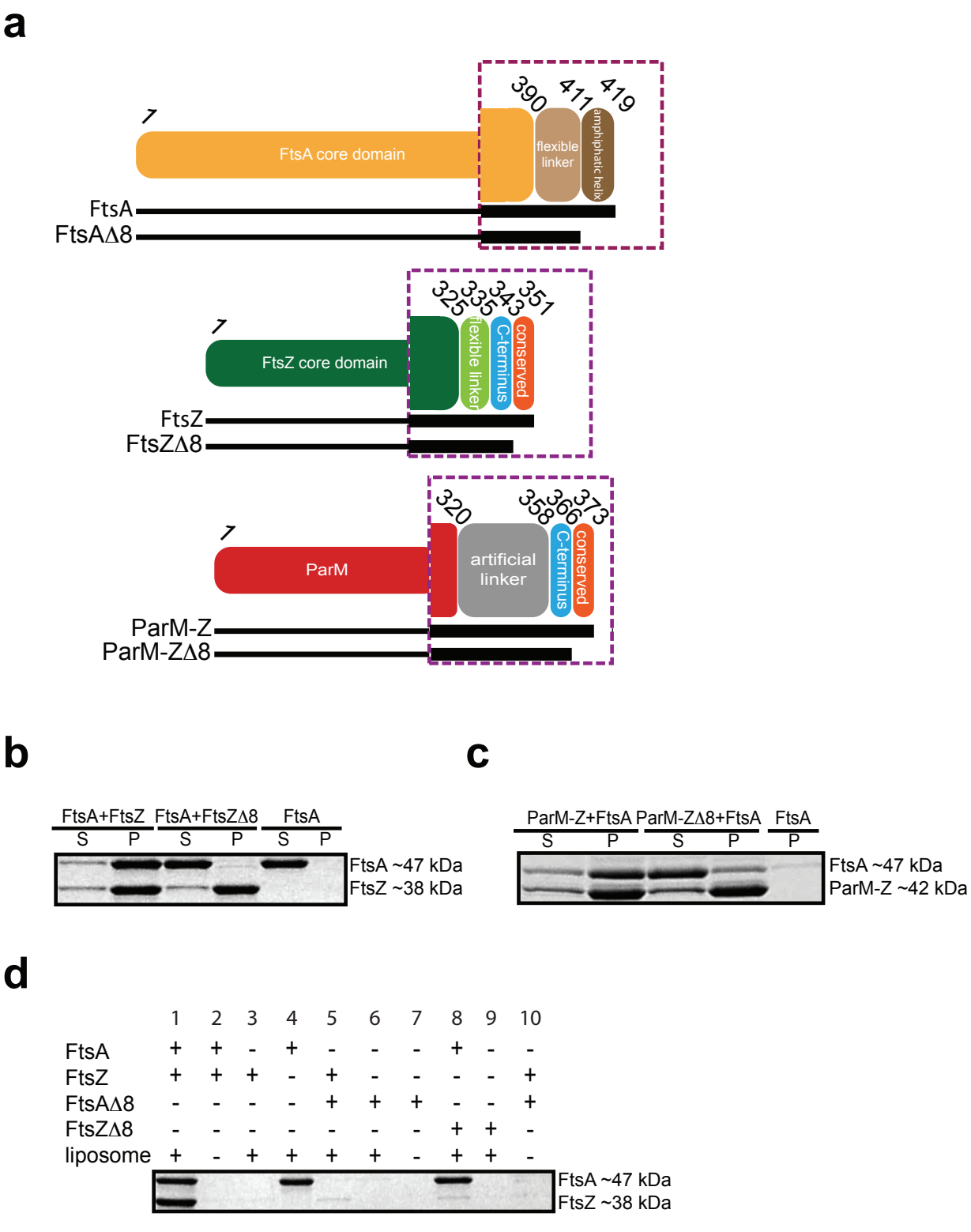
a
1
390
411
419
FtsA core domain
flexible linker
amphiphatic helix
FtsA
FtsAΔ8
1
325
335
343
351
FtsZ core domain
flexible linker
C-terminus
conserved
FtsZ
FtsZΔ8
1
320
358
366
373
ParM
artificial linker
C-terminus
conserved
ParM-Z
ParM-ZΔ8
b
FtsA+FtsZ
FtsA+FtsZΔ8
FtsA
S
P
S
P
S
P
FtsA ~47 kDa
FtsZ ~38 kDa
c
ParM-Z+FtsA
ParM-ZΔ8+FtsA
FtsA
S
P
S
P
P
FtsA ~47 kDa
ParM-Z ~42 kDa
d
1 2 3 4 5 6 7 8 9 10
FtsA + + - + - - - + - -
FtsZ + + + - + - - - - +
FtsAΔ8 - - - - + + + - - +
FtsZΔ8 - - - - - - - + + -
liposome + - + + + + - + + -
FtsA ~47 kDa
FtsZ ~38 kDa

polymerised, however, when the last 8 residues of this hybrid protein are removed (ParM-ZΔ8), the interaction is lost. I conclude that the last 8-16 residues of TmFtsZ are both necessary and sufficient for interaction with TmFtsA.

Which residues are then required for FtsA to tether itself and FtsZ to the membrane? To address this question I reconstituted the FtsZ:FtsA:membrane complex by performing a co-sedimentation assay in the presence of liposomes and in the absence of any nucleotides (Fig. 6d). This showed that TmFtsA recruits TmFtsZ to the membrane (lane 1) and TmFtsZ does not have an affinity for the lipid bilayer itself (lane 3). Also, this assay confirms that both truncated TmFtsA and TmFtsZ are not functional: TmFtsZΔ8 is not able to interact with TmFtsA (lane 8) whereas TmFtsAΔ8 does not bind to liposomes (lane 6), emphasising the role of the C-terminal amphipathic helix, as had previously been deduced for the *E. coli* proteins *in vivo* (Pichoff & Lutkenhaus, 2005).

Crystal structure of the FtsA binding motif of TmFtsZ bound to TmFtsA at 1.8 Å resolution

Having reconstituted the FtsZ:FtsA:membrane system *in vitro* I wanted to get structural insight into the complex formation and determine a crystal structure of TmFtsA bound to TmFtsZ. Crystallisation trials using the full-length proteins failed, probably due to the flexible linker connecting FtsZ's core and C-terminal subdomains. Since I revealed that residues 335-351 of TmFtsZ are necessary and sufficient and mimic the interaction of the full-length protein with TmFtsA I decided to co-crystallise TmFtsA with the peptide corresponding to the last 16 amino acids of TmFtsZ. The complex crystallised in space group $P2_1$ with two TmFtsA molecules per asymmetric unit, each with the TmFtsZ peptide bound on the surface of subdomain 2B of TmFtsA (Table 1, Fig. 7a left). The FtsZ peptide is far away from the nucleotide-binding site of FtsA (Fig. 7a right), which contains an endogenous ATP molecule at 0.65 occupancy. The peptide is in a predominantly helical conformation (Fig. 7c), but is not just a single, straight helix. I identified three salt bridges between the peptide and residues belonging to the H8 helix of the 2B domain, TmFtsA(Arg301) to TmFtsZ(Asp338), TmFtsA(Glu304) to TmFtsZ(Arg344) and one involving TmFtsA(Lys293) and the carboxyl group of the very last Leu351 of the

Figure 7. The crystal structure shows that FtsZ binds to FtsA's surface between helices H6 and H8 within subdomain 2B and does not directly interact with the nucleotide-binding site containing ATP.

a) Crystallographic asymmetric unit containing two FtsA molecules, each with the 16-residue FtsZ peptide bound (left). FtsA has been colour-coded according to the subdomain architecture of the conserved actin family of proteins. The peptide (purple) is bound on the surface of subdomain 2B (green). ATP is shown as spheres.
b) View of the FtsA/FtsZ interaction site. For the peptide, the final 2FoFc electron density map at 1.8 Å is shown.
c) A stereo representation of the FtsA-FtsZ interacting site. The peptide is depicted in purple, 2B subdomain in green. Three salt bridges have been identified: FtsA(Arg301) to FtsZ(Asp338), FtsA(Glu304) to FtsZ(Arg344), FtsA(Lys293) to the C-terminal carboxyl group of FtsZ(Leu351).
d) ITC analysis. Shown is the experiment where 500 μM FtsZ peptide was titrated into 55 μM FtsA.

Figure 7

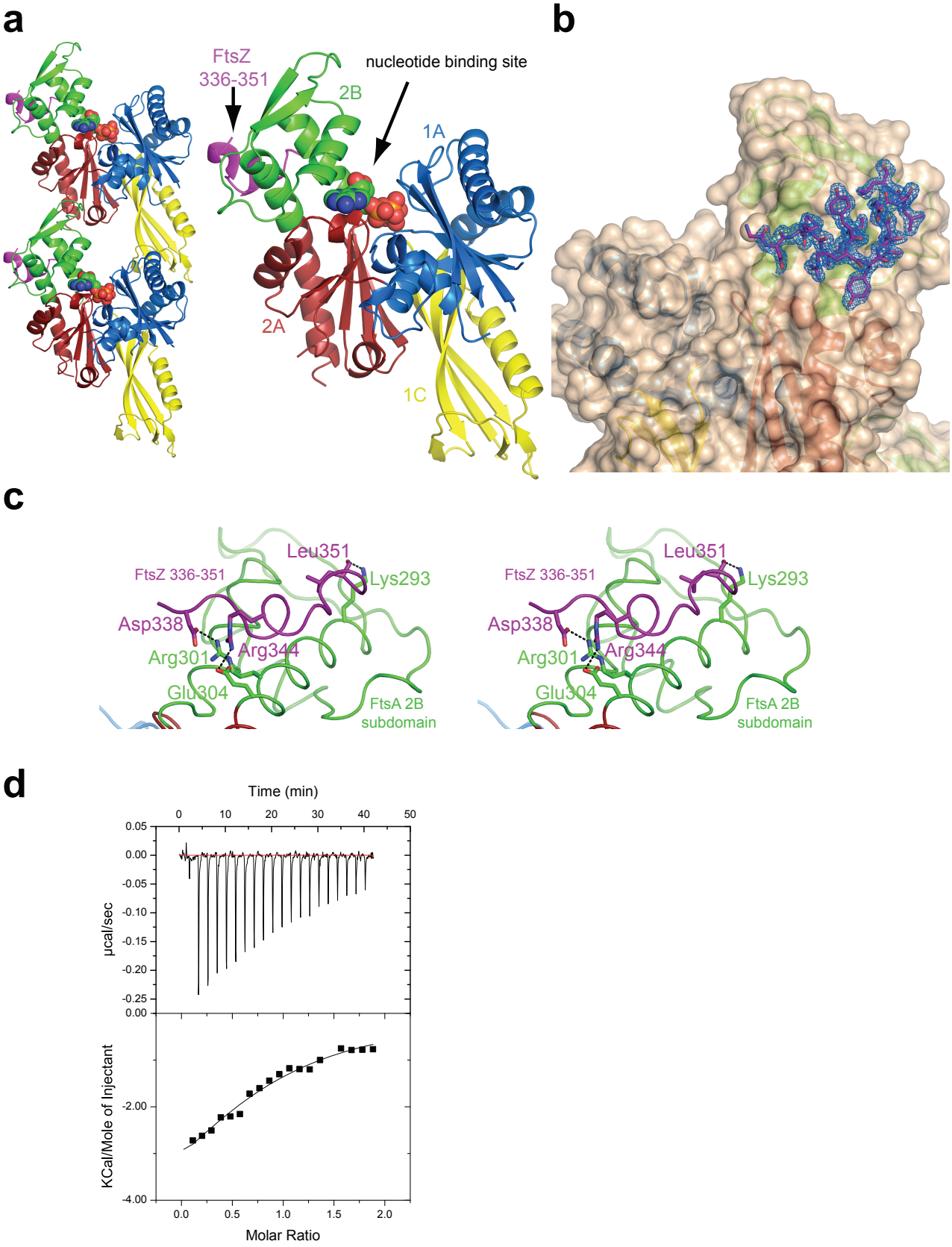
a
FtsZ
336-351
nucleotide binding site
2B
1A
2A
1C
b
c
Leu351
FtsZ 336-351
Lys293
Asp338
Arg301
Arg344
Glu304
FtsA 2B
subdomain
Leu351
FtsZ 336-351
Lys293
Asp338
Arg301
Arg344
Glu304
FtsA 2B
subdomain
d
Time (min)
0
10
20
30
40
50
0.05
0.00
-0.05
-0.10
-0.15
-0.20
-0.25
µcal/sec
0.00
-2.00
-4.00
KCal/Mole of Injectant
0.0
0.5
1.0
1.5
2.0
Molar Ratio

Figure 8

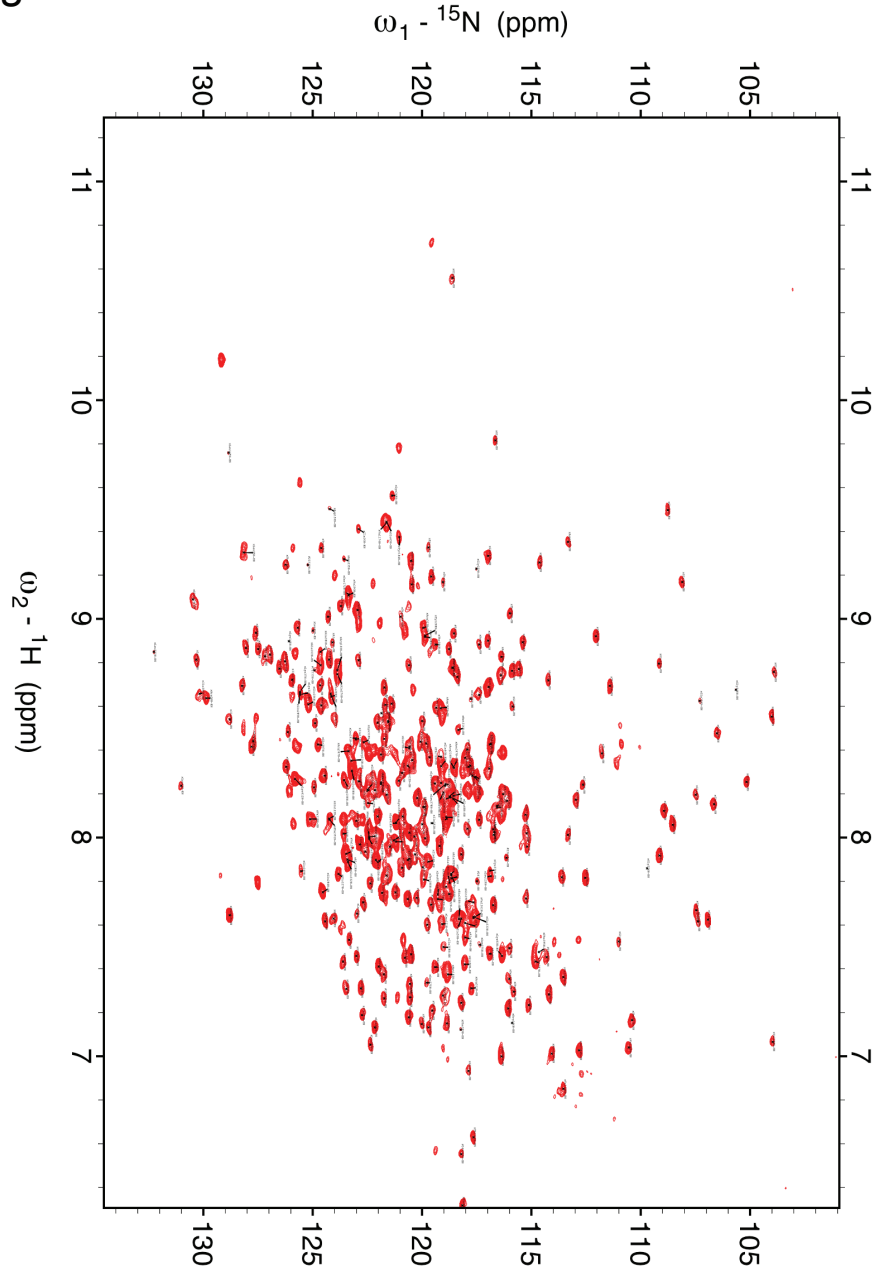

Figure 8. $^{1}H,^{15}N$ TROSY spectrum of a $^{15}N,^{13}C,^{2}H$ triple labelled sample of TmFtsA (~50 kDa) recorded at 50°C and 16.4 T.

Figure 9. Solution NMR analysis allowed me to independently confirm the FtsZ peptide-binding site on FtsA's surface.

a) Examples of exchange broadened (left) and shifted (right) resonances.
b) MAPPER program output showing that more than 80% of FtsA's primary sequence has been assigned.
c) A graph representing weighted chemical shift perturbation between TROSY HSQC spectra of FtsA with and without the 16-residue FtsZ peptide. Residues shifted more than the threshold (dotted line) and those that disappeared upon peptide binding have been mapped on the crystal structure.
d) Solution NMR studies identifying amide resonances perturbed upon addition of the FtsZ peptide (red). These results support the crystal structure as well as previous *in vivo* mutations by Pichoff and Lutkenhaus (Pichoff & Lutkenhaus, 2007; yellow). Residues highlighted by both *in vivo* and NMR studies are blue.

Figure 9

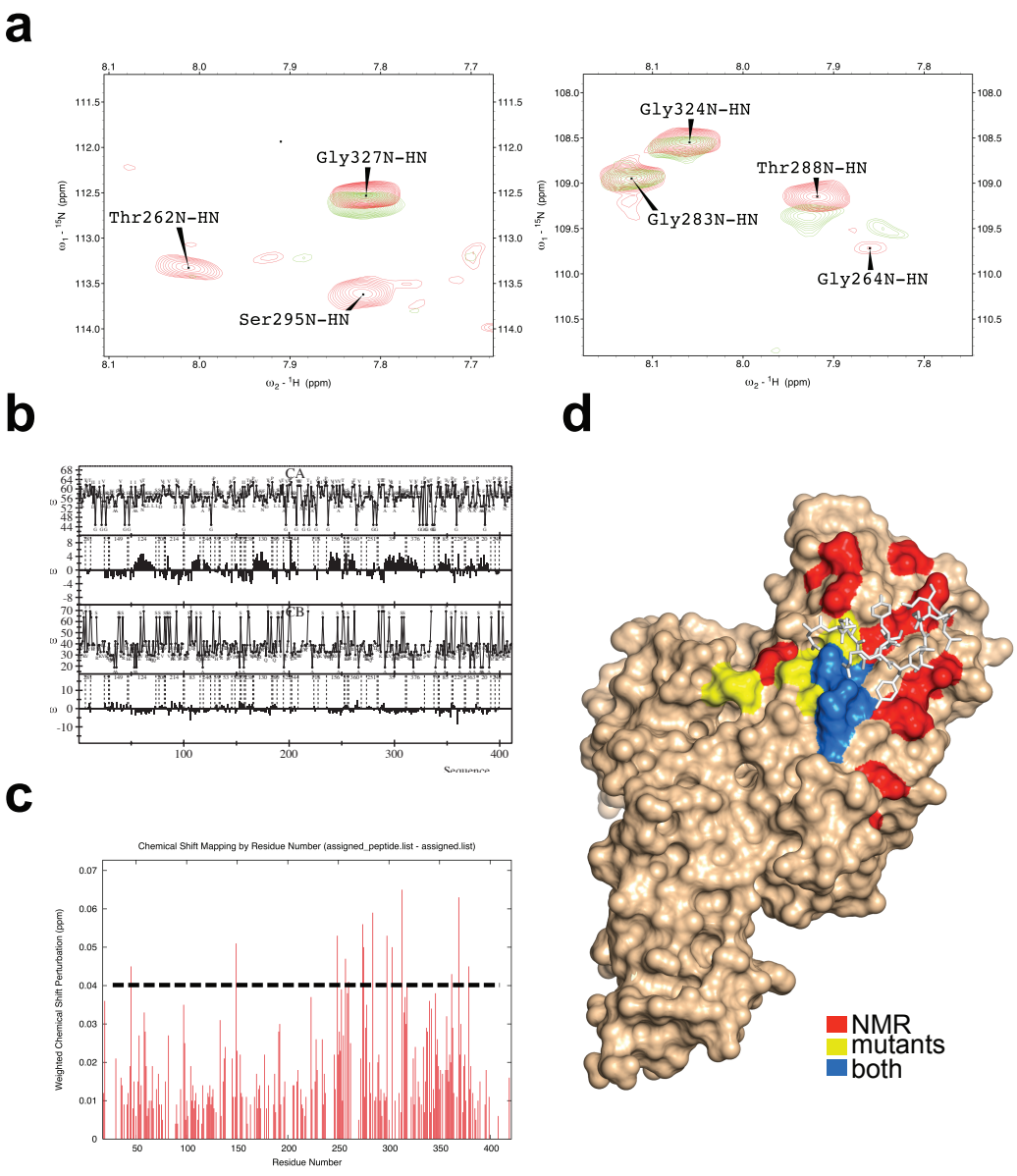
a
Gly327N-HN
Thr262N-HN
Ser295N-HN
Gly324N-HN
Thr288N-HN
Gly283N-HN
Gly264N-HN
ω1 - 15N (ppm)
ω2 - 1H (ppm)
b
CA
CB
Sequence
c
Chemical Shift Mapping by Residue Number (assigned_peptide.list - assigned.list)
Weighted Chemical Shift Perturbation (ppm)
Residue Number
d
NMR
mutants
both

TmFtsZ peptide. Binding of the FtsZ peptide to FtsA is in the micromolar range with a Kd of 51 ± 9.9 μM as determined by isothermal titration calorimetry (Fig. 7d).

Identification of the TmFtsZ binding site on TmFtsA by solution NMR

Although the peptide fitted very well into the electron density map (Fig. 7b) I aimed next at confirming the binding site by solution NMR. Since TmFtsA is a relatively large protein (47 kDa) it became necessary to deuterate the protein. Triple-labelled $^{15}N^{13}C^{2}H$ TmFtsA yielded high quality TROSY spectra at 50°C (Fig. 8). There were still some overlapping peaks on 2D TROSY-HSQC, however, 3D experiments managed to resolve them. Comparison of the spectra recorded in the absence and presence of the same 16 residue FtsZ peptide revealed chemical shift perturbations as well as resonances that were exchange broadened beyond detection as a result of FtsZ peptide binding (Fig. 9a). Based on a standard set of TROSY triple resonance experiments, over 80 % of backbone resonances of TmFtsA's primary sequence were assigned (see Methods and Fig. 9b). It was also necessary to label particular residues. Based on their frequency in the FtsA sequence as well as other factors (metabolism, crumbling) I decided to use ^{15}N-labelled Leu and Ile. This enabled me to identify all perturbed resonances (Fig. 9c) and map these onto the crystal structure (Fig. 9d). Satisfyingly, both solution NMR and the X-ray structure agree on the binding site of the FtsZ C-terminal tail on the surface of subdomain 2B of FtsA, and both agree well with prior knowledge from mutants (Pichoff & Lutkenhaus, 2007).

FtsA forms actin-like protofilaments

Based on its fold, FtsA was originally classified as a member of the actin/HSP70 family of proteins, alongside actin itself and prokaryotic actin-like MreB (Bork et al., 1992), although a large deviation from the canonical fold was reported, replacing subdomain 1B with 1C on the other side of the protein (van den Ent & Löwe, 2000). This raised the important question of whether FtsA would be able to polymerise into filaments. The canonical actin fold is shown in figure 4a using MreB (van den Ent et al., 2001b): it consists of subdomains 1A, 1B, 2A and 2B (Fig. 10a, b). In the protofilament, the conserved sub-filament that all polymerising members of the actin family share, polymerisation utilizes a contact between subdomains 1B and 2B on one subunit, and 1A and 2A on the other. FtsA has a distinct subdomain architecture: it contains subdomains 1A, 2A and 2B, but subdomain 1B is replaced with 1C, located

on the other side of the protein when interpreting it in terms of the protofilament architecture (Fig. 7a, 10).

Inspection of my new FtsA:FtsZ crystal structure (Fig. 7a, left) reveals that the TmFtsA dimer resembles an actin-like protofilament. Furthermore, when co-crystallised with ATPγS, TmFtsA produced new crystals containing continuous protofilaments that closely resemble the previous dimer and are again actin-like (Table 1, Fig. 10a, c). In the ATPγS crystals, the longitudinal axis of the protofilament is aligned with the crystallographic a axis, providing accurate measurement of the 48.0 Å repeat length (Fig. 10c). The protofilament structure clearly resembles that of MreB (longitudinal spacing 51.1 Å; van den Ent et al., 2001b) and all other polymerising actin-like proteins (Fig. 10a).

This leads to the question of how FtsA forms the same protofilament when it has a distinct subdomain architecture. FtsA and MreB comprise the 1A, 2A and 2B subdomains, which are similarly arranged in both proteins. However, the 1B subdomain of MreB, which in the polymer structure makes a contact with the 1A subdomain of the succeeding subunit (van den Ent et al., 2001b), is replaced in FtsA with the 1C subdomain occurring on the opposite side of the molecule, which in the polymer structure contacts the 1A subdomain of the preceding subunit (Fig. 10b). In other words: the subdomain can be loosely described as having been swapped from one side of the FtsA molecule to the other, but its relative position within the protofilament has been conserved when compared to canonical actin-like protofilaments (Fig. 15a).

This alteration has implications for the polymer's appearance. Firstly, the ends of the polymers will look very different, with the 1C subdomain of FtsA prominently projecting at one terminus and the 2B subdomain at the other. Secondly, since FtsA's 1C subdomain contains nearly twice the number of residues as MreB's 1B subdomain and has a dissimilar topology (Fig. 15b), there are important differences between the two polymer structures. MreB protofilaments are flat when observed along the longitudinal axis, whereas FtsA's 1C subdomain protrudes out, placing monomeric FtsA subunits at an angle with respect to the longitudinal axis and making the polymer structure thicker (Fig. 10a right). Also, in the structure of the MreB filament, the tip of the subdomain 2A consisting of helices H8 and H9 is inserted in

Figure 10. Crystallographic analysis reveals that FtsA, in spite of its unusual subdomain architecture, is able to form actin-like filaments.

a) FtsA in the presence of ATPγS crystallised as a continuous polymer. The packing remarkably resembles that of MreB, which has the canonical actin-like fold (subdomains 1A, 1B, 2A, 2B) and forms actin-like, straight protofilaments. The longitudinal spacings are 51.1 Å and 48.0 Å for MreB and FtsA, respectively.
b) A more detailed view of FtsA and MreB dimers. Monomeric subunits are rimmed in red. FtsA and MreB adopt a similar subdomain architecture, however, the 1B subdomain of MreB (yellow) is missing in FtsA and instead subdomain 1C in FtsA is located on the other side of the molecule. It therefore appears that FtsA is a subdomain variation of the actin fold that still enables the formation of similar protofilaments (‘domain-swap’).
c) Crystal packing of TmFtsA in complex with ATPγS. The longitudinal axis of the protofilament is aligned with the crystallographic a axis, providing the repeat of 48.0 Å.

Figure 10

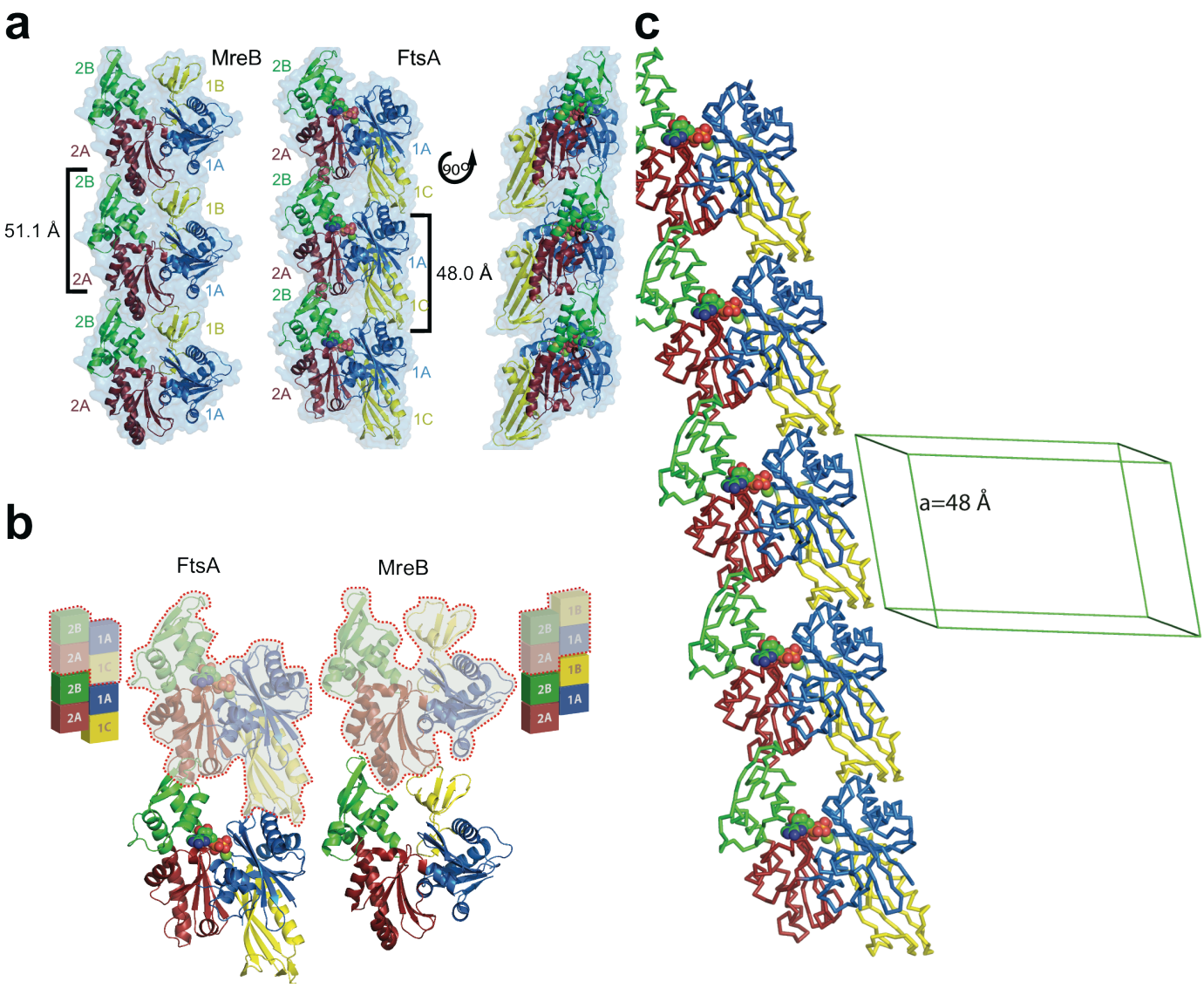

Figure 11. FtsA polymers visualised by electron microscopy on lipid monolayers are identical to those present in crystals.

a) A schematic of the lipid monolayer assay. 1. Drop of lipid solution added. 2. Monolayer forms as solvent evaporates. 3. Carbon-coated EM grid placed on monolayer. 4. Protein injected underneath monolayer 5. Incubation. 6. Negative staining and visualisation.
b) FtsA polymerises on a lipid monolayer forming long filaments, which often form doublets.
c) Occasionally, FtsA forms 2D sheets on the lipid monolayer. Fourier transformation of a sheet (white dotted square) reveals the same longitudinal spacing of about 48 Å, which matches the spacing present in the crystal structure very well.

Figure 11

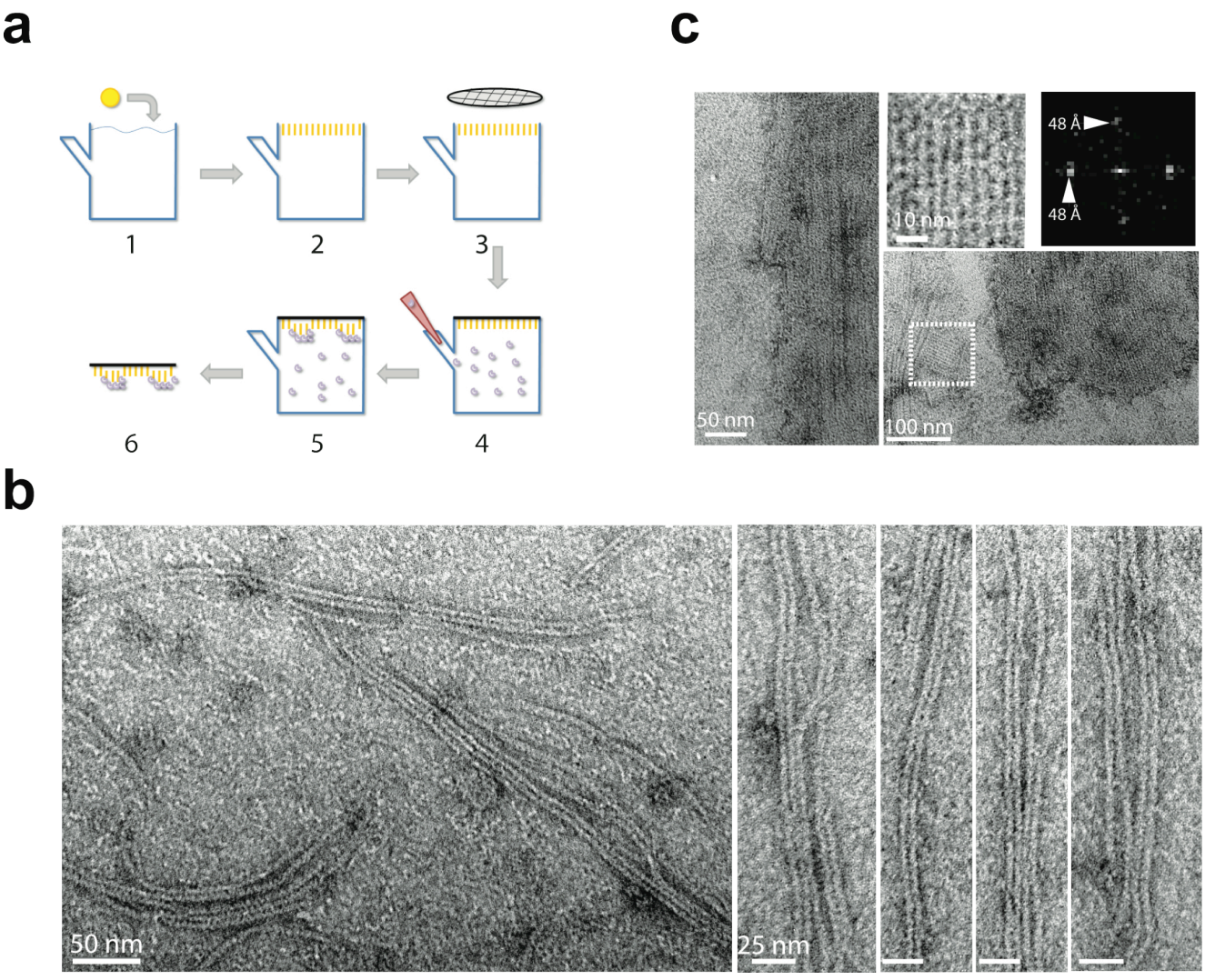

Figure 12. Fluorescence microscopy reveals FtsA fibers in *E. coli* cells. N-terminal mCherry fusions to EcFtsA and BsFtsA (C-terminal amphipathic helix removed; magenta) as well as to four BsFtsA mutants have been over-expressed in *E. coli* using a T7 expression system. Membranes were stained with FM1-43 (green).

a) The three top panels clearly show distinct, polymeric structures and the three bottom panels show that mutations introduced within the polymerisation interface prevent polymerisation, leading to diffuse localisation. The locations of these mutations are shown in section (b).
b) Rational design of FtsA polymerisation-deficient mutants. Marked mutations were introduced on the polymerisation interface (in red). *B. subtilis* residue numbers are shown.

Figure 12

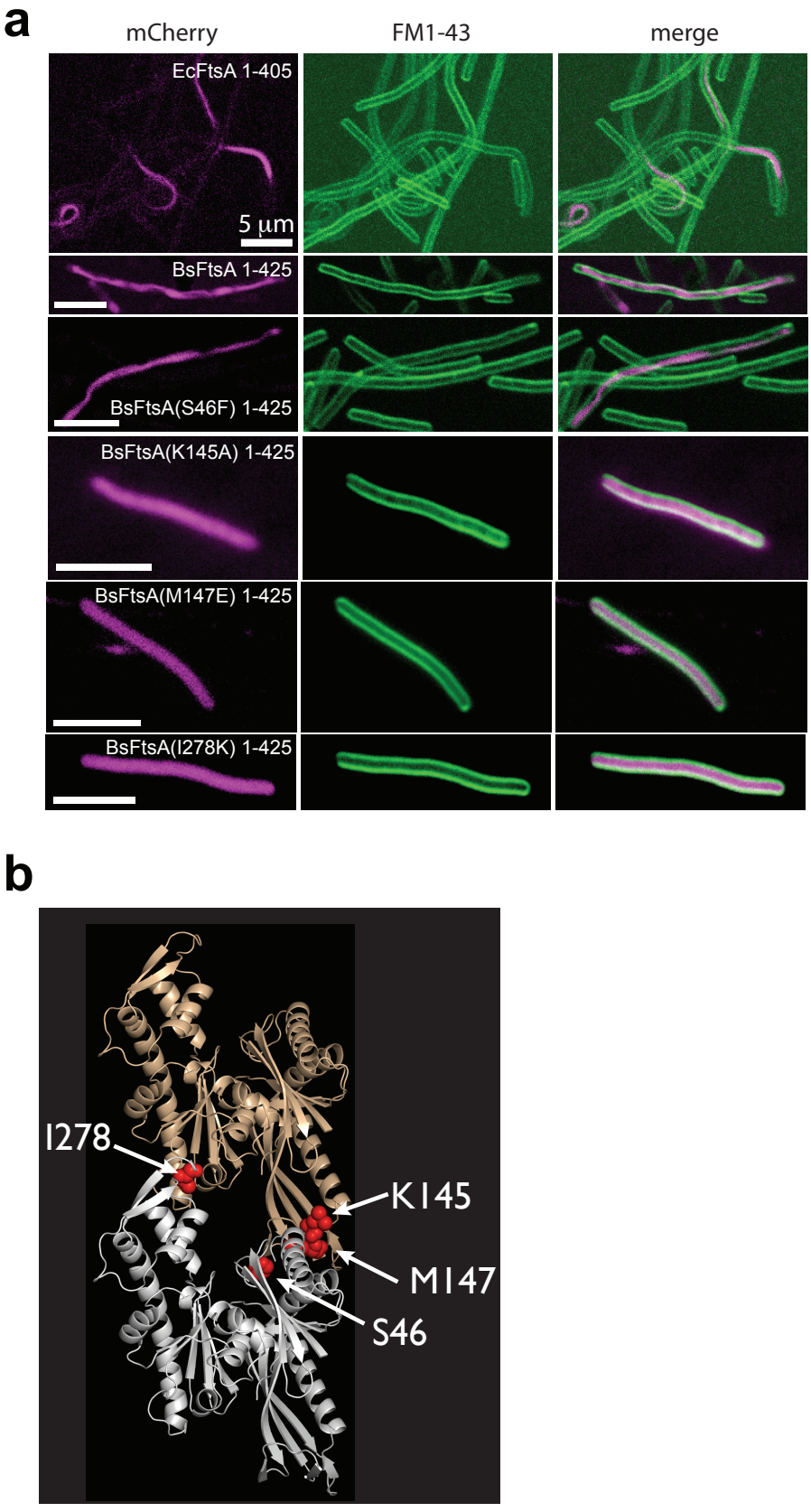
a
mCherry
FM1-43
merge
EcFtsA 1-405
5 µm
BsFtsA 1-425
BsFtsA(S46F) 1-425
BsFtsA(K145A) 1-425
BsFtsA(M147E) 1-425
BsFtsA(I278K) 1-425
b
I278
K145
M147
S46

Figure 13. FtsA polymers can be visualised in living cells by electron cryo-tomography (performed by Qing Wang).

a) Untagged *E. coli* and *B. subtilis* FtsA proteins were over-expressed in *E. coli* cells and imaged by electron cryo-tomography. EcFtsA without the amphipathic helix (left) forms long, straight bundles in the middle of the cell (navy blue dotted line represents cross-section's orientation). The middle panel shows similar filaments formed by BsFtsA truncated for the amphipathic helix. Full-length BsFtsA triggers membrane tubulation (right panel, red arrows). White dotted areas are shown enlarged in the insets. Red dotted area is shown enlarged in section (c).
b) Full-length TmFtsA causes membrane distortion and forming of lipid tubes (turquoise) that are coated with protein polymers (red) in the cell membrane's proximity. A cross-section through the middle of the cell does not show any polymeric structures present in the cytoplasm (left panel). Remarkably, the closer to the membrane, the more abundant the tubes become (middle and right panels).
c) Enlarged view of the red dotted area in (a), Fourier transform of this (bottom left) and filtered image (right).
d) Putative polymerisation-deficient mutant of TmFtsA (E49A, K51A, D52A). In this case round lipid vesicles rather than elongated tubes are formed.

Figure 13

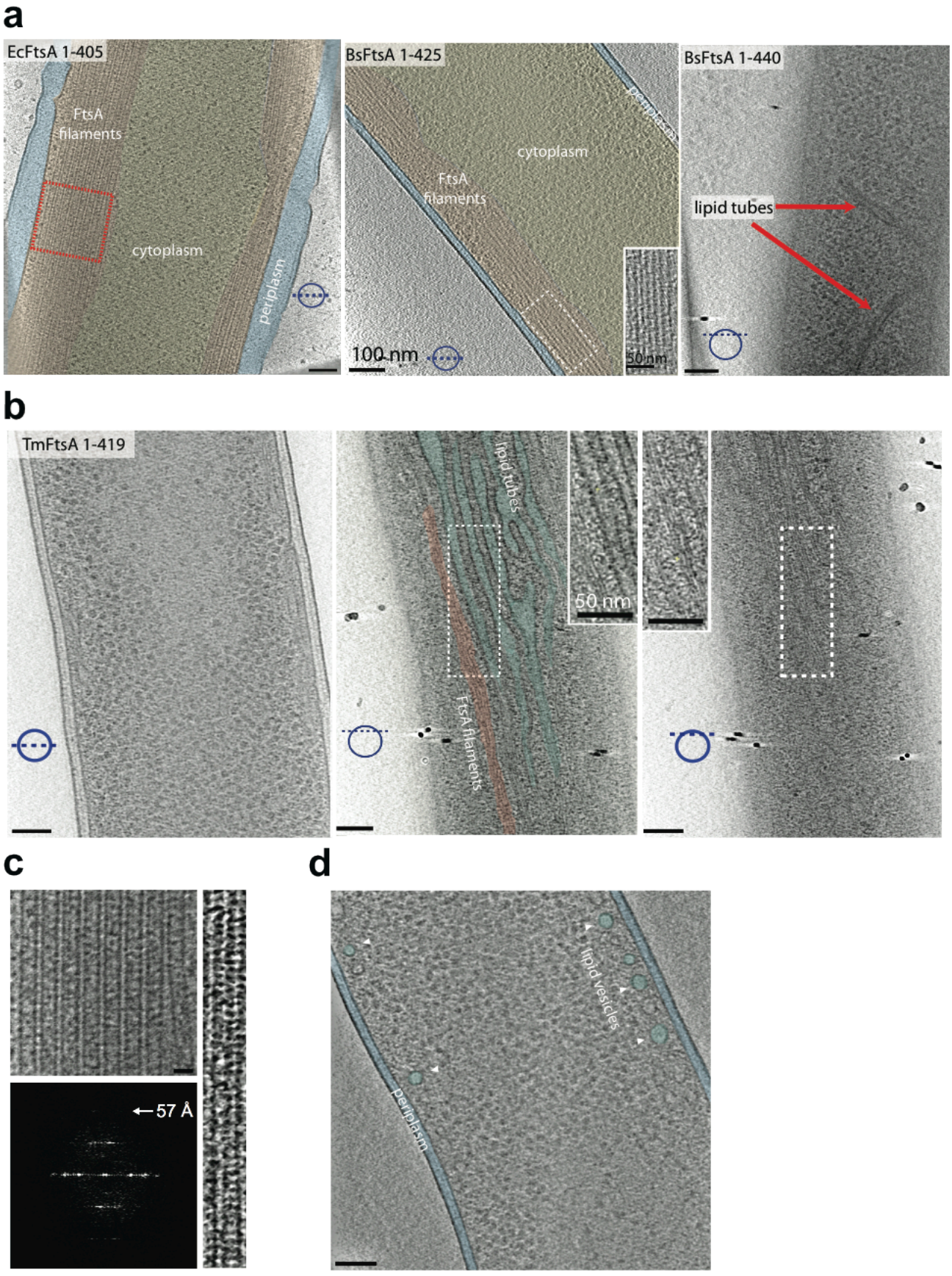
a
EcFtsA 1-405
FtsA filaments
cytoplasm
periplasm
BsFtsA 1-425
cytoplasm
FtsA filaments
periplasm
100 nm
50 nm
BsFtsA 1-440
lipid tubes
b
TmFtsA 1-419
lipid tubes
50 nm
FtsA filaments
c
57 Å
d
lipid vesicles
periplasm

the cleft between subdomains 1B and 2B. A similar arrangement in the FtsA protofilament is obviously not possible so the 2A subdomain stays in contact only with the 2B subdomain and is somewhat hidden behind it, when looking from the front of the molecule (Fig. 10a). This creates a hole in the polymerisation interface that is occluded by the interacting subdomains. However, given that FtsA and MreB (also actin and ParM) are only ~15 % identical in sequence, their protofilaments are remarkably analogous. I conclude that it appears that FtsA is a variation of the actin-like fold that still enables the formation of canonical actin-like protofilaments.

TmFtsA protofilaments formed on lipid monolayers are similar or identical to the filaments observed in crystals

To prove that FtsA filaments exist outside crystals I used purified TmFtsA for *in vitro* electron microscopy. Conventional negatively stained electron microscopy on carbon-coated grids failed, since the proteins (TmFtsA and TmFtsAΔ8) did not exhibit any polymeric structures but remained apparently monomeric. I then took advantage of FtsA's affinity for membranes through polymerisation on a lipid monolayer (Fig. 11a). Using this technique I revealed filaments several hundred nanometres in length, often present as doublets or higher-order structures (Fig. 11b). Interestingly, no exogenous nucleotide was required to obtain these, but it is important to note the protein contains some bound ATP carried over from the purification as is evident from the ATP in the crystal structure. Occasionally, two-dimensional sheets were observed (Fig. 11c). Fourier transformations of sheets (Fig. 11c, top right) revealed a longitudinal spacing of around 48 Å, corresponding to the spacing found in the crystals. This implies that the TmFtsA polymers visualised by electron microscopy and seen in atomic detail in the crystal structures are very similar or identical.

FtsA proteins from *T. maritima, E. coli* and *B. subtilis* all form filaments in *E. coli* cells when over-expressed

My previous experiments showed that *T. maritima* FtsA polymerises to form actin-like protofilaments *in vitro* on lipid monolayers. I investigated a broader range of species by including *E. coli* FtsA (EcFtsA) and *B. subtilis* FtsA (BsFtsA) proteins in my *in vivo* analysis. First, I over-expressed mCherry-tagged FtsAs deprived of the C-terminal amphipathic helices in *E. coli*. The amphipathic helices were removed for fluorescence microscopy in order to see filaments away from the cell membrane

where it would be difficult to distinguish between filaments and membrane localisation. The T7 system was used so not all cells showed strong fluorescence, but those cells that did showed long filaments: mCherry-EcFtsA 1-405, when over-expressed in *E. coli*, forms distinct, elongated polymer structures that tend to bend the cells into a tight curvature (Fig. 12a, top panels). Note that an earlier study found cytoplasmic aggregated structures formed by a similar C-terminal EcFtsA truncation (Gayda et al., 1992). mCherry-BsFtsA 1-425 produced large polymers as well (Fig. 12a, second row), however, in this case the cells remained straight. Over-expression of mCherry-TmFtsA 1-411 caused protein aggregation and accumulation as spots at the cell poles (data not shown) so it was not included in the subsequent analysis by electron cryo-tomography.

To investigate the subcellular organisation and appearance of FtsA filaments in more detail, Qing Wang imaged EcFtsA 1-405, BsFtsA 1-425, BsFtsA 1-440 and TmFtsA 1-419 in intact cells by electron cryo-tomography. Both BsFtsA 1-440 and TmFtsA 1-419 polymers, containing the C-terminal amphipathic helices, bind to the inner surface of the cytoplasmic membrane, thereby distorting it (Fig. 13a right panel, 13b). This causes formation of elongated lipid tubes coated with protofilaments roughly parallel to the long axis of these tubes. One has to assume that the protofilaments are made of FtsA. In the absence of the amphipathic helix, EcFtsA 1-405 and BsFtsA 1-425, formed long, straight filaments visible in the middle of the cell, that are not membrane-associated (Fig. 13a, left and middle panels). EcFtsA 1-405 filaments were exceptionally prominent and assembled into large sheets aligned along the direction of the long axis of the cell (Fig. 13a left panel). A Fourier transform of these shows a longitudinal repeat of 57 Å, which does not match the TmFtsA spacing of 48 Å I determined above (Fig. 13c). Because of the low resolution of the tomograms it is not clear from the pictures that this repeat actually measures along the protofilament axis since the *E. coli* polymers appear to be helical (Fig. 13c). In cells over-expressing BsFtsA 1-425, similar fibres and localisation patterns to those cells over-expressing EcFtsA 1-405 were observed (Fig. 13a middle panel). When cells over-expressing a putative triple TmFtsA 1-419 polymerisation mutant were imaged, small vesicles near the inner membrane were observed (Fig. 13d), which means that the protein is still associated with the membrane, but no filamentous structures were visible.

BsFtsA filaments are required for efficient cell division

Next I investigated whether polymerisation of FtsA is required for its function in cell division. For this I rationally designed potential polymerisation-deficient mutants (Fig. 12b) based on manual inspection of the protofilament crystal structures described above (Table 1, Fig. 7a, 10). The mutated proteins were then analysed by fluorescence microscopy after expressing them as mCherry fusion proteins in *E. coli* (Fig. 12a). The *in vivo* fluorescence assay seems to be the most reliable test for FtsA polymerization since it shows that the protein is made, does not form inclusion bodies and discrimination between fibres and uniform fluorescence is unambiguous. BsFtsA(S46F) 1-425 showed the same pattern as BsFtsA 1-425 (Fig. 12a, third row) demonstrating that it still polymerises. In contrast the three BsFtsA 1-425 mutants K145A, M147E and I278K displayed evenly distributed fluorescence in cells and did not feature any distinct polymer-like structures (Fig. 12a, three bottom panels). I conclude that BsFtsA(K145A), M147E and I278K are unable to form polymers, whereas BsFtsA(S46F) forms polymers similar or identical to the wild-type. Moreover, BsFtsA(I47D), P144K and G279R formed inclusion bodies (data not shown).

Having identified BsFtsA polymerisation-deficient mutants I wanted to study whether or not FtsA polymers are of biological significance *in vivo*. A complementation experiment was performed in a *Bacillus subtilis* FtsA temperature sensitive (ts) background at 42°C (see Methods and: Beall & Lutkenhaus, 1992; Karmazyn-Campelli et al., 1992). Under elevated temperature, the ts-FtsA protein is unable to support cell division and the cells acquire a filamentous appearance that is straightforward to distinguish and quantify. I then complemented the endogenous ts-FtsA with a series of mutant versions of FtsA, inserted into the *aprE* locus, under the control of the IPTG-inducible *Pspac* promoter (Fig. 14a). I tested six different variants: wild-type FtsA, FtsA(Q87Stop; truncated protein product), FtsA(K145A), FtsA(M147E), FtsA(I278K) and FtsA(S46F). I used this experimental setup since it has been shown (Beall & Lutkenhaus, 1992) that wild-type *ftsA* expressed from the *Pspac* promoter complemented the filamentation phenotype triggered by the ts-FtsA protein and I was wondering if my polymerisation-deficient mutants would behave similarly. As is shown in Fig. 14, the wild-type and S46F cells were of normal length, whereas the Q87Stop and the three polymerisation-deficient mutants K145A, M147E

and I278K grew as elongated, filamentous cells (Fig. 14b). These were long cells of varying length, similar to previous studies (Jensen et al., 2005) on an *ftsA*-null *B. subtilis* strain where the average cell length was 22.6 ± 11.9 μm. Quantification also reflects that fact (Fig. 14c), with significant standard deviations associated with the FtsA polymerisation-deficient mutants and the Q87Stop mutant. The average cell length of the FtsA mutants is larger than that of the wild-type, but the phenotype is not as severe as in the case of Q87Stop. Also, assuming that the length per nucleoid is constant and the wild-type FtsA cells undergo correct cell divisions I calculated a fraction of successful cell divisions (Fig. 14d). In the case of Q87Stop about 0.43 of divisions are working correctly and for the FtsA polymerisation-deficient mutants it varies between 0.59 (M147E) and 0.71 (K145A). This suggests that cell division in the absence of FtsA filaments (monomeric FtsA is still present) is much less efficient than usual. This strongly implies a role for FtsA polymerisation in bacterial cell division and Z-ring formation.

Figure 14. Replacing wild-type FtsA with either polymerisation-deficient mutants or a non-functional version has dramatic effects on cell division in *Bacillus subtilis*.

a) A scheme explaining the experimental design of the complementation assay. At 37°C and in the absence of IPTG only native *tsftsa* is expressed whereas at 42°C and in the presence of 1 mM IPTG the tsFtsA protein becomes non-functional and FtsA mutants inserted in the *aprE* locus are synthesised.
b) DIC images of genetically engineered *Bacillus subtilis* strains showing that non-polymerising FtsAs (K145A, M147E, I278K) do not fully complement the thermo-sensitive *spoIIN279(ts)* allele. As a control, non-functional FtsA (Q87Stop) shows a very severe cell division defect. S46F, which was found to still polymerise (Fig. 12a), shows no effect on cell division.
c) A chart showing the average cell lengths of strains bearing tested FtsA variants. The wild-type was 5.89 ± 1.74 μm and S46F exhibites similar values. Cells of the Q87Stop variant were 13.40 ± 8.30 μm and the three polymerisation-deficient mutants were as follows: K145A 8.29 ± 4.36 μm, M147E 9.93 ± 6.6 μm and I278K 9.04 ± 4.86 μm
d) Fractions of successful cell divisions were calculated referring to the wild-type FtsA variant.

Figure 14

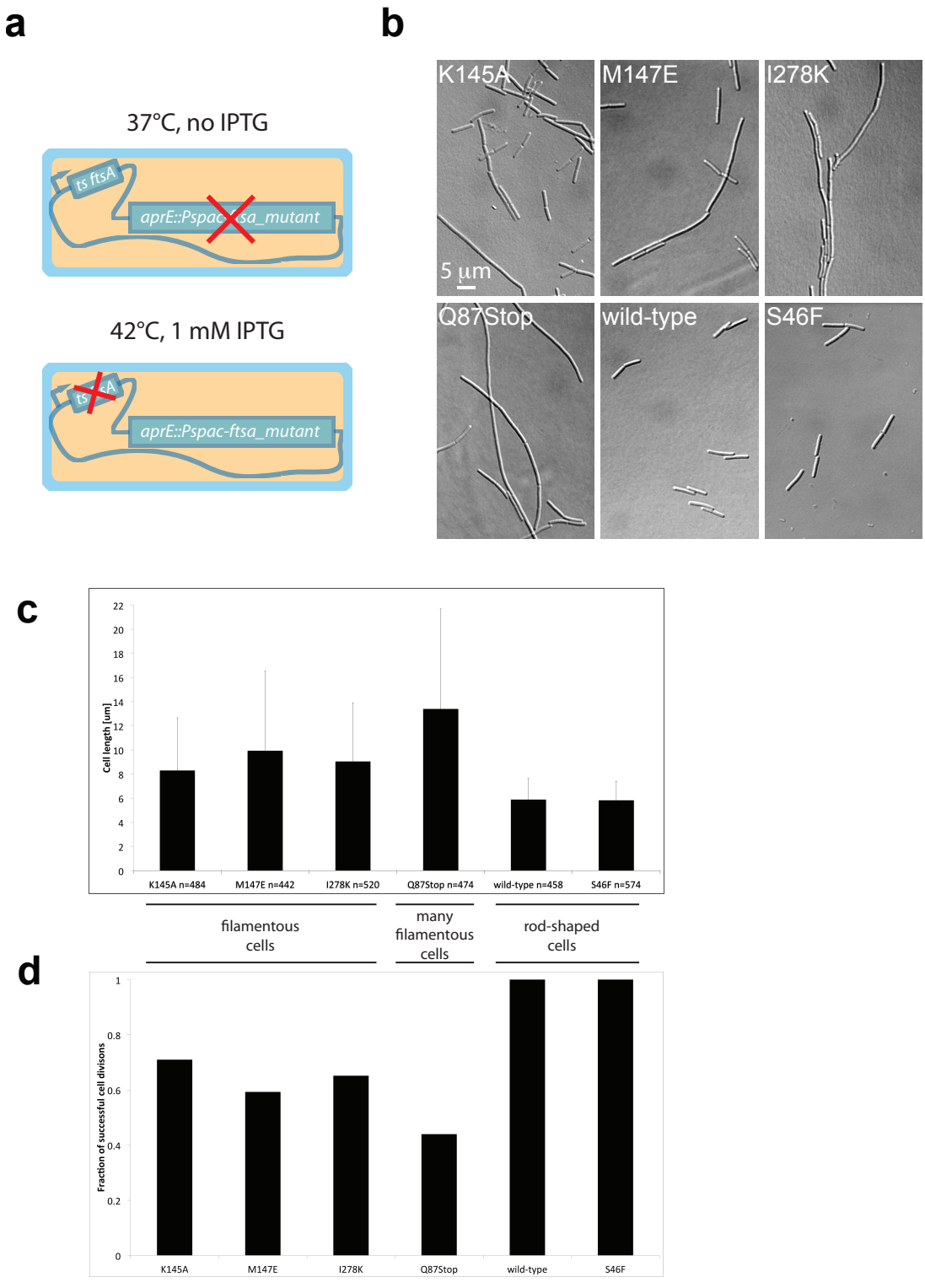
a
37°C, no IPTG
ts ftsA
aprE::Pspac-ftsa_mutant
42°C, 1 mM IPTG
ts ftsA
aprE::Pspac-ftsa_mutant
b
K145A
M147E
I278K
5 µm
Q87Stop
wild-type
S46F
c
Cell length [um]
0
2
4
6
8
10
12
14
16
18
20
22
K145A n=484
M147E n=442
I278K n=520
Q87Stop n=474
wild-type n=458
S46F n=574
filamentous cells
many filamentous cells
rod-shaped cells
d
Fraction of successful cell divisons
0
0.2
0.4
0.6
0.8
1
K145A
M147E
I278K
Q87Stop
wild-type
S46F

Discussion and future directions

I have reconstituted *in vitro* the *T. maritima* membrane-bound complex of FtsA and FtsZ and regions indispensable for complex formation have been identified. This work confirms and refines previous *in vivo* findings and leads to the FtsZ-tethering model depicted in Fig. 15c.

Importantly, the structural work on the FtsA:FtsZ complex led me to the discovery that FtsA is able to assemble into filaments that resemble actin-like protofilaments and I show that these filaments are formed by FtsAs from three different model organisms. The protofilaments are formed despite FtsA having an unusual subdomain architecture. Finally, I demonstrate that polymerisation-deficient FtsA mutants show a severe deficiency in cell division in a thermo-sensitive FtsA complementation assay in *Bacillus subtilis.*

It has previously been shown that the last 15-20 residues of FtsZ are highly conserved and form a region for interactions with other proteins, such as ZipA, MinC and FtsA (Shen & Lutkenhaus, 2009). I have now shown that the interaction between FtsZ and FtsA can be observed *in vitro* and I could identify and characterise the interactions in detail. I show the tail of FtsZ binding to subdomain 2B of FtsA, as was implied by earlier mutant work (Pichoff & Lutkenhaus, 2007). I could not find any effect of FtsZ tail binding on FtsA's nucleotide binding or hydrolysis activity, nor on FtsA polymerisation and it currently seems to be a purely architectural interaction leading to the membrane tethering of the Z-ring. My model in figure 15c does suggest that the Z-ring of bacterial cell division is some distance from the membrane and this has been reported earlier by electron cryo-tomography data (Li et al., 2007).

The structure of *E. coli* FtsZ peptide in complex with ZipA has previously been solved (Mosyak et al., 2000). Comparing the two structures unveils some similarities, although they are largely confined to a small alpha helical region and the termini point in different directions (Fig. 16a). Certainly, the binding pockets on ZipA and FtsA for the FtsZ tail seem to be quite diverse and it is not impossible that the same tail may adopt a couple of conformations, at least partly, to bind to both proteins (not simultaneously). This is conceivable in the light of overlapping functions of ZipA and FtsA (Pichoff & Lutkenhaus, 2002).

Figure 15. FtsA is a subdomain variation of the actin fold that still enables the formation of similar protofilaments.

a) The 1C subdomain is present on the other side of a monomeric subunit with respect to the 1B subdomain of MreB.
b) Both the 1C subdomain of FtsA and the 1B subdomain of MreB consist of an alpha helix and a three-stranded beta sheet, but the topology is different. For 1C it is S5-H2-S6-S7 and for 1B it is S4-S5-H1-S6.
c) Architecture of the FtsA:FtsZ membrane bound complex, as analysed here for *Thermotoga maritima*.
d) The Z-ring made of polymerised tubulin-like FtsZ may be attached to the membrane by an 'A-ring', made of polymerised actin-like FtsA or short stretches of FtsA polymers, based on the relative number of FtsZ and FtsA molecules in cells.

Figure 15

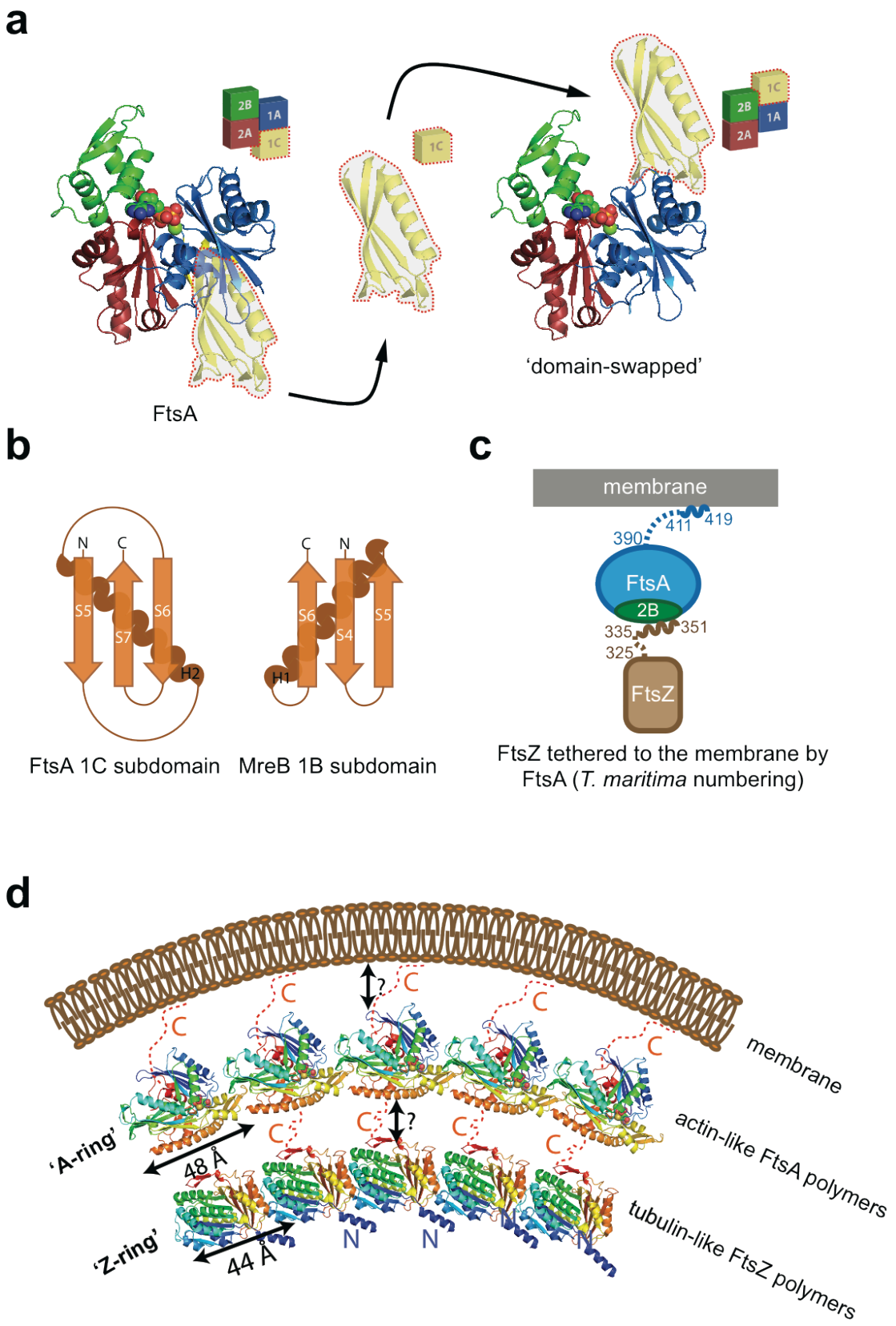
a
2B
1A
2A
1C
1C
2B
1A
2A
1C
FtsA
'domain-swapped'
b
N
C
S5
S7
S6
H2
C
N
S6
S4
S5
H1
FtsA 1C subdomain
MreB 1B subdomain
c
membrane
390
411
419
FtsA
2B
335
351
325
FtsZ
FtsZ tethered to the membrane by
FtsA (T. maritima numbering)
d
membrane
actin-like FtsA polymers
tubulin-like FtsZ polymers
'A-ring'
'Z-ring'
48 Å
44 Å
?
?
C
N

Figure 16. Analysis of FtsZ's C-terminal peptide conformation and FtsA's 1C subdomain topology.

a) Superposition of the TmFtsZ C-terminal peptide (this work) and the corresponding peptide of EcFtsZ when bound to ZipA.
b) The DALI server identified RNA polymerase II chain G as the one having the most similar fold to the 1C domain of FtsA with Z score 6.3 (PDB ID 3H0G).

Figure 16

a

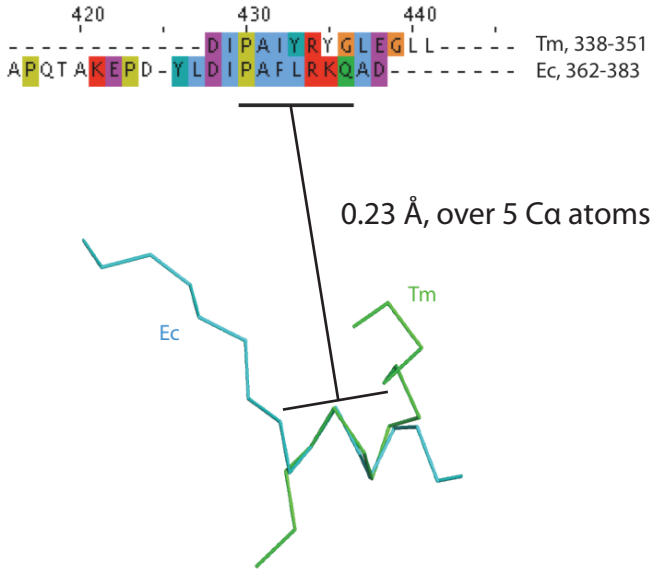

b

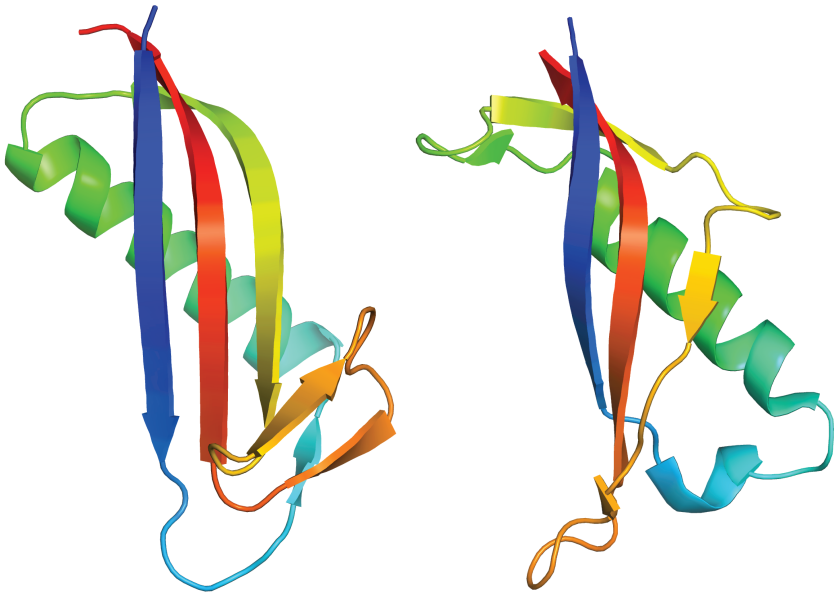

TmFtsA domain 1C

RNA polymerase II chain G
PDB 3H0G

My work shows that FtsA is more actin-like than was previously assumed. FtsA forms protofilaments on lipid monolayers and in cells when over-expressed. FtsA forms actin-like protofilaments although they diverge significantly from the ones formed by actin, MreB and ParM. These differences are most likely caused by the aberration in structure, fold and size of subdomain 1C that replaces 1B on the other side of the molecule (van den Ent & Löwe, 2000). The topology of FtsA's 1C subdomain is S5-H2-S6-S7 whereas MreB's 1B subdomain is S4-S5-H1-S6 (Fig. 15b). The origin of the 1C subdomain during evolution is unknown, although it seems unlikely that it is related to 1B. This suggests that 1C is not simply a domain swap (moving the subdomain into another loop region of the actin fold) but a more complicated domain replacement with something different, in a distinct location that still enables similar filament formation. A DALI search for the most similar fold to subdomain 1C returns RNA polymerase II chain G (PDB id: 3H0G) with a Z-score of 6.3 and 10 % sequence identity over 61 aligned residues (Fig. 16b). This is a significant hit, but to me does not provide any clues.

FtsA and FtsZ are the only nucleotide-binding components of the inner divisome machinery with the potential to produce energy. FtsZ's GTP binding and hydrolysis is now relatively well understood (Oliva et al., 2004) and the nucleotide is efficiently hydrolysed only upon filament formation. In contrast, less is known about FtsA's ATPase activity. Clearly, TmFtsA can bind ATP and ATPγS as demonstrated by the crystal structures (presented here and van den Ent & Löwe, 2000), but it still has not been shown conclusively that the protein, from any organism, exhibits ATPase activity (with one exception, which might represent contamination; Feucht et al., 2001). In the course of this work I performed ATPase assays with purified TmFtsA in the presence of miscellaneous ligands including divalent metal cations, the FtsZ C-terminal peptide and liposomes and they did not yield any detectable activity of the protein (data not shown). Also, in my *in vitro* experiment on lipid monolayers, polymers formed in the absence of exogenous nucleotide, although some ATP from purification is bound to the protein. Similarly, previous work on *S. pneumoniae* FtsA showed ATP-dependent polymerisation (Lara et al., 2005), however, no membrane was present. It is worth noting that my assay was performed with *Thermotoga* protein and this might be a special case because of the extreme temperature adaptation of this protein. Unfortunately, it has proven very difficult to produce very pure and well-

behaved FtsA proteins from other, mesophilic organisms, especially when full length, including the C-terminal amphipathic helix. This situation is somewhat similar to MreB, where it was very recently shown that an N-terminal amphipathic helix hinders biochemical experiments on most proteins, except that from *Thermotoga* (Salje et al., 2011). However, removal of the amphipathic helix will alter the protein's properties and polymerisation may then not be observed *in vitro*. *In vivo*, the system may be balanced so that membrane interaction and charge compensation are required for efficient polymerisation and it seems that ATP binding/hydrolysis are not required for polymerisation on the lipid surface (see Fig. 11b, c). However, in this case membrane binding might be the energy-reducing factor acting *in lieu* of ATP, which might still be essential in solution or in cells. To address this question more work using putative ATPase mutants *in vivo* will be needed.

Why might FtsA polymerisation be required in cells? It is thought that cell division in most bacteria proceeds through constriction of the Z-ring. The ring might either produce mechanical force or direct the position of cell-wall synthesising machinery in the periplasm, where force may then be generated. It has been shown in *C. crescentus* by tomography that the Z-ring may consist of short (~ 100 nm; Fig. 3d) filaments situated randomly near the division sites rather than one, long filament encircling the cell (Li et al., 2007). Also, it has been estimated in *B. subtilis* that there are around 1000 and 5000 molecules of FtsA and FtsZ, respectively, per cell (Feucht et al., 2001) and it still remains elusive whether this is enough to cover the cell circumference. Furthermore, this work shows that the Z-ring might be tethered to the membrane by an 'A-ring' made of FtsA polymer(s) (Fig. 15d). Because there is less FtsA in a cell than FtsZ, the A-ring would have to be non-continuous. This would lead to a constriction model, whereby FtsZ and FtsA polymers are parallel to the inner surface of the cytoplasmic membrane and the mismatch of spacings between the two proteins (FtsA ~48 Å and FtsZ ~44 Å) could trigger FtsZ:FtsA filament curvature and in turn membrane constriction (Li et al., 2007). An initial trial of lipid monolayer assay with purified FtsA and FtsZ has already been performed (Fig. 17) and interestingly, when both proteins are applied, one is able to see round structures, which might be a result of the mismatch of spacings. Alternatively, FtsZ filaments could be attached to the membrane by short stretches of FtsA only every several FtsZ subunits and then depolymerisation of the FtsZ protofilament, while still anchored in the membrane,

would also lead to constriction. FtsA could have a role in both scenarios. To distinguish between these two models more electron cryo-tomography will be required to determine how FtsA and FtsZ protofilaments are mutually oriented in cells, how they are arranged in respect to the membrane and how the flexible linkers in both proteins are organised.

Finally, how did the 1C/1B subdomain variation happen? The subdomains' fold topology is reversed and they vary in size. Analysis of actin-like protein sequences and structures, including actin, MreB (van den Ent et al., 2001b) and ParM (van den Ent et al., 2002b) reveals that the 1B subdomain is the most variable and FtsA is the most evolutionary distant from other actin-like proteins. All of these proteins play key roles in distinct cellular processes relying on their actin-like filamentous nature. Opposite orientations of the 1C and 1B subdomains could be explained by the fact that the former is preceded by S1-S2-S3-H1-S4 of the FtsA 1A subdomain, whereas the latter is preceded by only S1-S2-S3 and is followed by H2-S7 of the MreB 1A subdomain, thus it seems they are "inserted" in slightly different regions of 1A's primary sequence. It would be compelling to find out whether the last common ancestor of actin and FtsA was more "actin-like" or "FtsA-like" or of it rather existed as a three-subdomain protein (1A, 2A, 2B) and later acquired either the 1C or 1B subdomain.

Figure 17. Preliminary results of a monolayer assay employing both FtsA and FtsZ. When both proteins are present one can observe spiral-like structures. However, more EM and electron cryo-tomography will be needed to figure out how FtsZ and FtsA are arranged in such a structure. Representative images are shown.

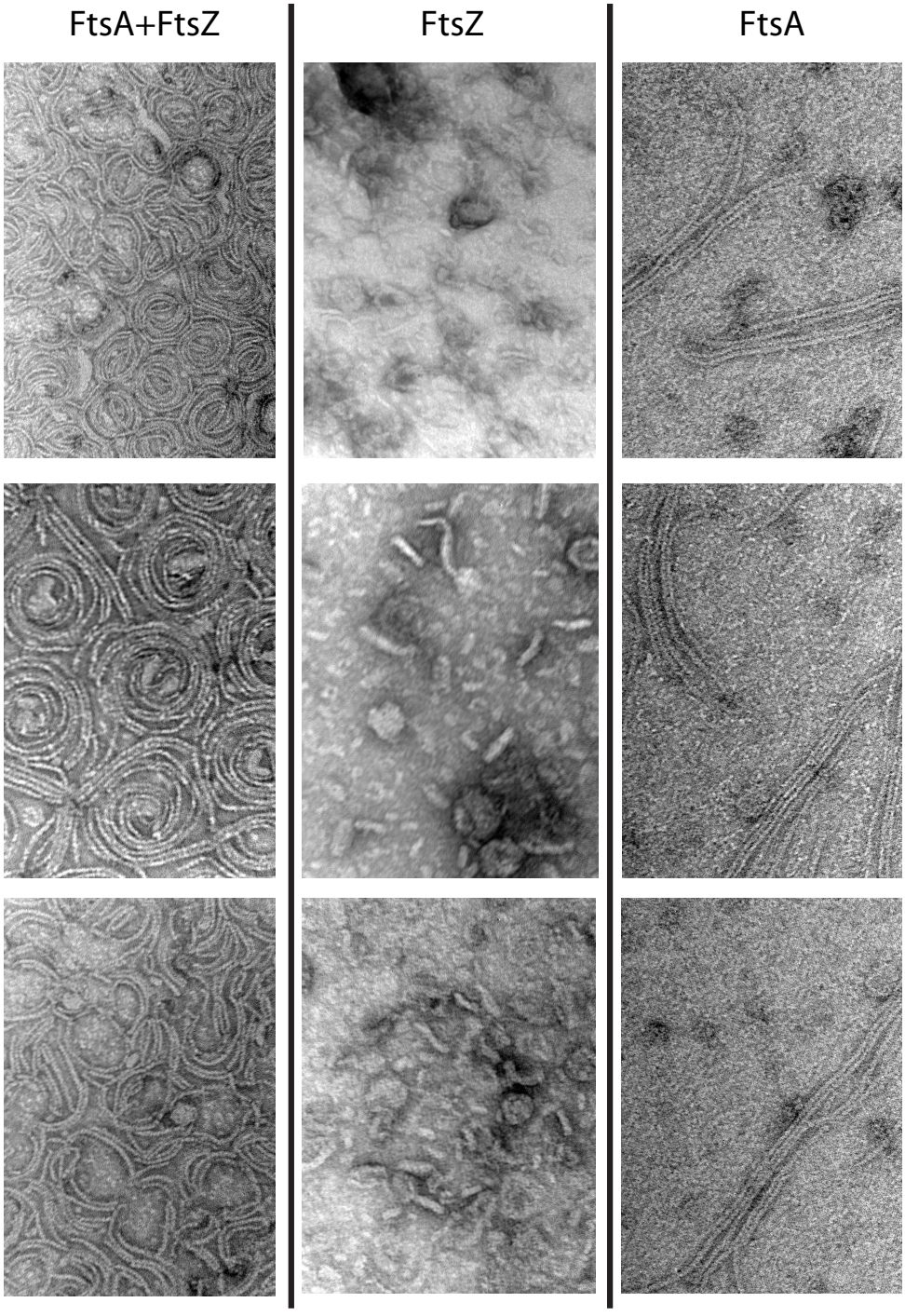

Figure 17

Appendix A

Plasmids

plasmid	descritption	tag	resistance	promoter	vector	ref
pSZ1	TmFtsA (1-419)	6xHis	Amp	T7	pET15b	this work
pSZ6	TmFtsA (1-419)	no	Kan	T7	pET9b	this work
pSZ7	TmFtsZ (1-351)	Intein-chitin	Amp	T7	pTXB1	this work
pSZ8	TmFtsA (1-419)	Intein-chitin	Amp	T7	pTXB1	this work
pSZ19	ParM-Z	Intein-chitin	Amp	T7	pTXB1	this work
pSZ25	TmFtsA495152A	no	Kan	T7	pET9b	this work
pSZ41	BsFtsA (1-440)	no	Kan	T7	pET9b	this work
pSZ47	BsFtsA (1-425)	no	Kan	T7	pET9b	this work
pMZ114	EcFtsA (1-405)	no	Kan	T7	pET9b	this work
pSZ49	EcFtsA (1-405)	mCherry	Amp	T7	pQW310	this work
pSZ50a	BsFtsA (1-425)	mCherry	Amp	T7	pQW310	this work
pSZ50b	BsFtsA_K145A (1-425)	mCherry	Amp	T7	pQW310	this work
pSZ50c	BsFtsA_M147E (1-425)	mCherry	Amp	T7	pQW310	this work
pSZ50d	BsFtsA_I278K (1-425)	mCherry	Amp	T7	pQW310	this work
pSZ50e	BsFtsA _S46F (1-425)	mCherry	Amp	T7	pQW310	this work
pSZ61a	BsFtsA (1-440)	no	Amp/Spc	Pspac	pAPNC213	this work
pSZ61b	BsFtsA_K145A (1-440)	no	Amp/Spc	Pspac	pAPNC213	this work
pSZ61c	BsFtsA_M147E (1-440)	no	Amp/Spc	Pspac	pAPNC213	this work
pSZ61d	BsFtsA_I278K (1-440)	no	Amp/Spc	Pspac	pAPNC213	this work
pSZ61e	BsFtsA _S46F (1-440)	no	Amp/Spc	Pspac	pAPNC213	this work
pSZ61f	BsFtsA_Q87Stop (1-440)	no	Amp/Spc	Pspac	pAPNC213	this work

Strains

strain	genotype	reference
Escherichia coli C41 (DE3)	BL21(DE3) derivative	(Miroux & Walker, 1996)
Bacillus subtilis S62	*ftsA279 trpC2 metE3 rpoB2*	(Karmazyn-Campelli et al., 1992)
Bacillus subtilis S62C	*ftsA279 trpC2 metE3 rpoB2 aprE::Pspac-ftsaK145A*	this work
Bacillus subtilis S62D	*ftsA279 trpC2 metE3 rpoB2 aprE::Pspac-ftsaM147E*	this work
Bacillus subtilis S62E	*ftsA279 trpC2 metE3 rpoB2 aprE::Pspac-ftsaI278K*	this work
Bacillus subtilis S62F	*ftsA279 trpC2 metE3 rpoB2 aprE::Pspac-ftsaQ87End*	this work
Bacillus subtilis S62G	*ftsA279 trpC2 metE3 rpoB2 aprE::Pspac-ftsa*	this work
Bacillus subtilis S62H	*ftsA279 trpC2 metE3 rpoB2 aprE::Pspac-ftsaS46F*	this work

Appendix B

Growth media

MD medium

Prepare 10x PC stock: (per litre)

K_2HPO_4	107 g
KH_2PO_4	60 g
$Na_3Citrate \times 5H_2O$	10 g

Then to make MD medium: (per 10 ml)

10x PC	1 ml
20% glucose	1 ml
L-tryptophan (2 mg/ml)	250 µl
Ferric ammonium citrate (2.2 mg/ml)	50 µl
L-aspartate (50 mg/ml)	500 µl
$MgSO_4$	30 µl

Adjust pH to 7.0 with KOH and membrane-filter.

MOPS medium

Make the following solutions:

A)

1.0 M MOPS
0.1 M Tricine

Buffer with KOH to pH 8.0

B)

1 mM $FeCl_2$

C)

1 M $CaCl_2$

D)

1 M $MgSO_4$

E)

20 mM H_3BO_3

5 mM $CoCl_2$

2 mM $CuCl_2$

10 mM $MnCl_2$

2 mM $ZnCl_2$

2 mM Na_2MoO_4

F)

4 M NaCl

G)

Thiamine	0.5 g/100 ml
d-Biotin	0.1 g/100 ml
choline chloride	0.1 g/100 ml
Folic acid	0.1 g/100 ml

To make 10x stock of MOPS mix:

A	800 ml
B	10 ml
C	10 ml
D	10 ml
E	10 ml
F	125 ml

To use:

Dilute 10x stock into $^{2}H_2O$ and sterilise. Add $^{15}NH_4Cl$ (20 mM final concentration), KPi (4 mM) and 0.4% ^{13}C glucose and relevant antibiotics. Add 1 ml of vitamin solution (G) per litre of media.

2xTY

tryptone	16 g
yeast extract	10 g
NaCl	5 g

make up to 1 litre with MiliQ water

pH 7.4

TYE agar plates

agar	15 g
NaCl	8 g

tryptone 10 g

yeast extract 5 g

make up to 1 litre with MiliQ water

pH 7.4

Buffers

1x SDS running buffer

Tris 30 g

glycine 144 g

SDS 10 g

make up to 10 litres with distiled water

Staining solution (for SDS-PAGE)

50% ethanol

10% acetic acid

0.5% PAGE blue 83

Destaining solution (for SDS-PAGE)

20% ethanol

10% acetic acid

10x TBE

Tris 108 g

$Na_2EDTA \times 2H_2O$	903 g
boric acid	55 g

make up to 1 litre with MiliQ water

8x DNA loading buffer

40% sucrose

0.25% bromophenol blue

Protein loading buffer

Tris	0.6 g
DTT	0.77 g
SDS	2 g
Sucrose	10 g
EDTA	0.095 g

0.25% bromophenol blue

make up to 50 ml with MiliQ water and adjust to pH 6.8

Appendix C

X-ray data collection

a) Crystals of TmFtsA in complex with the FtsZ peptide that were used for data collection.

b) A representative diffraction pattern from these crystals.

a

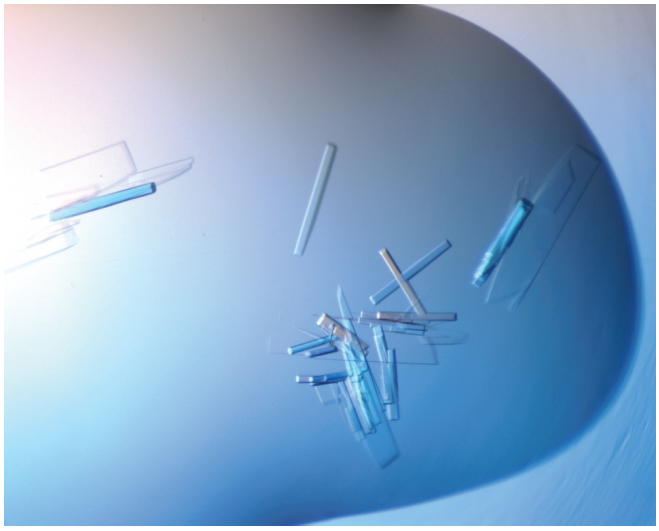

b

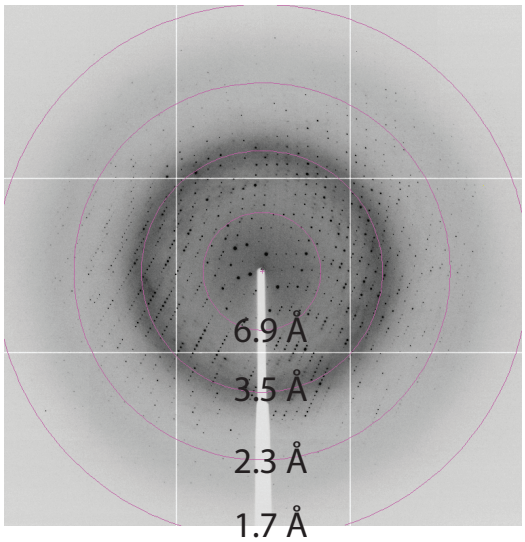

Table 1. Data collection and refinement

	T. maritima FtsA, UNIPROT **Q9WZU0** + *T. maritima* FtsZ peptide 336-EGDIPAIYRYGLEGLL-351 +ATP	*T. maritima* FtsA, UNIPROT **Q9WZU0** + ATPγS
Data collection		
Space group	$P2_1$	$P2_1$
Cell dimensions		
a, *b*, *c* (Å)	56.72, 75.72, 100.27	48.00, 64.59, 73.00
β (°)	93.64	102.93
Resolution (Å)	1.80 (1.90-1.80)	1.80 (1.90-1.80)
R_{merge}	0.072 (0.578)	0.073 (0.329)
$I / \sigma I$	10 (2.4)	10.6 (3.6)
Completeness (%)	99.8 (100)	99.6 (99.9)
Redundancy	3.6 (3.7)	3.5 (3.6)
Refinement		
Resolution (Å)	1.8	1.8
No. reflections	74365	38267
R_{work} / R_{free}	0.21/0.24	0.19/0.23
Model:		
Protein	FtsA: A 7-27, 32-319, 328-390 B 7-27, 29-74, 77-322, 327-390 FtsZ: C 338-351 D 337-351	FtsA: 7-392
ATPγS	-	1
ATP	2	-
Mg^{2+}	-	1
Waters	459	201
B-factors (Å^2)		
Protein	34.70	32.65
ATPγS	-	31.62
ATP	35.04	-
Mg^{2+}	-	52.30
Water	41.46	43.26
R.m.s. deviations		
Bond lengths (Å)	0.007	0.024
Bond angles (°)	1.078	2.179
Ramachandran (%)	91.2	91.4
PDB ID	4A2A	4A2B

Crystallography

Why do we need to use X-rays and protein crystals?

Seeing is believing, and this is why mankind has always endeavoured to image objects that are not visible with a naked eye. This all started when Antonie van Leeuwenhoek visualized microorganisms, whose size falls into the micrometer range, with a light microscope. Some 250 years later, electron microscopy and X-ray crystallography resolve sub-cellular and atomic details of living organisms.

In order to be seen, an object has to diffract electromagnetic radiation and this is only possible when the wavelength is no larger than the object. For instance, visible light (400 – 700 nm) cannot image individual atoms. The X-ray range of electromagnetic radiation comes to the rescue. X-rays have a wavelength in the range of 0.01 to 10 nm (0.1 – 100 Å) so they are diffracted by even the smallest molecules. The atoms comprising protein molecules are 1 – 2 Å apart. However, it is not possible to obtain a diffraction pattern of a single molecule, since it scatters X-rays very weakly. In contrast, a crystal contains many ordered, identically oriented molecules and under certain circumstances they might diffract in phase in order to produce a strong and detectable pattern.

Steps in a crystal structure determination

X-ray protein crystallography entails growing crystals of the purified protein, recording the diffraction pattern of X-ray beams scattered by the crystal(s), processing the collected data in a computer which simulates an image-reconstructing lens (there are no X-ray-focusing lenses, except of Fresnel lenses, whose resolution is limited to about 40 nm) and finally interpretation of the electron density map and building a molecular model.

Diffraction and coordinate systems in crystallography

Crystallographic data collection results in a diffraction pattern consisting of reflections. The positions and intensities of these reflections contain the information

Figure App C1. Principles of crystallography.

a) Reciprocal lattice. The dimensions of the reciprocal lattice are inverse of the real system (modified from www.ruppweb.org).
b) Bragg diffraction. Wave augmentation occurs when a ray's extra path length $2d \sin\theta$ equals an integer multiple of the wavelength (modified from www.wikipedia.org).

Figure App C1

a

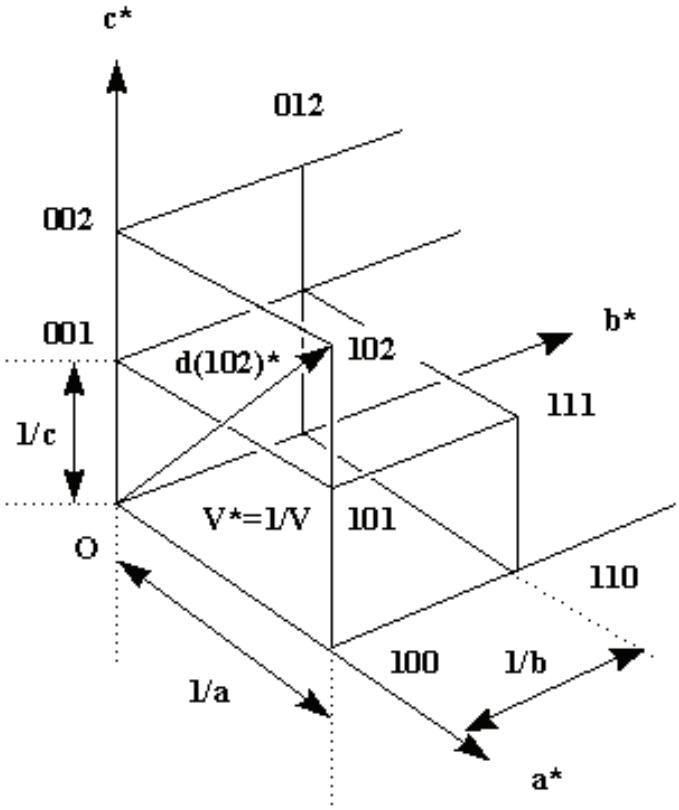

b

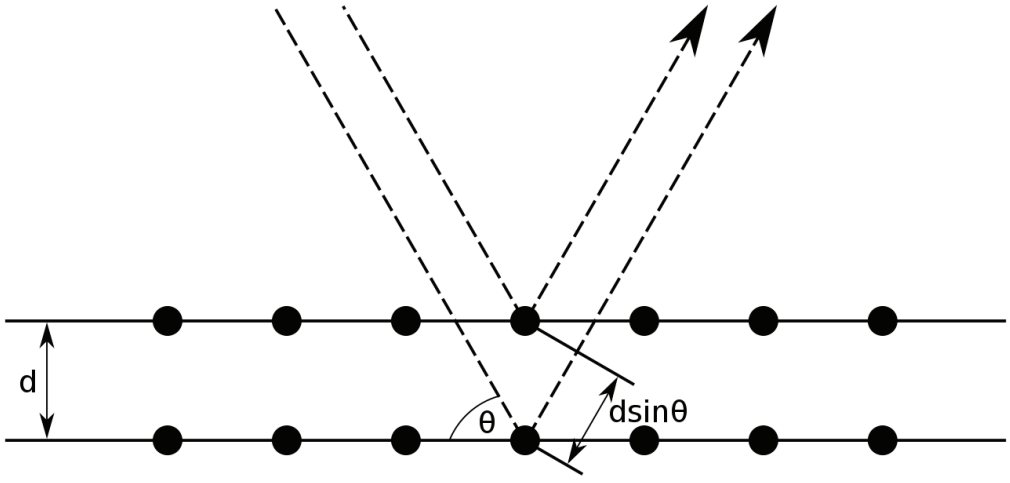

that is required to determine the structure. The spacing of the spots reflects the spacing of unit cells, which are crystal's building blocks. This relationship is inverse and this is why the crystalline lattice is called the real lattice and the lattice of reflections the reciprocal lattice. Each reflection is assigned three indices hkl and the intensity I_{hkl}. Furthermore, dimensions of reciprocal space are expressed in the units $Å^{-1}$ (Fig. App C1a).

Wave and diffraction theory

X-rays are electromagnetic waves and can be described by a periodic function such as:

$$f(x) = Fcos2\pi(hx + \alpha) \qquad \text{Eq. 1}$$

f(x) – vertical height of the wave at any position *x*, F – amplitude, *h* – frequency, α – phase of the wave. Also, waves can be represented as complex vectors. Then, the length of the vector is the amplitude and the angle is the phase (Fig. App C4a).

Each reflection is the product of diffraction from the molecules in the unit cell: in other words, each atom present in the unit cell contributes to each diffracted ray, so each spot can be described as the sum of the contributions of all scatterers in the unit cell in terms of wave theory. Such a sum is called the structure factor F_{hkl} and is a wave formed by many individual waves. For a unit cell containing *n* atoms the structure factor can be described as follows:

$$F_{hkl} = \sum_{j=1}^{n} f_j e^{2\pi i(hx_j + ky_j + lz_j)} \qquad \text{Eq. 2}$$

The term f_j is called the scattering factor and depends on the value of the atomic number Z. Moreover, as mentioned before, structure factors are defined in reciprocal space and they might be connected to electron density, found in the real space, through the Fourier transform (FT):

$$F_{hkl} = \int_x \int_y \int_z \rho(x,y,z)\, e^{2\pi i(hx+ky+lz)} dxdydz \qquad \text{Eq. 3}$$

where $\rho(x,y,z)$ is a value for electron density at every position *x,y,z* in the unit cell.

Because the Fourier transformation is reversible, one can write the electron density as:

$$\rho(x,y,z) = \frac{1}{V}\sum_h \sum_k \sum_l F_{hkl} e^{-2\pi i(hx+ky+lz)} \quad \text{Eq. 4}$$

This is a sum rather than an integral because structure factors are discrete rather than continuous values. Structure factors are complex numbers and can be dissected into its amplitudes $|F_{hkl}|$ and phases α_{hkl}. Consequently, electron density might also be represented as a function of intensities and phases.

$$\rho(x,y,z) = \frac{1}{V}\sum_h \sum_k \sum_l |F_{hkl}| e^{-2\pi i(hx+ky+lz-\alpha'_{hkl})} \quad \text{Eq. 5}$$

where $\alpha = 2\pi\alpha'_{hkl}$.

In order to simulate the effect of a lens, which is to perform the Fourier transformation on a set of structure factors, all the components have to be known. Amplitude |F| is proportional to $(I_{hkl})^{1/2}$, which is measureable. Also, the position *hkl* of each reflection specifies its frequency along the *x, y* and *z* axes, respectively. Only missing is the phase α that is not recorded on any kind of detector and it has to be calculated for every reflection. This is the so-called phase problem of crystallography.

Collecting diffraction data is a crucial step in X-ray analysis. Reflections appear only under certain conditions. It has been shown by W.L. Bragg that a set of parallel planes with an index (*hkl)* and spacing d_{hkl} produces a spot when incident X-rays of wavelength λ are reflected at an angle θ and fulfills the equation:

$$2d_{hkl}sin\theta = n\lambda \quad \text{Eq. 6}$$

This is because rays reflected from two successive planes have to be in phase with each other, which means the difference in path length for these rays has to be equal to an integral number of wavelengths (Fig. App C1b). Bragg's law also implies that large unit cells give reflections at small angles, since $sin\theta$ is proportional to $1/d_{hkl}$.

Reflections occupy the reciprocal lattice. To find a spot in reciprocal space, one has to draw a vector of length $1/d_{hkl}$ from the origin, which is normal to the plane (*hkl)*. The head of the vector indicates the reciprocal lattice point *hkl*. The reciprocal lattice is

Figure App C2. Ewald sphere.

a) Rotating the crystal triggers rotation of the reciprocal lattice. In turn, some reciprocal lattice points will move through the Ewald sphere (modified from www.ruppweb.org).
b) Reciprocal lattice point has to move through the Ewald sphere and must lie within the resolution sphere of the detector in order to yield a reflection that will be recorded (modified from www.ruppweb.org).

Figure App C2

a

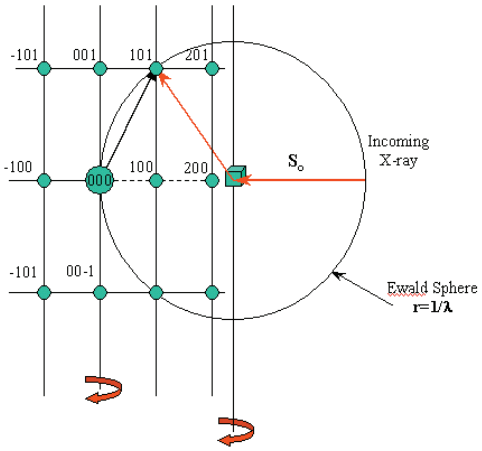

b

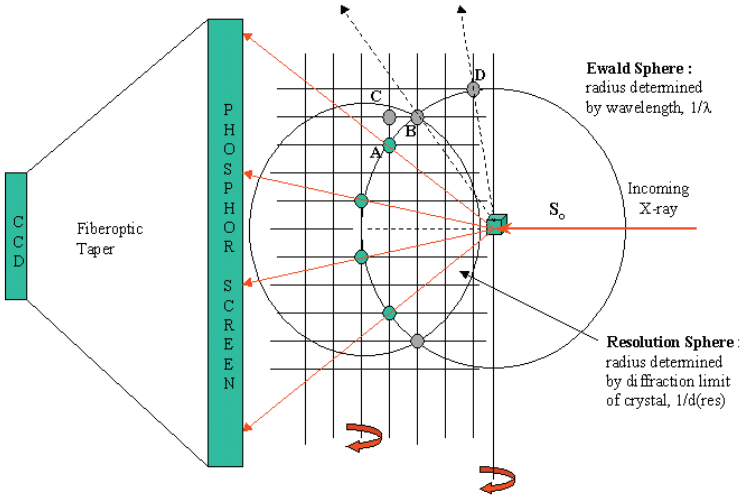

linked to the crystal, so when the crystal rotates, the reciprocal lattice tumbles as well. What sort of requirements has to be met in reciprocal space in order to obtain a diffraction spot? The Ewald sphere of radius 1/λ with the crystal in the middle might provide the answer. As the crystal is rotated, various reciprocal-lattice points cross the Ewald sphere and at that point they produce reflections with indices *hkl* (Fig. App C2a, b). The number of measurable reflections is limited to a distance of 2/λ from the origin, since any point within this limiting sphere can be rotated into contact with the Ewald sphere. This can produce an enormous amount of data, even from a moderate-sized crystal. Luckily, because of symmetry, not all reflections are unique. For instance, Friedel's law says that intensity of each reflection *hkl* is identical to the intensity of reflection $\overline{hkl}$ (Fig. App C4b). It implies that all reciprocal lattices possess a center of symmetry. This is why data collection around 180° of any reciprocal lattice axis will record all unique reflections. If there are any additional elements of symmetry in the crystal, the total angle of data collection might be reduced further, down to 1/48 for the space group P432.

Solving the phase problem

The main goal of X-ray crystallography is to calculate the function whose graph is the electron density map. In order to do so one has to know every reflection's phase. It is of crucial importance to accurately determine the phases since they contain relatively more information than the intensities (Fig. App C3).

At the moment there are three common methods to overcome this problem: isomorphous replacement, anomalous scattering and molecular replacement.

Isomorphous replacement

As mentioned before, every atom contributes to every reflection and the phase of a diffracted ray depends only on the atomic coordinates of the atom. So if one adds an atom, or a few of them to identical sites in the unit cell, and these atoms are sufficiently strong diffractors (for instance mercury, lead or gold), it will be possible to observe a slight perturbation in the diffraction pattern and this will allow an initial estimates of phases to be obtained.

Figure App C3

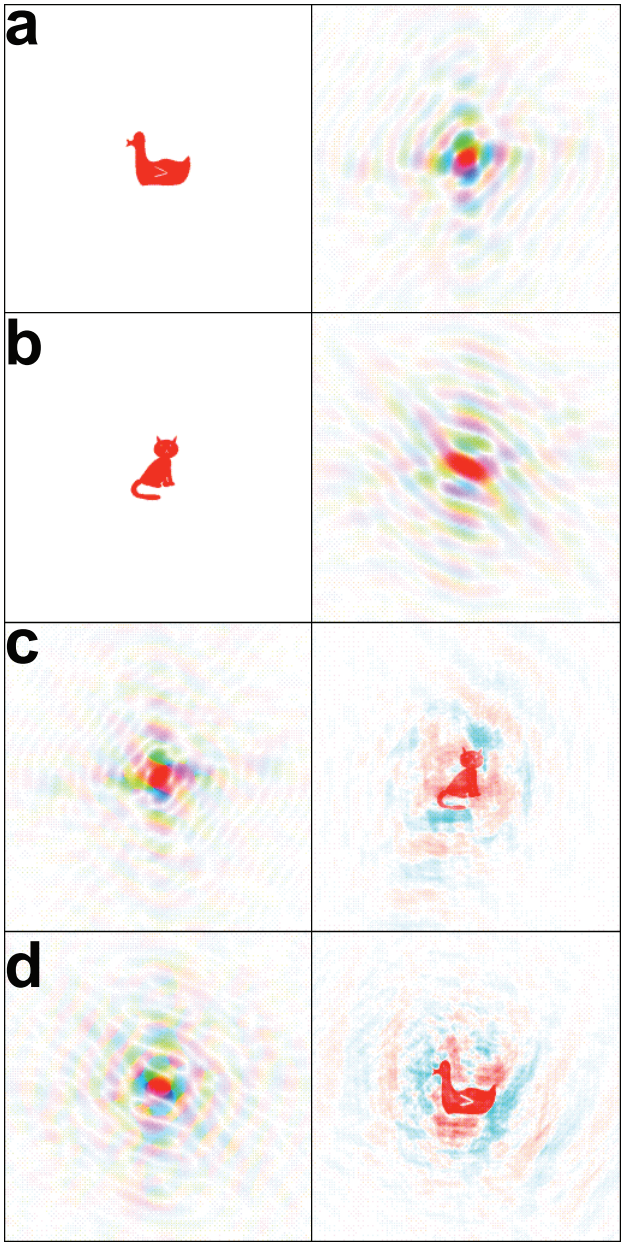

Figure App C3. The importance of phases. A duck image (a, left) has been Fourier transformed (a, right). The same procedure has been applied to a cat (b). Finally, the amplitudes from the duck transform were combined with the phases from the cat transform (c, left) and back-transformed in order to get the cat (c, right). The same thing was done other way round and the result was the duck (d). A significant phase contribution in each case is clearly visible (modified from www.ysbl.york.ac.uk/~cowtan/fourier/magic.html).

Figure App C4. Vector representation of structure factors.

a) Structure factors might be represented as vectors $A + iB$, and the length of vector F_{hkl} is $|F_{hkl}|$, therefore proportional to $(I_{hkl})^{1/2}$. The angle between F_{hkl} and the real axis is the phase angle (modified from www.ruppweb.org).
b) Structure factors of a Friedel pair. F_{hkl} is the reflection of $F_{\overline{hkl}}$ in the real axis (modified from www.ruppweb.org).

Figure App C4

a

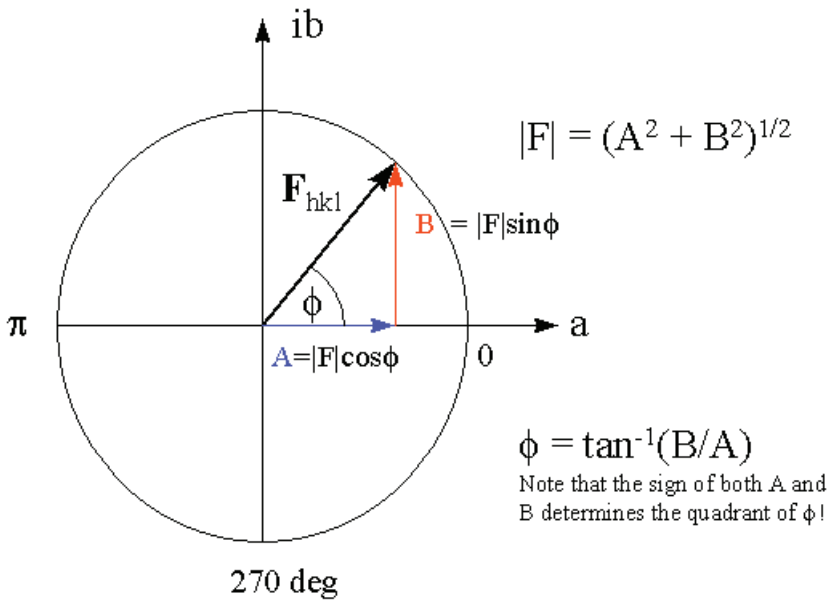

b

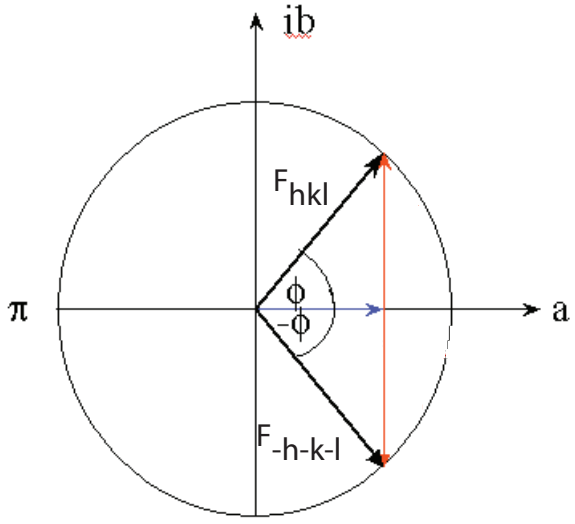

This strategy requires that the derivative crystals are isomorphous with native crystals, which means that the crystal packing and protein conformation remain unchanged. Apart from collecting data from the native crystal, one has to repeat the procedure for the heavy-metal derivative, and very often it involves recording diffraction data for several derivatives. Subtracting a single reflection of amplitude $|F_P|$ (native dataset) from the corresponding reflection of amplitude $|F_{PH}|$ (protein plus heavy atom) yields the amplitude contribution of the heavy atom and this diffraction pattern is relatively simple. Then it is easy to find the location of the heavy atom in the unit cell and subsequently determine the remaining phases.

Locating heavy atoms gives tools to calculate the structure factors F_{hkl}, including both amplitudes and phases for all the heavy atoms. The difference Patterson function gives the means to extract the simple diffraction pattern of the heavy atom and solve this simple structure. The difference Patterson function is:

$$\Delta P(u,v,w) = \frac{1}{V}\sum_h \sum_k \sum_l \Delta F_{hkl}^2 e^{-2\pi i(hu+kv+lw)} \qquad \text{Eq. 7}$$

Where $(\Delta F)^2 = (|F_{PH}| - |F_P|)^2$ and the coordinates (u,v,w) represent a vector between atom 1 at (x_1, y_1, z_1) and atom 2 at (x_2, y_2, z_2).

The Patterson function can be easily calculated from collected data since it does not contain phases. The resulting contour map displays peaks at locations corresponding to vectors between atoms. For n atoms there are $n\,(n-1)$ vectors. Usually this diagram is enough to identify positions of the heavy atoms in the unit cell. Sometimes it is possible to make use of unit-cell symmetry and look for vectors connecting symmetry-related atoms, for instance those along a 2_1 axis are connected by a vector $(2x, \left[\frac{1}{2}\right], 2z)$ and lie in the plane called a Harker section.

Once the above procedure is done, one can compute the structure factors F_H (both amplitudes and phases) and subsequently solve the equation:

$$F_P = F_{PH} - F_H \qquad \text{Eq. 8}$$

There are two solutions to this equation and to distinguish between them one has to prepare a second heavy-atom derivative and repeat the whole process (Fig. App C5a). Having determined the phases one can calculate the electron density using Eq. 5.

Anomalous scattering

This aims to solve the phase problem relying on a breakdown of Friedel's law so that the reflection hkl and $\bar{h}\bar{k}\bar{l}$ are not equal in intensity (Fig. App C5b). This is achieved by anomalous scattering as some heavy atoms absorb X-rays at specified wavelengths, which are called absorption edges. The structure factor for the heavy-atom derivative recorded at λ_2, where anomalous scattering occurs, might be described as:

$$F_{PH}^{\lambda 2} = F_{PH}^{\lambda 1} + \Delta F_r + \Delta F_i \qquad \text{Eq. 9}$$

where $F_{PH}^{\lambda 1}$ is a structure factor measured at λ_1, where there is no anomalous scattering and ΔF_r and ΔF_i are real and imaginary contributions to anomalous scattering, respectively.

For Friedel pairs, in the absence of anomalous scattering the following is true: $|F_{hkl}| = |F_{\overline{hkl}}|$ and $\alpha_{hkl} = -\alpha_{\overline{hkl}}$. This implies that $F_{PH}^{\lambda 1-}$ and ΔF_r^- are reflections of $F_{PH}^{\lambda 1+}$ and ΔF_r^+ in the real axis, respectively. However, the imaginary contribution ΔF_i^- is obtained by reflecting ΔF_i^+ in the real axis and then reversing its sign. This triggers the fact that under anomalous scattering that Friedel pairs are no longer equal in intensity, nor opposite in phase and from that one can extract phase information.

Once the heavy atom is located, the phases for ΔF_r and ΔF_i can be computed and subsequently Eq. 9 solved for $F_{PH}^{\lambda 1}$. Unfortunately, there are two solutions to this equation and to sort this out on has to reflect $F_{PH}^{\lambda 2-}$ across the real axis to obtain a second equation involving $F_{PH}^{\lambda 1+}$. Having found F_{PH} and F_H with both phases and amplitudes it is easy to obtain F_P with Eq. 8 (Fig. App C5c).

Molecular replacement

When a structure of a homologous protein is available, one can use the phases from structure factors of the known protein to initially estimate phases for a new protein. The known protein is called a phasing model and the new protein is a target (Fig. App C5d).

Figure App C5. Solving the phase problem.

a) Multiple isomorphous replacement. Two or more heavy-atom derivatives are enough to solve the phase problem since the three circles intersect at one point (modified from Taylor, 2003).
b) Breakdown of Friedel's law when an anomalous scatterer is present (modified from Taylor, 2003).
c) Harker construction for phasing using an anomalous scatterer (modified from Taylor, 2003).
d) Molecular replacement. Fourier transformation of a cat with a tail (top left) gives us only amplitudes (top right). In addition to these amplitudes we have phases from a tailless cat (middle). One can restore the image of the cat combining the known magnitudes and phases. This is analogous to solving a structure of the protein with a ligand (cat's tail) when the structure of the protein itself is available (modified from www.ysbl.york.ac.uk/~cowtan/fourier/magic.html).

Figure App C5

a

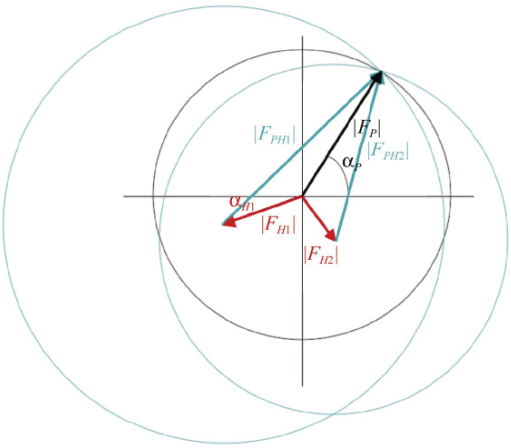

b

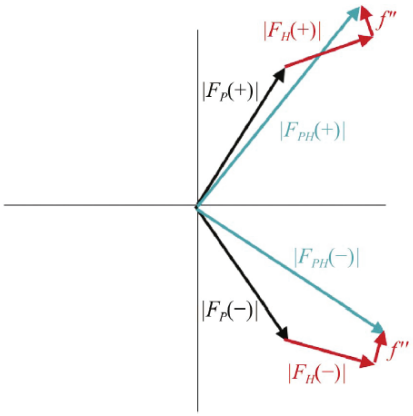

c

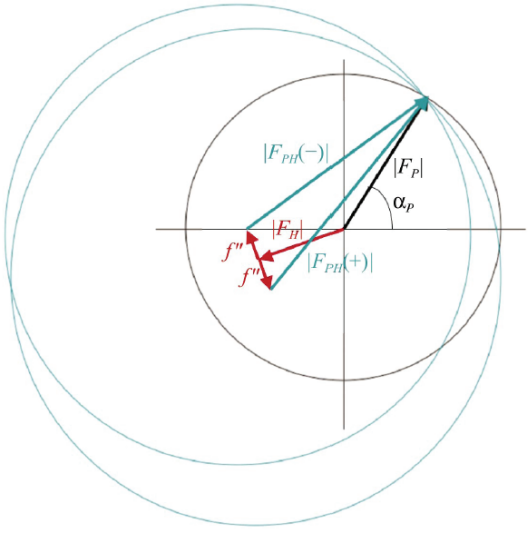

d

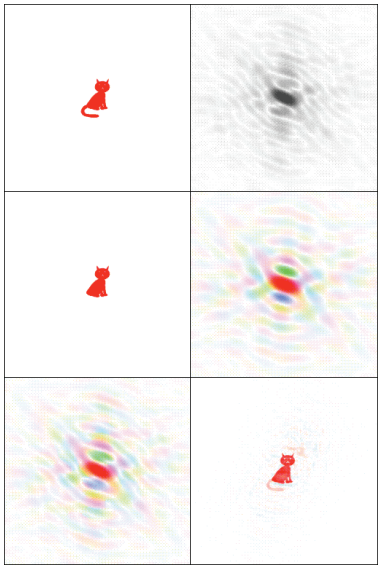

If the phasing model and the target are isomorphous, the procedure is straightforward and the phases from the known protein may be used directly to compute the electron density of the new protein using the equation:

$$\rho(x,y,z) = \frac{1}{V}\sum_h \sum_k \sum_l |F_{hkl}^{target}| e^{-2\pi i(hx+ky+lz-\alpha_{hkl}^{'model})} \quad \text{Eq. 10}$$

Since the phases depend on the location of atoms in the unit cell, the phasing is more difficult if the phasing model is not isomorphous with the target. In this case, to make use of the model phases, one has to superimpose the structure of the model on the structure of the target protein in its unit cell. How can this be achieved? Obviously, it might be feasible to search all of the orientations and positions of the model in the new unit cell. However, this would yield an enormous number of calculations. This is why the procedure has been simplified and divided into two searches: for the best orientation and for the best position. Then, a six-variable problem (three angle of rotation and three coordinates along the x, y and z axes) becomes two three-variable problems. Comparison of the orientations is performed by calculating a rotation function. It simply estimates the correlation between Patterson maps for the target and model proteins in various orientations:

$$R(\phi,\varphi,\chi) = \int_{u,v,w} P^{target}(u,v,w) P^{model}\{(u,v,w)\times[\phi,\varphi,\chi]\} dudvdw \quad \text{Eq. 11}$$

This function will display maxima when the two Patterson maps overlap and this will mark the best orientation for placing the phasing model. Once the model is oriented correctly, the translation search is carried out in order to find the position in the unit cell. This might be achieved by a brute-force search in real space where the comparison between the model and the native data structure factors is done and expressed as the R-factor:

$$R = \frac{\sum ||F_{obs}| - |F_{calc}||}{\sum |F_{obs}|} \quad \text{Eq. 12}$$

In ideal situation all the differences equal zero and R is zero. Usually for proteins R-values of 0.3-0.4 give good initial phase estimates. However, this approach is computationally expensive and fast translation functions based on fast Fourier transform techniques are now commonly in use. They, in turn, compare the observed

Fourier coefficients with the ones calculated from the transform of the intermolecular vector set.

Density, refinement and validation

Once the phase problem is solved one can apply Eq. 5 to calculate the electron density map. These initial phases are only rough estimates so they need some improvement. The refinement process might occur in real space (adding information to the map, improving the model) and in reciprocal space (improving phases). Atoms are fitted into the map and then structure factors might be calculated using equation Eq. 2, then the computed phases can be combined with measured amplitudes to obtain new, improved density. Simply modifying the model might bring some new phase information, for instance by adjusting the atomic coordinates. To avoid introducing excessive bias from the model into the density various difference Fourier syntheses have been introduced. They reduce model influence by subtracting $|F_{calc}|$ from some multiple of $|F_{obs}|$. For instance:

$$\rho(x,y,z) = \frac{1}{V}\sum_h \sum_k \sum_l (|F_0| - |F_c|)e^{-2\pi i(hx+ky+lz-\alpha'_{calc})} \qquad \text{Eq. 13}$$

Such a map display can be positive or negative. In the former case it means that some electron density should be added to this region of the model, and the latter indicates that some atoms have to be moved away.

A very easily interpreted map is the $2F_0$-F_c map, whose contours resemble a molecular model and is used for model building. The map is calculated as follows:

$$\rho(x,y,z) = \frac{1}{V}\sum_h \sum_k \sum_l (2|F_0| - |F_c|)e^{-2\pi i(hx+ky+lz-\alpha'_{calc})} \qquad \text{Eq. 14}$$

Using rational chemical knowledge, some constraints (for example fixed values for certain parameters) and restraints (conditions imposed upon the parameters) one can refine the structure to the point where the measured and calculated structure factors converge. A measure of convergence is the residual index, or R-factor defined by Eq. 12. For protein models a reasonable R-factor is about 0.2-0.3.

Appendix D

Publications

Szwedziak, P., Wang, Q., Freund, S. M. V. & Löwe, J. (2012). FtsA forms actin-like filaments. *Submitted.*

References

Abramoff, M. D., Magalhaes, P. J. & Ram, S. J. (2004). Image processing with ImageJ. *Biophotonics International*, *11*, 36-42.

Adams, D. W., & Errington, J. (2009). Bacterial cell division: assembly, maintenance and disassembly of the Z ring. *Nat Rev Microbiol*, *7*(9), 642-653.

Adams, P. D., Afonine, P. V., Bunkoczi, G., Chen, V. B., Davis, I. W., Echols, N. et al. (2010). PHENIX: a comprehensive Python-based system for macromolecular structure solution. *Acta Crystallogr D Biol Crystallogr*, *66*(Pt 2), 213-221.

Addinall, S. G., Bi, E., & Lutkenhaus, J. (1996). FtsZ ring formation in fts mutants. *J Bacteriol*, *178*(13), 3877-3884.

Addinall, S. G., & Lutkenhaus, J. (1996a). FtsZ-spirals and -arcs determine the shape of the invaginating septa in some mutants of Escherichia coli. *Mol Microbiol*, *22*, 231-237.

Addinall, S. G., & Lutkenhaus, J. (1996b). FtsA is localized to the septum in an FtsZ-dependent manner. *J Bacteriol*, *178*(24), 7167-7172.

Anagnostopoulos, C. S., J. (1961). Requirements for transformation in *Bacillus subtilis*. *Journal of bacteriology*, *81*, 741-746.

Ayala, J. A., Garrido, T., de Pedro, M. A. & Vicente, M. (1994). Bacterial cell wall. *Elsevier Science Publishers,* 73-101.

Beall, B., & Lutkenhaus, J. (1992). Impaired cell division and sporulation of a Bacillus subtilis strain with the ftsA gene deleted. *J Bacteriol*, *174*(7), 2398-2403.

Ben-Yehuda, S., & Losick, R. (2002). Asymmetric cell division in B. subtilis involves a spiral-like intermediate of the cytokinetic protein FtsZ. *Cell*, *109*(2), 257-266.

Bernander, R., & Ettema, T. J. G. (2010). FtsZ-less cell division in archaea and bacteria. *Current Opinion in Microbiology*, *13*, 747-752.

Bernhardt, T. G., & de Boer, P. A. (2005). SlmA, a nucleoid-associated, FtsZ binding protein required for blocking septal ring assembly over Chromosomes in E. coli. *Mol Cell*, *18*(5), 555-564.

Bi, E., & Lutkenhaus, J. (1991). FtsZ ring structure associated with division in Escherichia coli. *Nature*, *354*, 161-164.

Bork, P., Sander, C., & Valencia, A. (1992). An ATPase domain common to prokaryotic cell cycle proteins, sugar kinases, actin, and hsp70 heat shock proteins. *Proc Natl Acad Sci U S A*, *89*(16), 7290-7294.

Bramhill, D. (1997). Bacterial cell division. *Annu Rev Cell Dev Biol*, *13*, 395-424.

Bramhill, D., & Thompson, C. M. (1994). GTP-dependent polymerization of Escherichia coli FtsZ protein to form tubules. *Proc Natl Acad Sci U S A*, *91*, 5813-5817.

Carettoni, D., Gomez-Puertas, P., Yim, L., Mingorance, J., Massidda, O., Vicente, M. et al. (2003). Phage-display and correlated mutations identify an essential region of subdomain 1C involved in homodimerization of Escherichia coli FtsA. *Proteins*, *50*(2), 192-206.

Dai, K., & Lutkenhaus, J. (1992). The proper ratio of FtsZ to FtsA is required for cell division to occur in Escherichia coli. *J Bacteriol*, *174*(19), 6145-6151.

Davis, B. K. Molecular evolution before the origin of species. *Prog Biophys Mol Biol*, *79*, 77-133.

de Boer, P., Crossley, R., & Rothfield, L. (1992). The essential bacterial cell-division protein FtsZ is a GTPase. *Nature*, *359*, 254-256.

Dewar, S. J., Begg, K. J., & Donachie, W. D. (1992). Inhibition of cell division initiation by an imbalance in the ratio of FtsA to FtsZ. *J Bacteriol*, *174*(19), 6314-6316.

Dominguez-Escobar, J., Chastanet, A., Crevenna, A. H., Fromion, V., Wedlich-Soldner, R., & Carballido-Lopez, R. (2011). Processive movement of MreB-associated cell wall biosynthetic complexes in bacteria. *Science*, *333*, 225-228.

Erickson, H. P. (2000). Dynamin and FtsZ: missing links in mitochondrial and bacterial division. *Journal of Cell Biology*, *148*, 1103-1105.

Erickson, H. P., Anderson, D. E., & Osawa, M. (2010). FtsZ in bacterial cytokinesis: cytoskeleton and force generator all in one. *Microbiology and Molecular Biology Reviews*, *74*, 504-528.

Erickson, H. P., & Osawa, M. (2010). Cell division without FtsZ - a variety of redundant mechanisms. *Mol Microbiol*, *78*, 267-270.

Erickson, H. P., Taylor, D. W., Taylor, K. A., & Bramhill, D. (1996). Bacterial cell division protein FtsZ assembles into protofilament sheets and minirings, structural homiologs of tubulin polymers. *Proc Natl Acad Sci U S A*, *93*, 519-523.

Errington, J., Daniel, R. A., & Scheffers, D. J. (2003). Cytokinesis in bacteria. *Microbiol Mol Biol Rev*, *67*(1), 52-65.

Feucht, A., Lucet, I., Yudkin, M. D., & Errington, J. (2001). Cytological and biochemical characterization of the FtsA cell division protein of Bacillus subtilis. *Mol Microbiol*, *40*(1), 115-125.

Galkin, V. E., Orlova, A., Rivera, C., Mullins, R. D., & Egelman, E. H. (2009). Structural polymoprhism of the ParM filament and dynamic instability. *Structure*, *17*, 1253-1264.

Garner, E. C., Bernard, R., Wang, W., Zhuang, X., Rudner, D. Z., & Mitchison, T. (2011). Coupled, circumferential motions of the cell wall synthesis machinery and MreB filaments in B. subtilis. *Science*, *333*, 222-225.

Gasper, R., & Löwe, J. (2011). Das bakterielle Zytoskelett. *Biospektrum*, *17*, 396-398.

Gayda, R. C., Henk, M. C., & Leong, D. (1992). C-shaped cells caused by expression of an ftsA mutation in Escherichia coli. *J Bacteriol*, *174*(16), 5362-5370.

Geissler, B., Elraheb, D., & Margolin, W. (2003). A gain-of-function mutation in ftsA bypasses the requirement for the essential cell division gene zipA in Escherichia coli. *Proc Natl Acad Sci U S A*, *100*(7), 4197-4202.

Goddard, T. D., & Kneller, D. G. *SPARKY 3.* University of California, San Francisco.

Goehring, N. W., & Beckwith, J. (2005). Diverse paths to midcell: assembly of the bacterial cell division machinery. *Current Biology*, *15*, 514-526.

Goley, E. D., Yeh, Y. C., Hong, S. H., Fero, M. J., Abeliuk, E., McAdams, H. H. et al. (2011). Assembly of the Caulobacter cell division machine. *Mol Microbiol*, *80*(6), 1680-1698.

Graumann, P. L. (2007). Cytoskeletal elements in bacteria. *Annu Rev Microbiol*, *61*, 589-618.

Guntert, P., Salzmann, M., Braun, D., & Wuthrich, K. (2000). Sequence-specific NMR assignment of proteins by global fragment mapping with the program MAPPER. *J Biomol NMR*, *18*(2), 129-137.

Haney, S. A., Glasfeld, E., Hale, C., Keeney, D., He, Z., & de Boer, P. (2001). Genetic analysis of the Escherichia coli FtsZ.ZipA interaction in the yeast two-hybrid system. Characterization of FtsZ residues essential for the interactions with ZipA and with FtsA. *J Biol Chem*, *276*(15), 11980-11987.

Hirota, V., Ryter, A., & Jacob, F. (1968). Thermosensitive mutants of E. coli affected in the process of DNA synthesis and cellular division. *Cold Spring Harbor Symp Quant Biol*, *33*, 677-693.

Ikeda, M., Sato, T., Wachi, M., Jung, H. K., & Ishino, F. (1989). Structural similarity among Escherichia coli FtsW and RodA proteins and Bacillus subtilis SpoVE protein, which function in cell division, cell elongaton, and spore formation, respectively. *J Bacteriol*, *171*, 6375-6378.

Jensen, S. O., Thompson, L. S., & Harry, E. J. (2005). Cell division in Bacillus subtilis: FtsZ and FtsA association is Z-ring independent, and FtsA is required for efficient midcell Z-Ring assembly. *J Bacteriol*, *187*(18), 6536-6544.

Jimenez, M., Martos, A., Vicente, M., & Rivas, G. (2011). Reconstitution and organization of Escherichia coli proto-ring elements (FtsZ and FtsA) inside giant unilamellar vesicles obtained from bacterial inner membranes. *J Biol Chem*, *286*(13), 11236-11241.

Jones, L. J., Carballido-Lopez, R., & Errington, J. (2001). Control of cell shape in bacteria: helical, actin-like filaments in Bacillus subtilis. *Cell*, *104*, 913-922.

Jones, L. J., Carballido-Lopez, R., & Errington, J. (2007). Evolution of the cytoskeleton. *BioEssays*, *29*, 668-677.

Jung, Y. S., & Zweckstetter, M. (2004). Mars -- robust automatic backbone assignment of proteins. *J Biomol NMR*, *30*(1), 11-23.

Kabsch, W., & Holmes, K. C. (1995). The actin fold. *FASEB J*, *9*(2), 167-174.

Karimova, G., Dautin, N., & Ladant, D. (2005). Interaction network among Escherichia coli membrane proteins involved in cell division as revealed by bacterial two-hybrid analysis. *J Bacteriol*, *187*(7), 2233-2243.

Karmazyn-Campelli, C., Fluss, L., Leighton, T., & Stragier, P. (1992). The spoIIN279(ts) mutation affects the FtsA protein of Bacillus subtilis. *Biochimie*, *74*(7-8), 689-694.

Kawarabayasi, Y., Hino, Y., Horikawa, H., Yamazaki, S., & Haikawa, Y. (1999). Complete genome sequence of an aerobic hyper-thermophilic crenarchaein, Aeropyrum pernix K1. *DNA Res*, *6*, 83-101.

Kelly, A. J., Sackett, M. J., Din, N., Quardokus, E., & Brun, Y. V. (1998). Cell cycle-dependent transcriptional and proteolytic regulation of FtsZ in Caulobacter. *Genes Dev*, *12*, 880-893.

Kiefel, B. R., Gilson, P. R., & Beech, P. L. (2004). Diverse eukaryotes have retained mitochondrial homologues of the bacterial division protein FtsZ. *Protist*, *155*, 105-115.

Kremer, J. R., Mastronarde, D. N., & McIntosh, J. R. (1996). Computer visualization of three-dimensional image data using IMOD. *J Struct Biol*, *116*(1), 71-76.

Laemmli, U. K. (1970). Cleavage if structural proteins during the assembly of the head of bacteriophage T4. *Nature*, *227*, 680-685.

Lara, B., Rico, A. I., Petruzzelli, S., Santona, A., Dumas, J., Biton, J. et al. (2005). Cell division in cocci: localization and properties of the Streptococcus pneumoniae FtsA protein. *Mol Microbiol*, *55*(3), 699-711.

Leaver, M., Dominguez-Cuevas, P., Coxhead, J. M., Daniel, R. A., & Errington, J. (2009). Life without a wall or division machine in Bacillus subtilis. *Nature*, *457*, 849-853.

Levin, P. A., & Losick, R. (1996). Transcription factor Spo0A switches the localization of the cell division protein FtsZ from a medial to a bipolar pattern in Bacillus subtilis. *Genes Dev*, *10*, 478-488.

Li, Z., Trimble, M. J., Brun, Y. V., & Jensen, G. J. (2007). The structure of FtsZ filaments in vivo suggests a force-generating role in cell division. *EMBO J*, *26*(22), 4694-4708.

Lindas, A. C., Karlsson, E. A., Lindgren, M. T., Etterna, T. J., & Bernander, R. (2008). A unique cell division machinery in the Archaea. *Proc Natl Acad Sci U S A*, *105*, 18942-18946.

Lluch-Senar, M., Querol, E., & Pinol, J. (2010). Cell division in a minimal bacterium in the absence of ftsZ. *Mol Microbiol*, *78*, 278-289.

Longtine, M. S., & Bi, E. (2003). Regulation of septin organization and function in yeast. *Trends Cell Biol*, *13*, 403-409.

Löwe, J., & Amos, L. A. (1998). Crystal structure of the bacterial cell-division protein FtsZ. *Nature*, *391*, 203-206.

Löwe, J., & Amos, L. A. (2009). Evolution of cytomotive filaments: the cytoskeleton from prokaryotes to eukaryotes. *The International Journal of Biochemistry and Cell Biology*, *41*, 323-329.

Löwe, J., Ellonen, A., Allen, M. D., Atkinson, C., Sherratt, D. J., & Grainge, I. (2008). Molecular mechanism of sequence-directed DNA loading and translocation by FtsK. *Mol Cell*, *31*, 458-509.

Löwe, J., & van den Ent, F. (2001). Conserved sequence motif at the C-terminus of the bacterial cell-division protein FtsA. *Biochimie*, *83*(1), 117-120.

Lutkenhaus, J. F., Wolf-Watz, H., & Donachie, W. D. (1980). Organization of genes in the ftsA-envA region of the Escherichia coli genetic map and identification of a new fts locus (ftsZ). *J Bacteriol*, *142*(2), 615-620.

Ma, X., Ehrhardt, D. W., & Margolin, W. (1996). Colocalization of cell division proteins FtsZ and FtsA to cytoskeletal structures in living Escherichia coli cells by using green fluorescent protein. *Proc Natl Acad Sci U S A*, *93*(23), 12998-13003.

Ma, X., & Margolin, W. (1999). Genetic and functional analyses of the conserved C-terminal core domain of Escherichia coli FtsZ. *J Bacteriol*, *181*(24), 7531-7544.

Ma, X., Sun, Q., Wang, R., Singh, G., Jonietz, E. L., & Margolin, W. (1997). Interactions between heterologous FtsA and FtsZ proteins at the FtsZ ring. *J Bacteriol*, *179*(21), 6788-6797.

Martin, M. E., Trimble, M. J., & Brun, Y. V. (2004). Cell cycle-dependent abundance, stability and localization of FtsA and FtsQ in Caulobacter crescentus. *Mol Microbiol*, *54*(1), 60-74.

Martin, W., Rujan, T., Richly, E., Hansen, A., Comelsen, S., Lins, T. et al. (2002). Evolutionary analysis of Arabidopsis, cyanobacterial, and chloroplast genomes reveals plastid phylogeny and thousands of cyanobacterial genes in the nucleus. *Proc Natl Acad Sci U S A*, *99*, 12246-12251.

Mastronarde, D. N. (2005). Automated electron microscope tomography using robust prediction of specimen movements. *J Struct Biol*, *152*(1), 36-51.

McAdams, H. H., & Shapiro, L. (2009). System-level design of bacterial cell cycle control. *FEBS Letters*, *583*, 3984-3991.

McCoy, A. J., Grosse-Kunstleve, R. W., Adams, P. D., Winn, M. D., Storoni, L. C., & Read, R. J. (2007). Phaser crystallographic software. *J Appl Crystallogr*, *40*(Pt 4), 658-674.

Miroux, B., & Walker, J. E. (1996). Over-production of proteins in Escherichia coli: mutant hosts that allow synthesis of some membrane proteins and globular proteins at high levels. *J Mol Biol*, *260*(3), 289-298.

Mohammadi, T., van Dam, V., Sijbrandi, R., Vernet, T., Zapun, A., Bouhss, A. et al. (2011). Identification of FtsW as a transporter of lipid-linked cell wall precursors across the membrane. *EMBO J*, *8*, 1425-1432.

Moller-Jensen, J., Jensen, R. B., Löwe, J., & Gerdes, K. (2002). Prokaryotic DNA segregation by an actin-like filament. *EMBO J*, *21*, 3119-3127.

Moller-Jensen, J., Ringgaard, S., Mercogliano, C. P., Gerdes, K., & Löwe, J. (2007). Structural analysis of the ParR/parC plasmid partition complex. *EMBO J*, *26*, 4413-4422.

Morimoto, T., Loh, P. C., Hirai, T., Asai, K., Kobayashi, K., Moriya, S. et al. (2002). Six GTP-binding proteins of the Era/Obg family are essential for cell growth in Bacillus subtilis. *Microbiology*, *148*(Pt 11), 3539-3552.

Mosyak, L., Zhang, Y., Glasfeld, E., Haney, S., Stahl, M., Seehra, J. et al. (2000). The bacterial cell-division protein ZipA and its interaction with an FtsZ fragment revealed by X-ray crystallography. *EMBO J*, *19*(13), 3179-3191.

Mukherjee, A., & Lutkenhaus, J. (1994). Guanine nucleotide-dependent assembly of FtsZ into filaments. *Journal of bacteriology*, *176*, 2754-2758.

Murshudov, G. N., Vagin, A. A., & Dodson, E. J. (1997). Refinement of macromolecular structures by the maximum-likelihood method. *Acta Crystallogr D Biol Crystallogr*, *53*(Pt 3), 240-255.

Nanninga, N. (2001). Cytokinesis in prokaryotes and eukaryotes: common principles and different solutions. *Microbiology and Molecular Biology reviews*, *65*, 319-333.

Oda, T., Iwasa, M., Aihara, T., Maeda, Y., & Narita, A. (2009). The nature of the globular- to fibrous-actin transition. *Nature*, *457*, 441-445.

Oliva, M. A., Cordell, S. C., & Löwe, J. (2004). Structural insights into FtsZ protofilament formation. *Nat Struct Mol Biol*, *11*(12), 1243-1250.

Osawa, M., Anderson, D. E., & Erickson, H. P. (2008). Reconstitution of contractile FtsZ rings in liposomes. *Science*, *320*(5877), 792-794.

Osawa, M., Anderson, D. E., & Erickson, H. P. (2009). Curved FtsZ protofilaments generate bending forces on liposome membranes. *EMBO J*, *22*, 3476-3484.

Pelve, E. A., Lindas, A. C., Martens-Habbena, W., de la Torre, J., Stahl, D. A., & Bernander, R. (2011). Cdv-based cell division and cell cycle organization in the thaumarchaeon Nitrosopumilus maritimus. *Mol Microbiol*, *82*, 555-566.

Pichoff, S., & Lutkenhaus, J. (2002). Unique and overlapping roles for ZipA and FtsA in septal ring assembly in Escherichia coli. *EMBO J*, *21*(4), 685-693.

Pichoff, S., & Lutkenhaus, J. (2005). Tethering the Z ring to the membrane through a conserved membrane targeting sequence in FtsA. *Mol Microbiol*, *55*(6), 1722-1734.

Pichoff, S., & Lutkenhaus, J. (2007). Identification of a region of FtsA required for interaction with FtsZ. *Mol Microbiol*, *64*(4), 1129-1138.

Pollard, T. D. (2009). Actin, a central player in cell shape and movement. *Science*, *326*, 1208-1212.

Pollard, T. D. (2010). Mechanics of cytokinesis in eukaryotes. *Current Opinion in Cell Biology*, *22*, 50-56.

Popp, D., & Robinson, R. C. (2011). Many ways to build an actin like filament. *Mol Microbiol*, *80*, 300-308.

Raskin, D. M., & de Boer, P. A. (1999). Rapid pole-to-pole oscillation of a protein required for directing division to the middle of Escherichia coli. *Proc Natl Acad Sci U S A*, *96*(9), 4971-4976.

Rico, A. I., Garcia-Ovalle, M., Mingorance, J., & Vicente, M. (2004). Role of two essential domains of Escherichia coli FtsA in localization and progression of the division ring. *Mol Microbiol*, *53*(5), 1359-1371.

Salje, J., van den Ent, F., de Boer, P., & Löwe, J. (2011). Direct Membrane Binding by Bacterial Actin MreB. *Mol Cell*, *43*(3), 478-487.

Samson, R. Y., Obita, T., Freund, S.M.V., Williams, R.L. & Bell, S.D. (2008). A role for the ESCRT system in cell division in archaea. *Science*, 322. 1710-1713.

Sanchez, M., Valencia, A., Ferrandiz, M. J., Sander, C., & Vicente, M. (1994). Correlation between the structure and biochemical activities of FtsA, an essential cell division protein of the actin family. *EMBO J*, *13*(20), 4919-4925.

Shen, B., & Lutkenhaus, J. (2009). The conserved C-terminal tail of FtsZ is required for the septal localization and division inhibitory activity of MinC(C)/MinD. *Mol Microbiol*, *72*(2), 410-424.

Shen, B., & Lutkenhaus, J. (2010). Examination of the interaction between FtsZ and MinCN in E. coli suggests how MinC disrupts Z rings. *Mol Microbiol*, *75*(5), 1285-1298.

Shiomi, D., & Margolin, W. (2008). Compensation for the loss of the conserved membrane targeting sequence of FtsA provides new insights into its function. *Mol Microbiol*, *67*(3), 558-569.

Stephens, R. S., Kalman, S., Lammel, C., Fan, J., Marathe, R., & Aravind, L. (1998). Genome sequence of an obligate intracellular pathogen of humans: CHlamydia trachomatis. *Science*, *282*, 754-759.

Stricker, J., Maddox, P., Salmon, E. D., & Erickson, H. P. (2002). Rapid assembly dynamics of the Escherichia coli FtsZ-ring demonstrated by fluorescence recovery after photobleaching. *Proc Natl Acad Sci U S A*, *99*, 3171-3175.

Taylor, G. (2003). The phase problem. *Acta Crystallogr D Biol Crystallogr*, *59*, 1881-1890.

Thanbichler, M. (2010). Synchronization of chromosome dynamics and cell division in bacteria. *Cold Spring Harbor Perspectives in Biology*.

(1994). The CCP4 suite: programs for protein crystallography. *Acta Crystallogr D Biol Crystallogr*, *50*(Pt 5), 760-763.

van den Ent, F., Amos, L. A., & Löwe, J. (2001a). Bacterial ancestry of actin and tubulin. *Curr Opin Microbiol*, *6*, 634-638.

van den Ent, F., Amos, L. A., & Löwe, J. (2001b). Prokaryotic origin of the actin cytoskeleton. *Nature*, *413*(6851), 39-44.

van den Ent, F., & Löwe, J. (2000). Crystal structure of the cell division protein FtsA from Thermotoga maritima. *EMBO J*, *19*(20), 5300-5307.

van den Ent, F., Moller-Jensen, J., Amos, L. A., Gerdes, K., & Löwe, J. (2002a). F-actin-like filaments formed by plasmid segregation protien ParM. *EMBO J*, *21*, 6935-6943.

van den Ent, F., Moller-Jensen, J., Amos, L. A., Gerdes, K., & Löwe, J. (2002b). F-actin-like filaments formed by plasmid segregation protein ParM. *EMBO J*, *21*(24), 6935-6943.

Vicente, M., & Rico, A. I. (2006). The order of the ring: assembly of Escherichia coli cell division components. *Mol Microbiol*, *61*(1), 5-8.

Waller, B. J., & Alberts, A. (2003). The formins: active scaffolds that remodel the cytoskeleton. *Trends Cell Biol*, *13*, 435-446.

Wang, X., Huang, J., Mukherjee, A., Cao, C., & Lutkenhaus, J. (1997). Analysis of the interaction of FtsZ with itself, GTP, and FtsA. *J Bacteriol*, *179*(17), 5551-5559.

Woldringh, C.L. (1976). Morphological analysis of nuclear separation and cell division during the life cycle of Escherichia coli. *J Bacteriol*, *125*, 248-257.

Yim, L., Vandenbussche, G., Mingorance, J., Rueda, S., Casanova, M., Ruysschaert, J. M. et al. (2000). Role of the carboxy terminus of Escherichia coli FtsA in self-interaction and cell division. *J Bacteriol*, *182*(22), 6366-6373.